NASA/TM—2010–216373

Pyroelectric Materials for Uncooled Infrared Detectors: Processing, Properties, and Applications

M.D. Aggarwal, A.K. Batra, P. Guggilla, and M.E. Edwards
Alabama A&M University, Normal, Alabama

B.G. Penn and J.R. Currie, Jr.
Marshall Space Flight Center, Marshall Space Flight Center, Alabama

March 2010

The NASA STI Program…in Profile

Since its founding, NASA has been dedicated to the advancement of aeronautics and space science. The NASA Scientific and Technical Information (STI) Program Office plays a key part in helping NASA maintain this important role.

The NASA STI Program Office is operated by Langley Research Center, the lead center for NASA's scientific and technical information. The NASA STI Program Office provides access to the NASA STI Database, the largest collection of aeronautical and space science STI in the world. The Program Office is also NASA's institutional mechanism for disseminating the results of its research and development activities. These results are published by NASA in the NASA STI Report Series, which includes the following report types:

- TECHNICAL PUBLICATION. Reports of completed research or a major significant phase of research that present the results of NASA programs and include extensive data or theoretical analysis. Includes compilations of significant scientific and technical data and information deemed to be of continuing reference value. NASA's counterpart of peer-reviewed formal professional papers but has less stringent limitations on manuscript length and extent of graphic presentations.

- TECHNICAL MEMORANDUM. Scientific and technical findings that are preliminary or of specialized interest, e.g., quick release reports, working papers, and bibliographies that contain minimal annotation. Does not contain extensive analysis.

- CONTRACTOR REPORT. Scientific and technical findings by NASA-sponsored contractors and grantees.

- CONFERENCE PUBLICATION. Collected papers from scientific and technical conferences, symposia, seminars, or other meetings sponsored or cosponsored by NASA.

- SPECIAL PUBLICATION. Scientific, technical, or historical information from NASA programs, projects, and mission, often concerned with subjects having substantial public interest.

- TECHNICAL TRANSLATION. English-language translations of foreign scientific and technical material pertinent to NASA's mission.

Specialized services that complement the STI Program Office's diverse offerings include creating custom thesauri, building customized databases, organizing and publishing research results…even providing videos.

For more information about the NASA STI Program Office, see the following:

- Access the NASA STI program home page at <http://www.sti.nasa.gov>

- E-mail your question via the Internet to <help@sti.nasa.gov>

- Fax your question to the NASA STI Help Desk at 443–757–5803

- Phone the NASA STI Help Desk at 443–757–5802

- Write to:
  NASA STI Help Desk
  NASA Center for AeroSpace Information
  7115 Standard Drive
  Hanover, MD 21076–1320

Pyroelectric Materials for Uncooled Infrared Detectors: Processing, Properties, and Applications

M.D. Aggarwal, A.K. Batra, P. Guggilla, and M.E. Edwards
Alabama A&M University, Normal, Alabama

B.G. Penn and J.R. Currie, Jr.
Marshall Space Flight Center, Marshall Space Flight Center, Alabama

Acknowledgments

TABLE OF CONTENTS

LIST OF FIGURES

LIST OF TABLES

LIST OF ACRONYMS AND SYMBOLS

AAMU	Alabama A&M University
ABO_3	oxygen octahedral ferroelectric
ac	alternating current
ADTGSP	alanine-doped deuterated triglycine phosphate-sulfate
AES	auger electron spectrometry
AFM	atomic force microscopy
AIN	aluminum nitride
As	arsenic
ATGS	alanine-doped triglycine sulfate
ATGSP/As	alanine-doped triglycine sulfate-phosphate/arsenate
Au	gold
B	boron
Ba	barium
$BaTiO_3$	barium titanate
BITO	bismuth titanate
Bi	bismuth
BLT	bismuth lanthanum titanate
BNN	barium sodium niobate
BSN	barium strontium niobate
BST	barium strontium titanate
BTO	barium titanate
Ca	calcium
$CaTiO_3$	calcium titanate
CCD	charge-coupled device
Cd	cadmium
CdTGS	cadmium-doped triglycine sulfate
Cl	chlorine
CO_2	carbon dioxide
Cr	chromium
CrLATGS	chromium L-alanine-doped triglycine sulfate
Cs	cesium
CsLATGS	cesium L-alanine-doped triglycine sulfate

CST calcium strontium titanate
Cu copper
CuTGS copper-doped triglycine sulfate
CVD chemical vapor deposition
CZ Czochralski
D_2O deuterium oxide
dc direct current
dc-UBMS direct current-unbalanced magnetron sputtering
DLATGS L-alanine-doped deuterated triglycine sulfate
DRAM dynamic random access memory
DTA differential thermal analysis
DTGFB deuteration of triglycine fluoroberyllate
DTGPS deuterated triglycine phosphate-sulfate
DTGS deuterated triglycine sulfate
ECR electron cyclotron resonance
EO electrooptical
Er erbium
Eu europium
Fe iron
FOM figure of merit
FRAM ferroelectric random access memory
g-c glass-ceramic
Ga gallium
GaN gallium nitride
GFD graded ferroelectric device
GMO gadolinium molybdate
H_2O water
Hg mercury
IC integrated circuit
In indium
IR infrared
ITO indium tin oxide
K potassium

KDA	potassium dihydrogen arsenate
KDP	potassium dihydrogen phosphate
KLN	potassium lithium niobate
KN	potassium niobate
KNN	potassium sodium niobate
KT	potassium titanate
KTN	potassium tantalate niobate
KTP	potassium titanyl phosphate
La	lanthanum
LAO	lithium aluminum oxide
LATGS	L-alanine-doped triglycine sulfate
LGO	lead germanium oxide
Li	lithium
LiTGS	lithium-doped triglycine sulfate
LN	lithium niobate
Ln	lanthanoid
LSBN	lanthanum-doped strontium barium niobate
LT	lithium tantalate
M	morphotropic
MCT	mercury cadmium telluride
MEK	methyl-ethyl-ketone
MFS-FET	metal-ferroelectric-semiconductor-field effect transistor
Mg	magnesium
ML	multilayer
Mn	manganese
MnTGS	manganese-doped triglycine sulfate
MOCVD	metallo-organic chemical vapor deposition
MOD	metallo-organic deposition
MSPZT	manganese- and antimony-doped lead zirconium titanate
Na	sodium
NAFP	NASA Administrator's Fellowship Program
Nb	niobium
NBT	sodium bismuth titanate

Nd:YAG	neodymium-doped yttrium aluminum garnet
NEP	noise equivalent power
Ni	nickel
NiLATGS	nickel L-alanine-doped triglycine sulfate
NLO	nonlinear optical
O	oxygen
P	polarization
P(VDF-TrFE)	polyvinylidene fluoride-trifluoroethylene
Pb	lead
PbO	lead oxide
$Pb(Zr,Ti)O_3$	lead zirconate titanate
PCLT	calcium (11%)-modified lead titanate
PCT	lead calcium titanate
PECVD	plasma-enhanced chemical vapor deposition
PErT	erbium-doped lead titanate
PET	porous silicon and plastic
PETM	lead europium titanate manganate
PIR	pyroelectric infrared
PLAD	pulse laser ablation deposition
PLTM	lead lanthanum titanate manganate
PLT	lead lanthanum titanate
PLZT	lead lanthanum zirconate titanate
PMN-PT	lead magnesium niobate-lead titanate
PMZT	manganese-doped lead zirconate titanate
PPR	photoplaner-radiometer
PMN-PZT	lead magnesium niobate-lead zirconate titanate
PMNZTU	uranium-doped lead magnesium niobate-lead zirconate titanate
PST	lead scandium titanate
PSTM	lead samarium titanate manganate
PT	lead titanate
Pt	platinum
PTB	pyroelectric thermistor bolometer
PTCR	positive temperature coefficient resistance
PU	polyurathane

PVDF	poly(vinylidene fluoride)
PVF	polyvinyl fluoride
PZ	lead zirconate
PZFNT	lead zirconate iron niobate titanate
PZT	lead zirconate titanate
RDA	rubidium dihydrogen phosphate
RF	radio frequency
RIE	reactive ion etching
rms	root mean square
RTA	rapid thermal annealing
Ru	ruthenium
RuO_2	ruthenium oxide
SAW	surface acoustic wave
Sb	antimony
SBN	strontium barium niobate
SbSI	antimony sulphoiodide
SBST	silicon dioxide-doped barium stontium titanate
Si	silicon
Sm	samarium
Sn	tin
Sr	strontium
STN	sodium tantalate niobate
Ta	tantalum
TCD	temperature coefficient of dielectric constant
Te	tellurium
TGFB	triglycine fluoroberyllate
TGS	triglycine sulfate
TGSe	triglycine selenate
Ti	titanium
TiO_2	titanium dioxide
TM	Technical Memorandum
TrFE	trifluoroethylene
U	uranium
UFPA	uncooled infrared focal plane array

VDF	vinylidene fluoride
VDF-TrFE	vinylidene fluoride-trifluoroethylene
W	tungsten
XRD	x-ray diffraction
Y	yttrium
YBCO	yttrium barium copper oxide
YSZ	yttria-stabilized zirconia
Zn	zinc
ZnO	zinc oxide
ZnTGS	zinc-doped triglycine sulfate
Zr	zirconium
ZrO_2	zirconium dioxide

NOMENCLATURE

A	area
C	elastic stiffness
C_V	volume specific heat
c	elastic stiffness
c'	specific heat
D^*	detectivity
D	electric displacement
d	piezoelectric coefficient
dE	change of electric field
dE/dT	change in the electric field with respect to the change in temperature
dP	change in polarization
dP/dE	change in polarization with respect to the change in the electric field
dT	temperature variation
dT/dt	rate of change of temperature
E	electric field
e	strain
F_D	figure of merit for high detectivity
F_{D^*}	figure of merit of detectivity
F_I	figure of merit for high current responsivity
F_i	figure of merit for high current responsivity without volume specific heat
F_V	figure of merit for high-voltage responsivity
I_p	pyroelectric current
H_{rms}	root mean square value of the fundamental component of the irradiance
k	thermal conductivity
P	polarization
P_r	remnant polarization
P_s	switchable polarization
p	pyroelectric coefficient
p_p	primary pyroelectric coefficient
p_s	secondary pyroelectric coefficient
R	responsivity
R_I	current responsivity

R_V	voltage responsivity
T	temperature
T_c	Curie temperature
t	thickness of film
$\tan \delta$	dielectric loss
V_n	root mean square noise value
V_s	detector root mean square output signal
α	thermal expansion
Δf	noise bandwidth
ε	permittivity
ε'	real part of dielectric constant
ε''	imaginary part of dielectric constant
ϕ_λ	incident radiant power
σ	stress
τ_E	electrical time constant
τ_T	thermal time constant

TECHNICAL MEMORANDUM

**PYROELECTRIC MATERIALS FOR UNCOOLED INFRARED DETECTORS:
PROCESSING, PROPERTIES, AND APPLICATIONS**

1. INTRODUCTION

Outside the visible spectrum, at its red end, exists the infrared (IR) region with wavelengths longer than visible light. The IR region of electromagnetic radiation spans photon wavelengths from 0.7 to 1,000 μm. The origins of IR photons are gases, liquids, and solids that make up the universe. These IR sources can both absorb and emit IR radiation. The dependence of radiation absorption and emission spectra on wavelength identifies and provides detailed information about the materials in our universe. Infrared detectors bring this valuable information within the purview of human observation through their use in a wide variety of optical characterization instruments, planetary exploration, space and astrophysics, atmosphere radiation measurements, and numerous commercial military applications such as occupancy and motion detection in security systems, military surveillance, manufacturing processes, gas sensing, industrial and medical thermal imaging, etc.

Uncooled pyroelectric IR (PIR) imaging systems, such as night vision goggles, offer important strategic advantages in battlefield scenarios and reconnaissance surveys. They include commercial applications such as fire rescue equipment, medical imaging, security surveillance systems, and imaging systems for cars, ships, and aircraft. In recent years, requirements in the field of IR sensors have turned increasingly towards technologies with the potential to deliver lightweight, compact, low-power, and low-cost IR detectors and imaging heads using thin- or thick-film elements integrated with silicon (Si) technology. It means that they are required both in peace and war.

Infrared radiation sensors can be generally classified into two classes: (1) Photon detectors in which the radiation absorption process directly produces a measurable effect (e.g., generation of photoelectrons or charge carrier pairs in a photoconductor) and (2) thermal detectors that are also considered as indirect optical detectors, as they first convert the absorbed incident radiation into heat, which then produces a measurable effect. Pyroelectric, along with bolometer, Golay cells, and thermopiles, belong to the latter class.

While photon detectors such as mercury (Hg) cadmium (Cd) telluride (MCT) have their highest responsivity (R) in the 8- to 14-μm region, their spectral range is very narrow (i.e., they are spectral selective). In addition, cryogenic cooling is often required to provide optimum operation, which adds significantly to the cost and complexity of these detectors. On the other hand, thermal detectors are of considerable interest due to the fact they can deliver relatively high performance at low cost when operated at room temperature. PIR detectors fall in the category of thermal detectors.

PIR sensing devices have the following five main advantages over photon IR sensors:

(1) Sensitivity in a very large spectral bandwidth limited only by the ability of the sensor to absorb the incident radiation.
(2) Sensitive in a very wide temperature range without the need of cooling.
(3) Low power requirements.
(4) Relatively fast response.
(5) Generally low-cost materials.

Furthermore, it is worthy to mention that uncooled PIR imaging systems, such as night vision goggles, offer important strategic advantages in battlefield scenarios and reconnaissance surveys due to their lightweight.

In this Technical Memorandum (TM), an overview is presented of pyroelectricity and its application in PIR detectors along with the physics of pyroelectric single-element sensors and how they are integrated with Si-substrate sensors, measurement of physical parameters, and pyroelectric materials (both bulk and films); this includes their growth, properties, and selection. An account is given of their wide range of applications.

2. FERROELECTRICS AND PYROELECTRICS

All crystals can be categorized into 32 different classes. These classes are point groups divided by using the following symmetry elements: (1) Center of symmetry, (2) axes of rotation, (3) mirror planes, and (4) several combinations of them. The 32 point groups are subdivisions of 7 basic crystal systems that are, in order of ascending symmetry, triclinic, monoclinic, orthorhombic, tetragonal, rhombohedral (trigonal), hexagonal, and cubic. Of the 21 classes of the 32 point groups that are noncentrosymmetric, which is a necessary condition for piezoelectricity to exist, 20 of them are piezoelectric. Of the 20 piezoelectric crystal classes, 10 crystals have pyroelectric properties. Within a given temperature range, this group of materials is permanently polarized. Compared to the general piezoelectric polarization produced under stress, the pyroelectric polarization is developed spontaneously and kept as permanent dipoles in the structure. Because this polarization varies with temperature, the response is termed as pyroelectricity.

The ferroelectric group is a subgroup of the spontaneously polarized pyroelectric crystals. On one hand, the polarization of ferroelectric is similar to the polarization of pyroelectric. On the other hand, there is a difference between the two polarizations because the ferroelectric polarization is reversible by an external applied electric field, provided that the applied field is less than the dielectric breakdown of the materials. Therefore, materials that can be defined as ferroelectrics must have two characteristics: (1) The presence of spontaneous polarization and (2) reversibility of the polarization under an electric field. A ferroelectric material is therefore pyroelectric, piezoelectric, and noncentrosymmetric.

Table 1 lists the important ferroelectric/pyroelectric materials being investigated and/or are being used in the various devices.[1–5] Figure 1 shows some important ferroelectric materials and their uses in various devices based on their unique piezoelectric, pyroelectric, ferroelectric, electrooptic, acoustooptic, and dielectric properties. The most commonly used materials for pyroelectric applications include triglycine sulfate (TGS); lead (Pb) zirconate titanate, $PbZrTiO_3$ (PZT); Pb titanate, $PbTiO_3$ (PT); poly (vinylidene fluoride) (PVDF); and lithium (Li) tantalate, $LiTaO_3$ (LT).

2.1 Pyroelectric Phenomenon

Since time immemorial, people in India and Ceylon—where tourmaline crystals were easily found—had observed that such crystals, when thrown into ashes, would strongly attract surrounding ash particles after a few moments, only to repel them again a little later. Dutch merchants brought this knowledge, together with the first tourmaline crystal, to Europe around 1703, where tourmaline was often called "Ceylon magnet." Carl Linnaeus gave it the scientific name "Lapis Electricus" in 1747. Aepinus proved the electrical nature of this phenomenon in 1756 when he noted the opposite polarities at two ends of a heated tourmaline crystal. Brewster named this effect "pyroelectricity" (from Greek "pyro," which means fire) in 1824.[7]

Table 1. Important pyroelectric and ferroelectric materials.

Ferroelectric Family	Ferroelectric Material	Chemical Formula	Abbreviation
Perovskite type	Barium (Ba) titanate	$BaTiO_3$	BTO
	Potassium (K) niobate	$KNbO_3$	KN
	K titanate	$KTiO_3$	KT
	K tantalate-niobate	$KTa_{1-x}Nb_xO_3$	KTN
	Pb zirconate titanate	$PbZrxTi_{1-x}O_3$	PZT
	Pb scandium titanate	$PbSc_xTi_{1-x}O_3$	PST
	Ba strontium (Sr) titanate	$Ba_xSr_{1-x}TiO_3$	BST
Li niobate family	Li niobate	$LiNbO_3$	LN
	Li tantalate	$LiTaO_3$	LT
Tungsten-bronze type	Ba Sr niobate	$Ba_{5x}Sr_{5(1-x)}Nb_{10}O_{30}$	BSN
	Ba sodium niobate	$Ba_{5x}Na_{5(1-x)}Nb_{10}O_{30}$	BNN
	K Li niobate	$K_5Li_2Nb_5O_{15}$	KLN
KDP family	K dihydrogen phosphate	KH_2PO_4	KDP
	K dihydrogen arsenate	KH_2AsO_4	KDA
	Rubidium dihydrogen phosphate	RbH_2PO_4	RDP
TGS type	Triglycine sulfate	$(NH_2CH_2COOH)_3 \cdot H_2SO_4$	TGS
	Triglycine selenate	$(NH_2CH_2COOH)_3 \cdot H_2SeO_4$	TGSe
KTP family	K titanyl phosphate	$KTiOPO_4$	KTP
Bismuth titanate	Bismuth titanate	$Bi_4Ti_3O_{12}$	BITO
Rare earth molybdate	Gadolinium molybdate	$\beta\text{-}Gd_2(MoO)_3$	GMO
Pb germanium oxide	Pb germanium oxide	$5PbO \cdot 3GeO_2$ or $Pb_5Ge_3O_{11}$	LGO
Antimony sulphoiodide	Antimony sulphoiodide	SbSI	SbSI
Polymer	Poly (vinylidene fluoride)	–	PVDF
	Poly (vinylidene fluoride-trifluoroethylene)	–	P(VDF-TrFE)

Pyroelectric detectors are thermal detectors and use the pyroelectric effect to detect incident IR radiation. The pyroelectric effect or pyroelectricity refers to the change of internal polarization of a material due to small changes in temperature.

Pyroelectric materials are dielectric materials and possess a spontaneous electrical polarization that appears in the absence of an applied electrical field or stress. Since pyroelectricity is the electrical response of a polar material as a result of a change of temperature, the pyroelectric effect at constant electric field (E) and stress (σ) are defined as follows:[8]

$$\left(\frac{\partial D}{\partial T}\right)_{E,\sigma} = \left(\frac{\partial D}{\partial T}\right)_{E,e} + \left(\frac{\partial D}{\partial e}\right)_{E,T}\left(\frac{\partial e}{\partial T}\right)_{E,\sigma}, \tag{1}$$

4
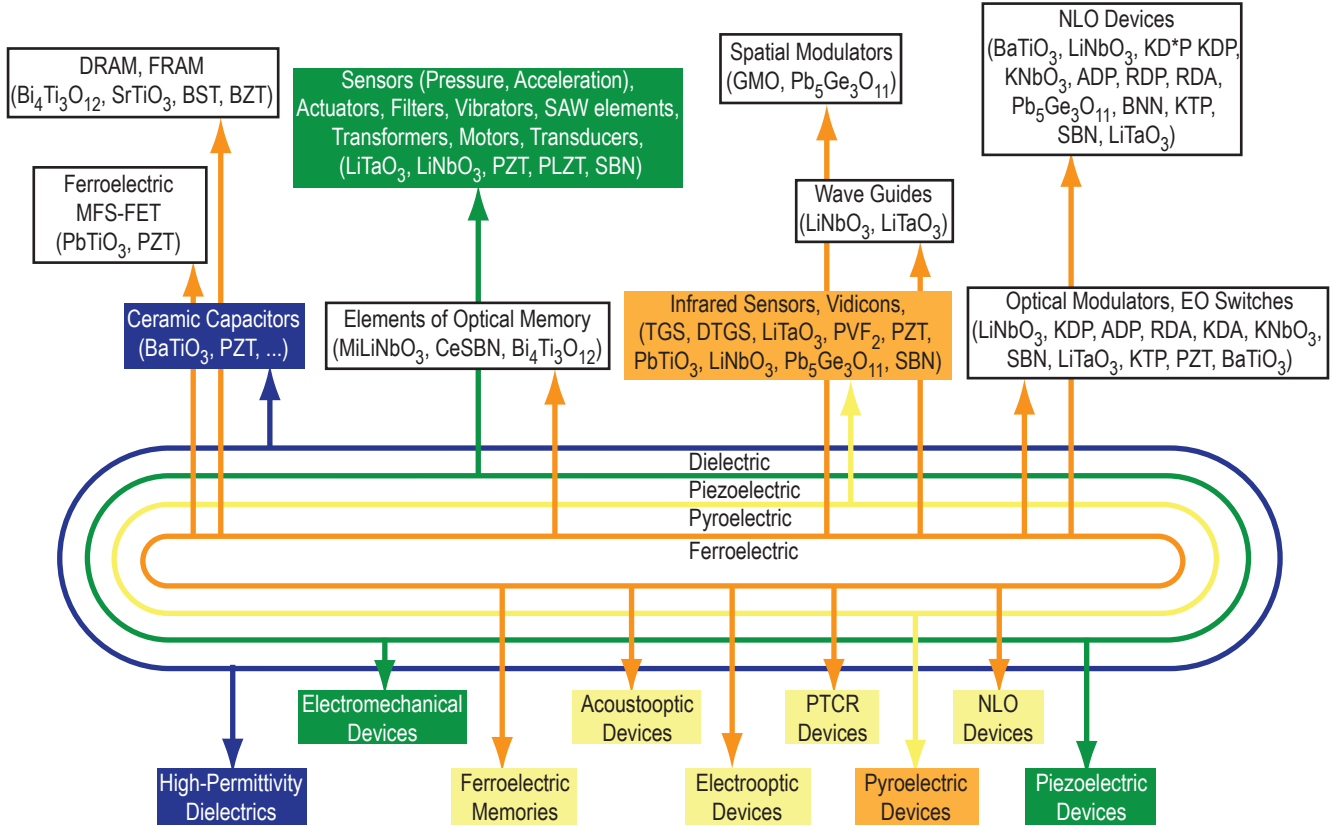
Figure 1. Important ferroelectric materials and selected applications. The color scheme illustrates that ferroelectrics are a subclass of pyroelectrics and that pyroelectrics are a subclass of piezoelectrics.[6]

where D is the electric displacement, e is the strain, and T is the temperature of the pyroelectric material. The first term on the right side of the equation is called the primary pyroelectric response or effect. This effect is due to charge produced owing to a change in the polarization with temperature when dimensions of pyroelectric materials are kept constant. If dimensions change with temperature for materials under constant stress, an additional charge is produced due to the piezoelectric effect. This phenomenon leads to the secondary pyroelectric effect. The second term on the right side of equation (1) represents the secondary pyroelectric effect.

For ferroelectrics, D is related as,

$$D = P + d\sigma \ , \tag{2}$$

where P is the polarization (which is switchable and abbreviated as P_s) and d is the piezoelectric coefficient of the ferroelectric materials. Polarization is defined as

$$P = P_s + \varepsilon E \ , \tag{3}$$

where ε is the permittivity and E is the electric field of the ferroelectric materials. From equations (1) and (2), one can derive,

$$p = \left(\frac{\partial \boldsymbol{D}}{\partial T}\right)_{E,\sigma} = \left(\frac{\partial \boldsymbol{P_s}}{\partial T}\right)_{E,\sigma} + E\left(\frac{\partial \boldsymbol{\varepsilon}}{\partial T}\right)_{E,\sigma}, \tag{4}$$

where the first term on the right side of equation (4) is the primary pyroelectric coefficient (p_p) at zero applied field and below the Curie temperature (T_c) of the material. The T_c is the temperature at which a material changes from the ferroelectric (polar) phase to the paraelectric (nonpolar) phase. The second term on the right side of equation (4) is significant near T_c, where the change of dielectric ε due to temperature is quite large. From equation (4), if $E=0$, or ε of the material does not change with temperature, then the p_p is the change of spontaneous polarization with temperature, provided the dimensions of the material do not change (first term). One can write,

$$p_p = \left(\frac{\partial P_s}{\partial T}\right)_{E,\sigma}. \tag{5}$$

The secondary pyroelectric coefficient (p_s)is described as,

$$p_s = \left(\frac{\partial \boldsymbol{D}}{\partial e}\right)_{E,T}\left(\frac{\partial e}{\partial T}\right)_{E,\sigma} = \left(\frac{\partial \boldsymbol{D}}{\partial \boldsymbol{\sigma}}\right)_{E,T}\left(\frac{\partial \boldsymbol{\sigma}}{\partial e}\right)_{E,T}\left(\frac{\partial e}{\partial T}\right)_{E,\sigma} = dc\alpha, \tag{6}$$

where c is the elastic stiffness and α is the thermal expansion coefficient of the material. Contribution to p_s is induced by thermal deformation and piezoelectricity.

It is worthwhile to explain that the two modes of operation for a pyroelectric detector are "pyroelectric" and "dielectric" (bolometer). The pyroelectric mode of operation is in the pyroelectric or ferroelectric state of the material (i.e., below the T_c of the material). The dielectric mode becomes operative through the application of a biasing field near T_c. It can also be operated in both ferroelectric and paraelectric phases of the material but near the T_c. In the pyroelectric mode, large changes in the spontaneous polarization with temperature near ferroelectric phase transitions lead to large p; thus, the detector sensitivity increases. In the dielectric bolometer mode, a larger p can be achieved for operation with an electric field and low losses, which are typically realized by the application of an electric field that impedes domain boundary motion. The optimum bolometer detector response is a function of the applied electric field and temperature. However, additional equipment is required to control the temperature near T_c.

A pyroelectric detector is basically a capacitor whose spontaneous polarization vector is oriented normal to the plane of the electrodes. Incident radiation absorbed by the pyroelectric material is converted into heat. This results in a temperature variation (dT) and varying of the magnitude of the spontaneous polarization. Changes in polarization alter the surface charge of the electrodes, and charges are expelled from the surface to keep neutrality, which results in a pyroelectric current (I_p) in the external circuit.

The I_p depends on the temperature change with time. Therefore, pyroelectric devices are considered to be alternating current (ac) coupled devices. Pyroelectric current is proportional to the area (A) and rate of change of temperature (dT/dt) of the detecting element. One can write,

$$I_p = p \cdot A \frac{dT}{dt} \tag{7}$$

and

$$p = I_p \left(\frac{1}{A \cdot dT/dt} \right) , \tag{8}$$

where p is the pyroelectric coefficient.

2.2 Performance Parameters of Pyroelectric Detectors

The performance of pyroelectric detectors is generally determined in terms of the parameters described in sections 2.2.1–2.2.3.

2.2.1 Responsivity

Responsivity is the detector root mean square (rms) signal per unit incident power. It is expressed as

$$R = \frac{V_s}{\phi_\lambda} , \tag{9}$$

where V_s is the detector rms output signal and ϕ_λ is the incident radiant standard power.

Responsivity is expressed as amps/watt if the detector output signal is measured as current and it is a function of wavelength, operating frequency, operating temperature, bias voltage, and input circuit parameters.

2.2.2 Noise Equivalent Power

Noise equivalent power (NEP) is defined as the amount of required radiant power incident on the active area that will yield a signal-to-noise ratio of 1:1 by

$$\text{NEP} = H_{\text{rms}} A \frac{V_n}{V_s} , \tag{10}$$

where H_{rms} is the rms value of the fundamental component of the irradiance, A is the detector area, V_n is the rms noise value, and V_s is the rms signal value. NEP is a function of source, operating frequency, area of detector, and noise bandwidth (Δf) (in hertz).

2.2.3 Detectivity

Detectivity (D^*) is the figure of merit (FOM) that is normalized with respect to the detector A and the Δf such that

$$D^* = \frac{1}{\text{NEP}} \sqrt{A\Delta f} \;. \tag{11}$$

From the definition of NEP,

$$D^* = \frac{(V_s / V_n)}{W} \sqrt{A\Delta f} \;, \tag{12}$$

where W is the radiant power incident on the detector's active area.

From the expression above for D^* and R, it is seen that, when H_{rms} (in watts/square centimeters) is selected so that W equals the product $(H_{\text{rms}}A)$, the expression reduces to,

$$D^* = \frac{R}{V_n} \sqrt{(A\Delta f)} \;. \tag{13}$$

The important properties to look at in order to assess the material performance of IR sensors are low ε' and loss, high p, and low volume specific heat (c'). However, important material FOMs are as follows:[1]

• FOM for high current responsivity (R_I),

$$F_I = p/c' \;, \tag{14}$$

• FOM for high voltage responsivity (R_V),

$$F_V = p/c'\varepsilon' \;, \tag{15}$$

and

• FOM for high D^*,

$$F_D = p/c'(\varepsilon'')^{1/2} \;, \tag{16}$$

where p is the pyroelectric coefficient, c' is the volume specific heat of the element, ε' is the real part of dielectric constant, and ε'' is the imaginary part of the dielectric constant (dielectric loss).

Bauer et al.[9] have developed the following FOMs for when the pyroelectric element is placed on a substrate that is acting as a heat sink (i.e., whose thermal conductivity is infinite),

- FOM for high current R_I,

$$F_I = p/k \quad, \tag{17}$$

- FOM for high R_V,

$$F_V = p/k\varepsilon' \quad, \tag{18}$$

and

- FOM for high D^*,

$$F_D = p/k(\varepsilon'')^{1/2} \quad, \tag{19}$$

where k is the thermal conductivity of the pyroelectric element.

3. PROCESSING OF IMPORTANT PYROELECTRIC MATERIALS

3.1 Single Crystals

The growth of single crystals, although simple in principle, requires meticulous attention to details. Knowledge of the phase diagram of the constituents of the crystals and any solvent involved is essential. The mechanical and electrical equipment involved must be such to ensure uniformity of conditions over the extended period needed to grow a single crystal of any size; furthermore, the apparatus must avoid excessive vibrations and thermal disturbances.

3.1.1 Growth of Crystals From Solution

Highly homogeneous crystals can be grown by the slow cooling of saturated solutions of salt or, sometimes, by slow evaporation of a solution at constant temperature.

The growth of crystals from solution from low-temperature solutions occupies a prominent place, especially when materials are not stable at elevated temperatures. A number of concepts for solution crystal growth systems are found in the literature.[1] One of the best concepts for growth of both inorganic and organic crystals from solution is by temperature lowering of a solution, provided the material has a positive temperature coefficient of solubility.

Using this method in a proper solvent, a saturated solution of the material to be grown is prepared at a chosen temperature and kept at this temperature for 24 hr. Then, the seed-holding rod is inserted in the growth chamber and its rotation is initiated. The growth process is initiated by lowering the temperature slowly. The temperature of the solution is lowered at a preprogrammed rate, typically 0.05–2 °C per day, depending on the solubility of the chosen material. The complete crystallization process may take a week to several weeks. To terminate the growth process, the grown crystals are taken out of the solution without thermal shock. The necessary conditions for the solution growth technique are the availability of a proper solvent for the pyroelectric material and that the material has a positive temperature coefficient of solubility.

The pyroelectric large crystals of TGS and K dihydrogen phosphate (KDP) type have been successfully grown by this method. Single crystals of TGS usually have been grown from an aqueous solution by the temperature-lowering or solvent evaporation method. The authors have successfully grown the large TGS crystals using the crystallizer illustrated and described in detail elsewhere.[10] The authors' design of a typical crystallizer illustrating all the major components is shown in figure 2.

Brezina et al.[11] designed a crystallizer for growing L-alanine-doped deuterated TGS (DTGS) crystals by isothermal evaporation of deuterium oxide (D_2O). Satapathy et al.[12] have described a novel technique for mounting the TGS seeds and a crystallizer. Banan[13] has also described a crystallizer and a seed holder for growing pure and doped TGS crystals. TGS crystals weighing more than 100 g have been grown from solution with ethyl alcohol additions.[14] When
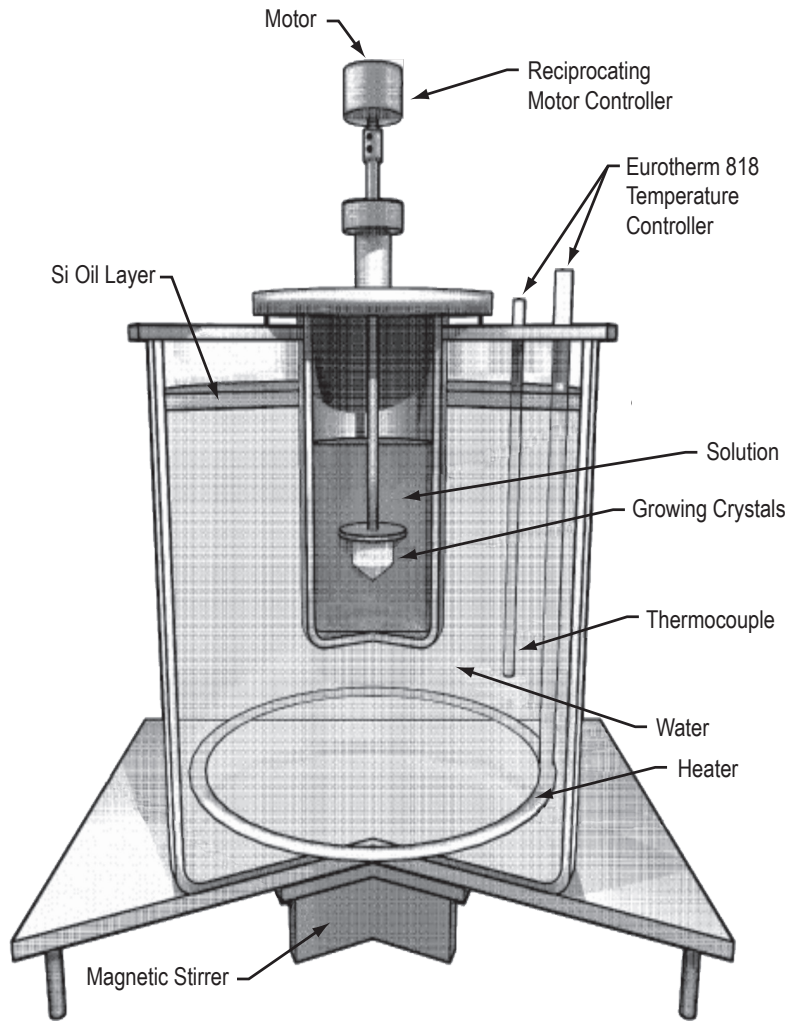
Figure 2. Schematic of a solution growth crystallizer designed
and fabricated at Alabama A&M University (AAMU).

alcohol is mixed in an aqueous solution of TGS, a part of the water in the solution associates with alcohol, which concentrates the solution. Thus, the supersaturation can be controlled to a certain degree, making it easier to grow TGS crystals.

To achieve success in growing crystals from aqueous solutions, it is important to prepare a solution with a well-determined saturation temperature, solubility profile, and absence of any foreign particles.

3.1.2 Crystal Growth From Melt

A basic diagram of the Czochralski (CZ) method with various components to explain the process is illustrated in figure 3.[15] The material should have a relatively low vapor pressure to be considered as a possible candidate for crystal growth by the CZ technique. The crucible material should be nonreactive with the crystal growth material above its melting point.
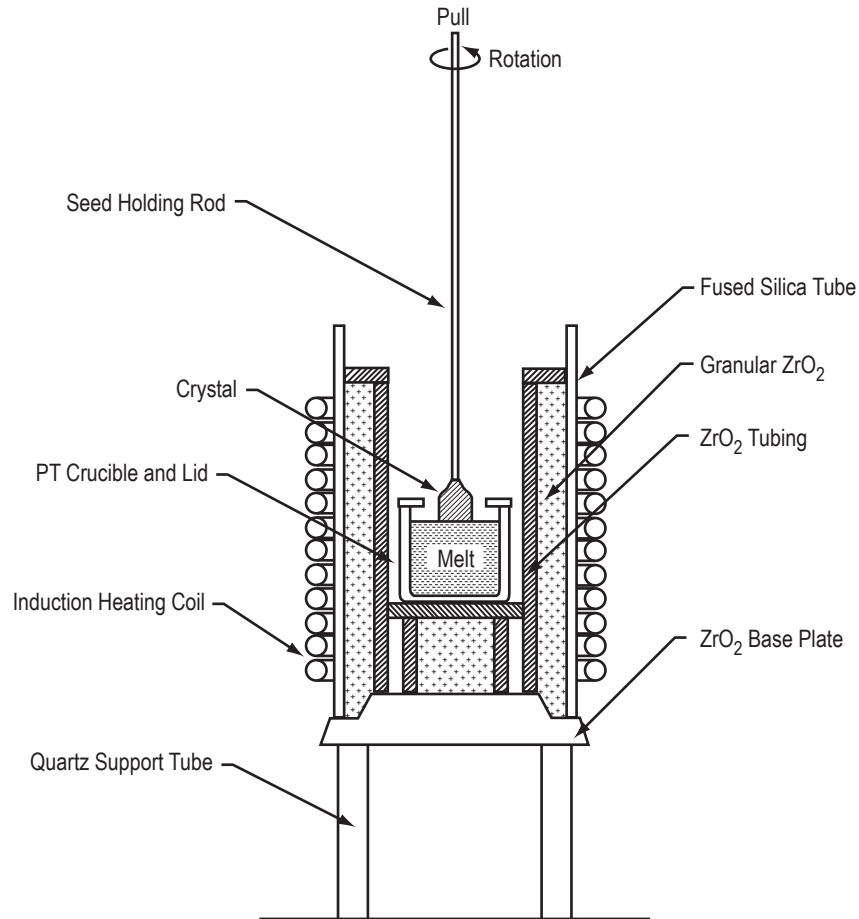
Figure 3. Schematic of the CZ crystal growth technique.[15]

The CZ system is based on the following principle. The material is melted in a crucible and is kept for a certain time at a temperature above the melting point. The temperature is then reduced to a value slightly above the freezing point. The freezing point is judged by cooling the melt until crystals start to appear on the surface; then, the temperature is slightly lowered and a seed (cut in the appropriate orientation) is inserted into the melt. It is kept at that position for ≈10 min. Then the pulling mechanism of the seed is started. The seed forms the crystallization center if the temperatures have been chosen correctly.

If the crystal starts growing very fast and becomes visible to the naked eye, the temperature of the melt needs to be increased by a degree or so. The melt must not be overheated because that would cause the crystal to dissolve and separate from the melt. Manipulating the temperature of the melt and the pulling rate controls the diameter of the pulled crystal. Suitable engineering of both axial and radial temperature gradients is needed to reliably grow single crystals of desired dimensions.

12

Pyroelectric single crystals of Li titanate, Li niobate (LN), K tantalate niobate (KTN), and others have been successfully grown by the CZ method.[16]

3.2 Preparation of Ceramics

Ceramic oxide compositions can generally be produced by thoroughly mixing the constituents as oxides or compounds, such as carbonates and nitrates, that readily decompose to oxides and where the calcination of the mixture is at a temperature that gives substantial interdiffusion of the cations. The calcine is then finely ground and compressed into the desired shape, which is then sintered at a temperature normally a few hundred degrees above the calcination temperature.[17]

For example, for the calcination of PZT, the starting raw materials Pb oxide (PbO), titanium (Ti) dioxide (TiO_2), and zirconium (Zr) dioxide (ZrO_2) are mixed in the molar ratio of 2:1:1, pressed into lumps, and then calcined in ambient air at 800 °C to obtain the perovskite phase. The calcining temperature is of great value as it influences the density and hence the electromechanical and other properties of the final product. However, calcining PZT at $T > 800$ °C could lead to Pb loss, resulting in a detrimental effect on the electrical properties. Therefore, calcination at the appropriate temperature is necessary to obtain the best electrical and mechanical properties.

After calcining, the lumps are ground by milling. The green bodies should have a certain minimum density before they can be sintered. The desired shape and a minimum green density can be provided by various techniques including powder compaction, slip casting, and extrusion. The choice of the method depends on the type of powder used, particle size distribution, and state of agglomeration, desired shape, and thickness of the part. After shaping, the green bodies are heated slowly to between 500 and 600 °C in order to remove any binder that is present. The binder amount burnout rate should be ≤1–2 °C/min in order to allow the gasses to come out slowly without forming cracks and blisters in the ceramic parts.

After the binder burnout is over, the samples are taken to a higher temperature for sintering to take place. The sintering temperature and time should be optimum for proper densification to occur without abnormal grain growth. The sintering of oxide ceramics must be carried out in an oxidizing atmosphere or in air. For Pb containing ceramics such as PZT, PT, Pb lanthanum (La) zirconate titanate (PLZT), etc., Pb loss occurs at temperatures above 800 °C. In order to reduce the Pb loss during sintering, the samples are kept in a sealed crucible containing saturated vapor. Figure 4 shows the flowchart of fabrication of ceramics and sample preparation for characterization.

3.3 Thin-Film Deposition Techniques

Fabrication of ferroelectric thin films has been of interest for some time. It originally started with simple thermal evaporation of barium (Ba) titanate ($BaTiO_3$) (BTO) by Feldman in 1956.[18] A number of deposition techniques have been developed since then. The various techniques can be simply classified into the two categories of solution deposition and nonsolution deposition. In the following sections, different techniques for the fabrication of PZT films are briefly reviewed.
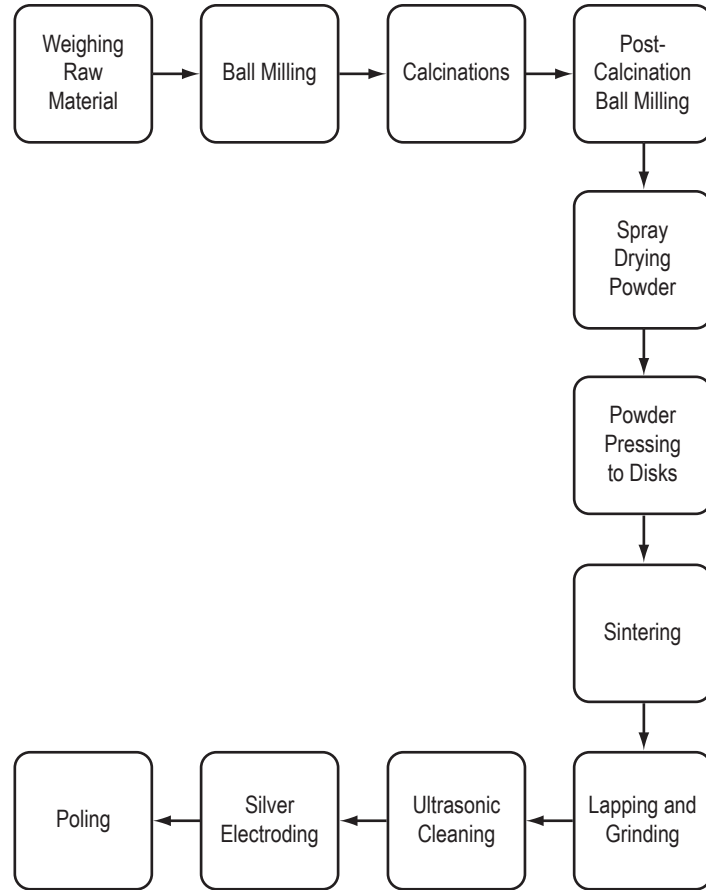
Figure 4. Flowchart for fabrication and processing of ferroelectric ceramics.

3.3.1 Nonsolution Deposition Techniques

　　3.3.1.1 Sputtering Technique. The sputtering methods (i.e., direct current (dc), radio frequency (RF) magnetron, electron cyclotron resonance (ECR) magnetron, and ion beam) have been the most widely used techniques to fabricate ferroelectric thin films because of their convenience and the high melting point of the PZT materials.[19] During the sputtering process, the material to be sputtered is made the sputtering target, which serves as the cathode in the electric circuit. The substrates to be coated are placed on a grounded anode a certain distance away. The target might consist of a series of individual elements aligned on a rotatable stage or a ceramic target that contains the required compositions. During the sputtering process, compositional ions are knocked from the surface of the target and deposited on the substrates. Both cold and hot stages are used in the PZT film preparation. The major problem associated with the sputtering process is stoichiometric control because the sputter rate of each element is different. The basic concept of a sputtering principle is illustrated in figure 5.

Figure 5. Schematic of a simple sputtering system.

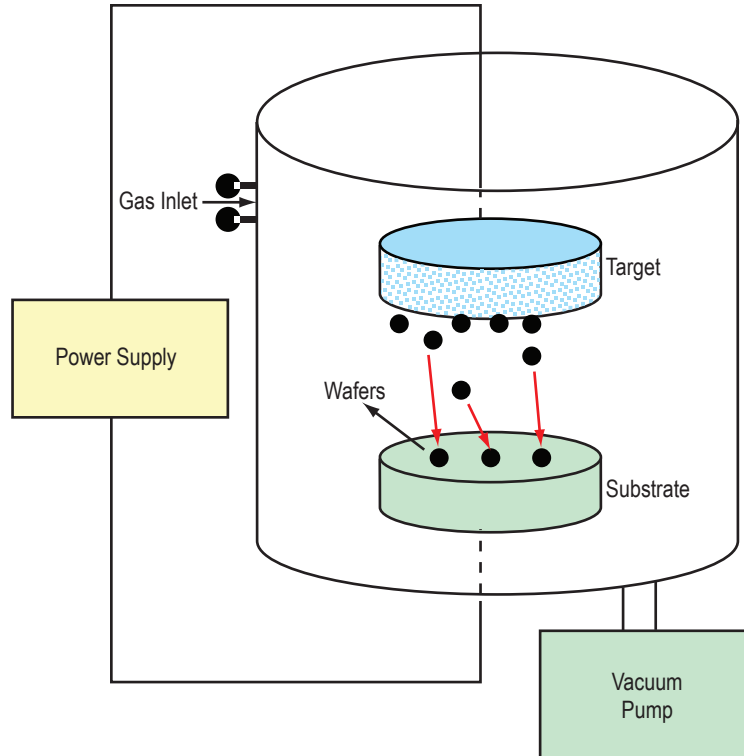**3.3.1.2 Laser Ablation Technique.** Pulse laser ablation deposition (PLAD) has been found to be a promising method for producing ferroelectric films because of its high depositing rate and stoichiometric control. It can be used to produce stoichiometric films even from a target material composed of five elements. The studies of PZT thin films have shown that the compositional uniformity of the fluence and the target-substrate distance are the two major factors that affect PZT thin-film quality. The higher the fluence the higher the deposition rate, but larger particles emitted from the target impair the quality of the films. To date, particulate-free PZT films have not been achieved by the PLAD technique.[20] A basic apparatus used for fabricating thin films by PLAD is illustrated in figure 6.

3.3.1.3 Chemical Vapor Deposition Technique. Chemical vapor deposition (CVD) involves the transportation of volatile compounds by carrier gas to the reaction chamber where they are exposed to the substrates. Chemical reactions take place at or near the substrate surface, resulting in a solid phase that condenses on the substrates. The CVD process can be significantly improved by making use of energy sources such as a laser beam, an electron beam, and an ion beam. The plasma formed by a focused energy source accelerates the decomposition of gases and improves the quality of the films. This type of technique is called plasma-enhanced CVD (PECVD). The PECVD technique is able to provide good quality PZT films at low processing temperatures.[21] A schematic of a CVD apparatus is shown in figure 7.
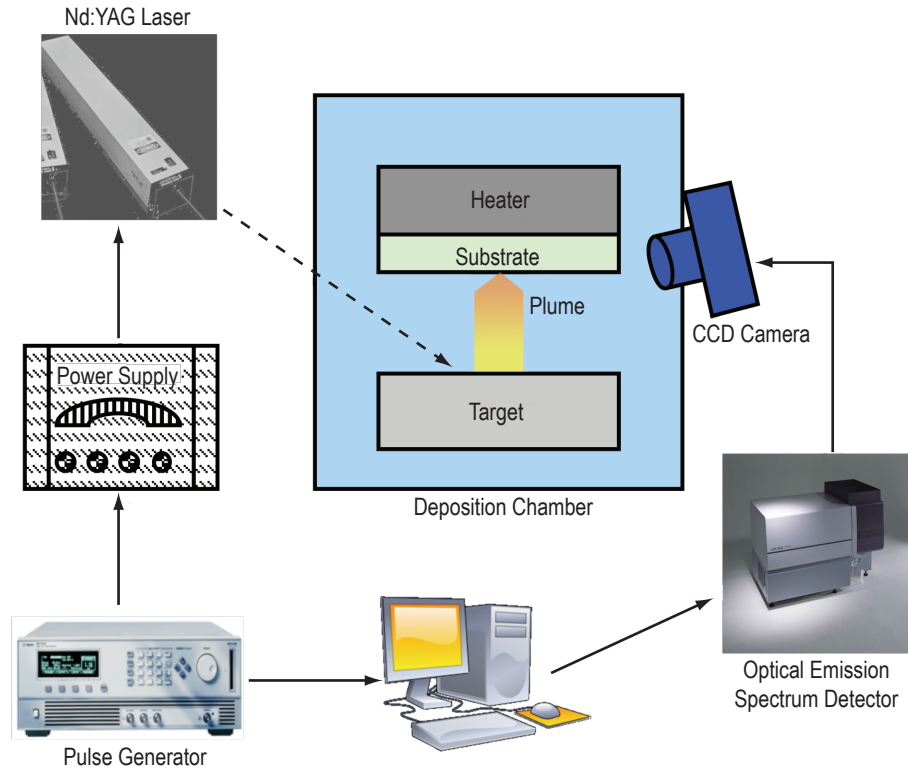
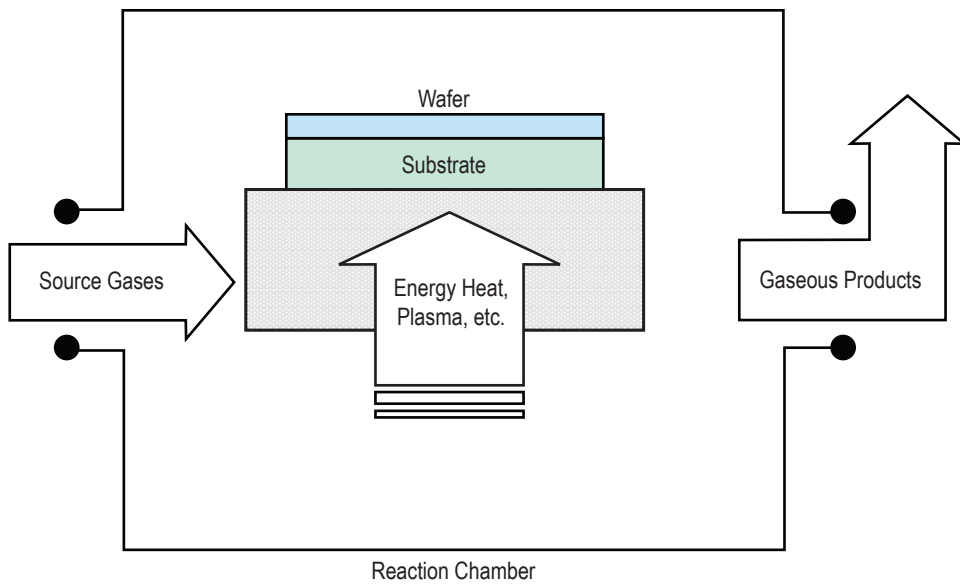Figure 6. Schematic of an experimental setup for the PLAD technique.
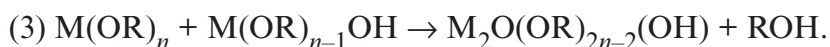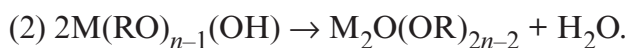

Figure. 7. Schematic of CVD.

If metallo-organic compounds are used as volatile reactants, the CVD process is called the metallo-organic CVD (MOCVD) technique. Recently, interest in using the MOCVD method to fabricate PZT films has increased because of its usefulness, high potential, and recent development of new source materials. The advantages of MOCVD processes include composition and crystalline structural control, high growth rate, and especially good step coverage.[22] By using the MOCVD technique, it has been shown that uniform PZT and PLZT thin films with variation in the film thickness is less than $\pm 1.5\%$ on a 6- to 8-in Si wafer, and both variations in Pb/(Zr + Ti) and Zr/(Zr + Ti) are below 5%.[23] Auger electron spectrometry (AES) depth profiling indicated a uniform composition through the thickness of the PZT films.[24]

3.3.2 Solution Deposition Technique

A solution deposition technique enables excellent stoichiometric control of complex mixed oxide systems and is a fast, cost-efficient method to prepare oxide thin films. The most used solution techniques are the sol-gel and metallo-organic deposition (MOD) methods. In the solution deposition for PZT films, metallo-organic starting reagents such as alkoxide $M(OR)_n$ (where M is a metal element and R is an alkyl group), carboxylate $(M(OOCR)_n)$, and β-biketonate $(MO_x(CH_3COCHCOCH_3)_n)$ compounds of Pb, Zr, and Ti are widely used as precursor compounds.[25–27]

3.3.2.1 Sol-Gel Technique. Sol-gel technology is one of the most popular methods for PZT thin deposition because it offers advantages such as high chemical purity, good stoichiometric control, low temperature processing, simple techniques for thin-film deposition, and microstructure control via chemical reactions. The basic steps in sol-gel processing involve the synthesis of a gel-precursor solution, or sol, that is applied to a substrate using a spin- or dip-coating technique. The resulting gel layer is then pyrolyzed to form an oxide ceramic film. J. Fukushima and coworkers were the first to report using sol-gel techniques to prepare PZT films.[28] They used butanol as the solvent for Pb ethylhexanate, Ti tetrabutoxide, and Zr acetalacetonate. Since then, great effort has been made to use the sol-gel technique to prepare PZT films. So far, the sol-gel route process can be classified into two categories: (1) Processes based on the use of 2-methoxyethanol as a reactant and solvent and (2) hybrid processes based on chelating ligands such as acetic acid or ethanolamine to reduce alkoxide reactivity.

In the 2-methoxyethanol process, metal-oxygen-metal bonds are formed as follows:

(1) $M(OR)_n + H_2O \rightarrow M(RO)_{n-1}(OH) + ROH$.

(2) $2M(RO)_{n-1}(OH) \rightarrow M_2O(OR)_{2n-2} + H_2O$.

(3) $M(OR)_n + M(OR)_{n-1}OH \rightarrow M_2O(OR)_{2n-2}(OH) + ROH$.

A key step in the 2-methoxyethanol process is the substitution of methoxyethoxy with Ti and Zr propoxide starting reagents, which produces the less-sensitive precursor solution of

$M(OR)_n + nR'OH \rightarrow M(OR')_n + nROH$.

17
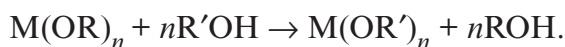
The hybrid process also utilizes alkoxide compounds as starting reagents but modifies the reaction with other reagents such as acetic acid or acetylacetone diethanolamine. The key reaction is chelation, which for acetic acid is

$$M(OR)_n + xCH_3COOH \rightarrow M(OR)_{n-x}(OOCCH_3)_x + xROH.$$

Acetic acid serves to reduce the susceptibility of the starting reagent to hydrolysis and condensation. A typical flowchart showing the various processing steps for growing PZT films is demonstrated in figure 8.
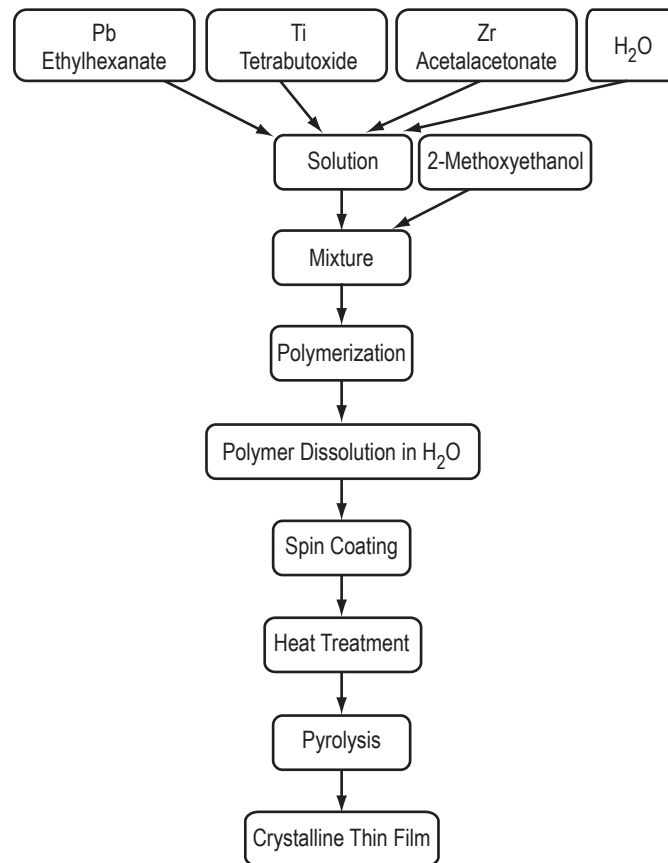
Figure 8. Flowchart of sol-gel processing of thin films.

A typical sol-gel process yields a single-layer PZT film about 0.1 μm thick. Multicoating is generally used in order to obtain thicker films (0.5 μm). Tu and Miline modified the sol-gel technique/process and used a diol-based sol-gel process to deposit PZT films.[29,30] They obtained 0.5-μm-thick, or thicker, films in a single coating. This technique could provide great advantages in the preparation of thicker films for film utilization, such as microactuators, pyroelectric sensors, and multilayer capacitors.

3.3.2.2 Metallo-Organic Deposition Method. The MOD method for thin-film fabrication has been known for more than 100 yr.[31] The process starts with dissolving precursor compounds in a proper solvent to obtain a true solution. This precursor solution is then coated onto a substrate by spin coating or spraying. The wet films are subsequently heated to remove any remaining solvent not evaporated during the deposition step, followed by pyrolyzing the organic films into inorganic films. If a thicker film is required, the coating and pyrolysis process are normally repeated several times until the required thickness is achieved. Finally, the films are postannealed to the desired crystalline phase, grain size, orientation, and oxygen content of the films.

The advantages associated with MOD are as follows:

• All the desired cations are mixed at the molecular level.
• Use of a low processing temperature.
• Precursor solution is very stable in air.
• In almost all cases, the deposition process can be conducted in air.
• It is easily applicable to substrates of any size and shape.

Recently, the MOD method has arisen as a promising technique for oxide film preparation.

3.3.2.2.1 Precursor Synthesis. In the molecular structure of precursor compounds using MOD, the ligands are bonded to the center metal ion through a heteroatom bridge. The bridge atom can be O, S, P, or N. The schematic of metallo-organic compounds is given as follows:

$$
\begin{array}{cc}
R_1 & O \\
| & \| \\
(R_2-C-C\text{-}O)_n-M \\
| \\
R_3
\end{array} \ .
$$

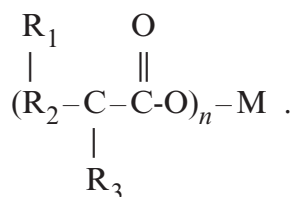Because most of the metallo-organic compounds suitable for oxide film fabrication are not commercially available, the success of oxide film fabrication from MOD processes strongly depends on the availability or the synthesis of metallo-organic compounds. So far, a number of methods have been developed to synthesize various metal precursors for producing oxide films by the MOD process. The major methods include the following:

• Double decomposition from ammonium soap.
• Neutralization.
• Metathesis reaction from metal acetate.
• Metathesis reaction from metal alkoxide.

Metal carboxylates are the most used starting materials in the MOD process for oxide films. According to the double decomposition reactions, metal carboxylate salts are synthesized by the reaction between the metal salt (typically hydrated nitrates or chlorides) and ammonium soap of the carboxylic acid, which is prepared before the reactions as follows:

- $NH_4OH + RCOOH \rightarrow RCOONH_4 + H_2O$

- $MX_n + nRCOONH_4 \rightarrow M(RCOO)_n + n(NH_4)X$.

When the resulting metal carboxylate is solid particles, the powder is filtered and washed to separate it from the solution. If it is a liquid, it can be extracted from the aqueous solution by using a nonpolar solvent such as xylene or benzene.

3.3.2.2.2 Solvent. In MOD, a liquid solution of organic compounds is prepared by dissolution of metal precursors with a suitable solvent that should have the following characteristics:

- High solvency for the precursors and does not interact with them.
- Adjustable viscosity.
- Adequate vapor pressure.
- Low cost, nontoxic, and noncorrosive.

Commonly used solvents for a MOD process are xylene and propionic acid. In cases where a single solvent does not meet all the requirements, mixed solvents are always utilized. With a combination of two or three solvents, the solvency capability of the solvent usually can be greatly improved. During the precursor solution preparation process, the addition order of precursor compounds is very important because of the micelle nature of the soap solutions. Micelles are aggregates of three or more soap molecules existing in the liquid in a thermodynamically stable state.[32] The aggregation of polar carboxylate molecules could form a compact, closed configuration rather than linear chains, which produces a nonpolar structure. These cause the carboxylate soaps to have a low viscosity in low-polarity solvents.

The advantage of the micelle nature of soap solutions in organic solvents is their ability to dissolve certain compounds by enclosing the molecules in the core of the micelles, which are otherwise not dissolved in the solvent. For example, La acetate is difficult to dissolve in xylene, but it is easily dissolved in a xylene solution of Ti dimethoxy dineodecanoate. To achieve this, the order of the addition of precursors is important, since it will decide what kinds of micelles exist in the solution and their solubility, which in turn will determine the solubility of precursors in the solvent. In the PZT film studies carried out by Yi et al., it was found that Zr propoxide must be added before Ti isopropoxide in solution preparation to avoid the formation of mono or diacetylated that will cause easy hydrolyzation.[27] A typical process of fabricating films by MOD is illustrated in figure 9.

3.3.2.2.3 Spin-Coating and Pyrolysis Processes. Spinning is the technique used most for depositing a uniform coating on a substrate in the MOD process. Regardless of the solvent system used, the solvent evaporation of the precursor solution can cause inhomogeneity during the coating process, especially in a multicomponent system because of the difference in solubility of each metallo-organic compound in the solvent. Therefore, the deposition step should occur as fast as possible to avoid any segregation. In spin coating, the spinning starts with a slow rate to spread
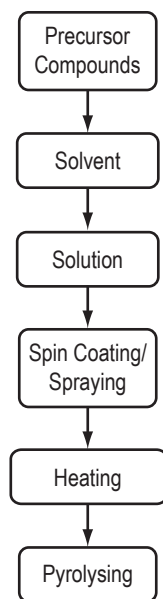
Figure 9. Flowchart for the MOD method.

the solution. As soon as the precursor solution completely covers the substrate, a spinning rate (≈3,000 rpm) is accelerated, quickly followed by a longer duration (30 s to 5 min).

After spin coating, the green organic films are usually heat treated in air or oxygen at 300 to ≈500 °C to remove any remaining solvent not evaporated during the deposition step and to convert the organic film into an inorganic film. Homogeneous thermal decomposition is critical in order to avoid elemental segregation and to form uniform phases and properties in a multicomponent system. In the whole MOD process, the pyrolysis process is the most important step, because the microstructure of the film is developed during this step. The volume change typically is very large, with typical ratios of deposited-to-fired thickness of 6:1 to 30:1. An inadequate heating rate during this phase can cause various defects such as cracks and voids in the fired film. Unfortunately, there is no rule to select an optimized heating rate.

To explain the thermal decomposition of carboxylates, a free radical mechanism is suggested. According to this mechanism, decomposition reactions go through the following three steps:

(1) Generation of the free radicals by thermal fission.
(2) Fragmentation and/or rearrangement of organic ligands.
(3) Oxidation of fission fragments of organic ligands by an oxidative chain reaction.

In a mixture of metallo-organic compounds, the free radicals generated by the decomposition of the least-stable metallo-organic compound will trigger the decomposition of the other precursors if their decomposition temperatures are not too different. This effect will lower the overall decomposition temperature, as compared to that of the individual components in the system.

3.3.2.2.4 Lead Zirconate Titanate Films by the Metallo-Oxide Deposition Technique. So far, the PZT films prepared by the MOD technique are comparable to the films fabricated by other techniques. Among the precursors used for MOD, metal neopentanoate, neoctoate, and neodecanoate salts are the most commonly used precursor compounds. Xylene, propionic acid, and butanol are the most widely used solvents. Vest and coworkers use Pb 2-ethylhexanoate $(Pb(C_7H_{15}COO)_2)$, Ti dimethoxy dineodecanoate $(Ti(OCH_3)_2(C_9H_{19}COO)_2)$, and Zr octanoate $(Zr(C_7H_{15}COO)_4)$ as precursor compounds to prepare PZT films. Xylene is used as the solvent.[26] The remnant polarization (P_r) of the PZT films was $P_r = 25$ µC/cm^2 and the dielectric constant was 600.

Klee et al. used Pb 2-ethylhexanoate, Ti-tetra-n-butylate, and Zr-acetylacetonate as starting compounds and butanol as the solvent to prepare PZT films.[33] It was found that a high weight loss occurred during annealing due to the high carbon content of MOD films. High weight loss usually is accompanied by a large volume change, which causes a cracking problem. Their results suggested that MOD-derived films crystallized into a single-phase perovskite phase at a lower temperature than sol-gel processes.

In order to minimize the cracking problem, Haertling used short-chain caraboxylate and β-diketonate as precursors.[34] The precursor solution not only showed an improved aging rate but also less film cracking due to small shrinkage associated with lower organic content precursors.

In most of the thin-film deposition techniques, the as-deposited PZT films have an amorphous structure. Therefore, postannealing is necessary to convert this amorphous phase into the desired ferroelectric perovskite phase. A typical microstructure of PZT films is of a rosette-type structure, where the rosette-like or spherulitic grains (perovskite phase) coexist with a nanocrystalline matrix (pyrochlore phase).[35,36] The existence of the pyrochlore phase in the PZT films is attributed to the loss of PbO during the phase evolution, which inhibits the pyrochlore to perovskite phase transformation. It is widely accepted that pyrochlore has a cubic structure with a formulation of $A_2B_2O_{7-x}$, richer in Zr and deficient in Pb than the perovskite structure.

Two mechanisms have been suggested to explain the mixed phase structure of PZT films. One suggestion is that as-deposited amorphous films first crystallize as a fine-grained intermediate, nonferroelectric pyrochlore phase. The pyrochlore phase is converted into the perovskite phase during a high-temperature treatment. Because of the high surface-to-volume ratio, the evaporation of Pb from PZT films is favored during the postanneal process. The consequence is the presence of the Pb-deficient pyrochlore phase in the films. The composition deviation of the pyrochlore phase from the oxygen octahedral ferroelectrics (ABO_3) stoichiometry increases with temperature and time of annealing and also depends on the substrate. Another mechanism proposes simultaneous crystallization of both pyrochlore and perovskite phases at high temperature from the amorphous films, which causes the two-phase structure.

Studies have shown that the amorphous to pyrochlore phase transformation takes place in the temperature range of 400 to 550 °C; whereas, the transformation between the pyrochlore-perovskite phases occurs from 450 °C, depending on the film composition. The transformation

between the pyrochlore-perovskite phase is a nucleation-controlled process, and the activation energies for nucleation and growth of 53:47 type PZT are 441 kJ/mol and 112 kJ/mol, respectively.[37,38] The volume change accompanying the pyrochlore to perovskite formation is ≈13%.[39] Microstructure studies also demonstrate that the Zr-rich films not only have a larger grain size but also more pyrochlore phases, which is attributed to a higher nucleation barrier and high tendency of Zr to form the pyrochlore phase.[38]

3.4 Thick-Film Fabrication

3.4.1 Thick-Film Transfer Technology (Screen Printing)

In this method, to prepare the ink for screen printing, organic ingredients (including solvent, dispersing agent, and plasticizer) are first incorporated with the binder and then blended. The active pyroelectric powder is subsequently added and mixed. In order to screen print, a desired unmasked feature of the screen is placed over the substrate on which the film is to be printed. A dollop of ink is placed on the screen at a point behind the unmasked area, thereby stretching in an orthogonal direction across it. A squeegee is placed behind the ink dollop onto the screen while holding the squeegee at a 45° angle. Then, in a smooth motion having minimal downward force, the squeegee is gently drawn towards the body and across the top of the unmasked screen feature. The screen is then gently lifted off the substrate. Next, the sample is removed from the fixture and allowed to rest for 10 min. The sample is dried on a hot plate set at 100 °C for 15 min. The process is repeated to coat additional layers onto the substrate. After the screen printing is completed, the film is sintered at an appropriate temperature and for the proper time. A.K. Batra et al. describe the detailed description of the laboratory screen printing machine and the process for fabricating PZT films on various substrates in detail.[40]

Besides the above-cited techniques, ferroelectric films have also been fabricated with spray coating,[41] rapid quenching,[42] jet printing,[43] aerosol deposition,[44] and gas deposition[45] methods.

3.5 Fabrication of Polymer-Ceramic Composites

The 0-3 connectivity composites are easy to fabricate, which allows for commercial production of these composites in a cost-effective manner.[46] The composites that have shown some promising results and are prepared by simple composite fabrication routes are described in this section. As a result, most composites are fabricated as active pyroelectric- and polymer-based diphasic samples. A polymer component can be either polar or nonpolar. The second, more popular approach is using the sol-gel synthesis route. Though the glass-ceramics (g-cs) have also shown noticeable pyroelectric sensing elements, this section does not include specific description sections on such materials.

The 0-3 connectivity composite may be prepared by mixing the ceramic particles in a hot rolling mill with a softened thermoplastic polymer. High-pressure casting at the softening temperature of the polymer can then be used to produce thin films of composites. With a thermoset polymer such as epoxy, the mixing can be made at room temperature with the right proportion of the resin, hardener, and ceramic powder.[46,47]

In solvent casting, a polymer is first dissolved in a suitable solvent and then electroactive ceramic powder is added and mixed/dispersed. A mixture so obtained is kept in a suitable container for the solvent to evaporate. The film so obtained is hot pressed at the crystallization temperature of the polymer. The problems faced during the mixing operation are linked to a poor distribution of the ceramic inclusions, poor adhesion of component phases, or air bubbles in the composites. An agglomeration of ceramic particles is also present in the solution, which may be overcome by lowering the polymer viscosity via heating during the ultrasonic mixing process.

Use the spin-coating technique for the fabrication of 0-3 connectivity composites. The following is a typical example for the preparation of a polyvinylidene fluoride-trifluoroethylene (P(VDF-TrFE)):PZT composite. First of all, a suitable amount of polymer, P(VDF-TrFE), is dissolved in methyl-ethyl-ketone (MEK) to form a solution (PMix). A requisite amount of nano-ceramic (PZT) powder is then added and the mixture is ultrasonically agitated for several hours to break up the agglomerates and to disperse the ceramic powder uniformly in the copolymer solution. With this composite solution (nPMix), a thin film can be deposited on conducting electroded substrate using a spin-coating technique. The steps involved in fabricating films by spin coating are illustrated in figure 10. The film is then annealed for 2–3 hr in air at 130 °C for the present case, and the top electrode is deposited for testing.[48–50] The flowchart illustrating various steps involved in fabricating composite films is shown in figure 11.
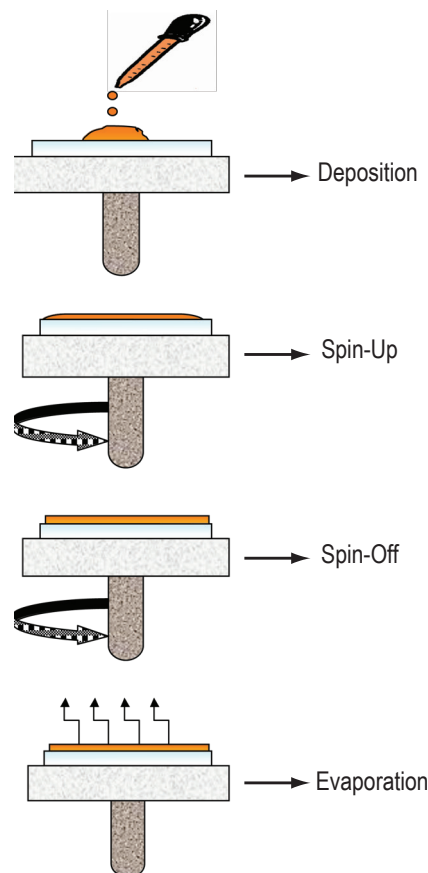
Figure 10. Spin-coating technique processing steps.

```
┌─────────────────────────────────┐
│   P(VDF-TrFE) + MEK = PMix      │
└─────────────────────────────────┘
                │
                ▼
┌─────────────────────────────────┐
│  Nanoparticles + PMix = nPMix   │
│     (Ultrasonic Dispersion)     │
│          (Stirring)             │
└─────────────────────────────────┘
                │
                ▼
┌─────────────────────────────────┐
│    nPMix Film Spin Coating      │
│              or                 │
│        Solution Casting         │
└─────────────────────────────────┘
                │
                ▼
┌─────────────────────────────────┐
│           Annealing             │
└─────────────────────────────────┘
                │
                ▼
┌─────────────────────────────────┐
│          Electroding            │
└─────────────────────────────────┘
                │
                ▼
┌─────────────────────────────────┐
│            Poling               │
└─────────────────────────────────┘
                │
                ▼
┌─────────────────────────────────┐
│            Testing              │
└─────────────────────────────────┘
```
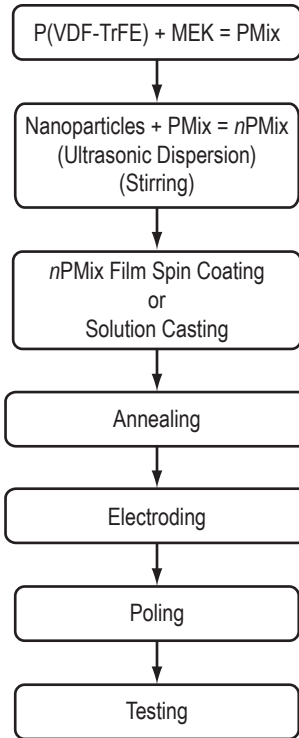
Figure 11. Flowchart for fabrication of polymer-ceramic composite films.

4. PROPERTIES AND PERFORMANCE PARAMETERS
OF IMPORTANT PYROELECTRICS

4.1 Triglycine Sulfate Crystals and Their Isomorphs

The TGS crystal family, with the chemical formula $(NH_2CH_2COOH)_3.H_2SO_4$, is one of the well-known ferroelectric materials useful for room temperature IR detector applications.[51] Pyroelectric detectors based on TGS are uniformly sensitive to radiations in the wavelength range from ultraviolet to far IR and do not require cooling as compared to quantum detectors, where low cooling is required. The crystal structure of TGS is monoclinic below T_c (49 °C). There are two chemical formulas in the elementary cell of the lattice and the crystal is monoclinic with space group $P2_1$ in the ferroelectric phase. Above the T_c, in the paraelectric phase, there are two mirror planes at $y = 0.25$ and 0.75 and space group $P2_{1/m}$. The ferroelectric effect is associated with the asymmetrical arrangement of the glycine group G I versus the mirror plane and the proton exchange between glycine groups G II and G III associated with the exchange role of zwitterions between two groups.[51] The b-cut/(010) crystals are used for detector fabrication, which is also a cleavage plane.

Single crystals of TGS are usually grown from an aqueous solution by the method of temperature lowering or solution evaporation.[52–57] TGS crystals weighing more than 100 g have also been grown from solution with ethyl alcohol additions.[58] By mixing alcohol in an aqueous solution of TGS, part of the water in the solution associates with alcohol; this concentrates the solution. Thus, the supersaturation can be controlled to a certain degree, making it easier to grow TGS crystals. A typical growth habit of a TGS crystal grown at AAMU is shown in figure 12.
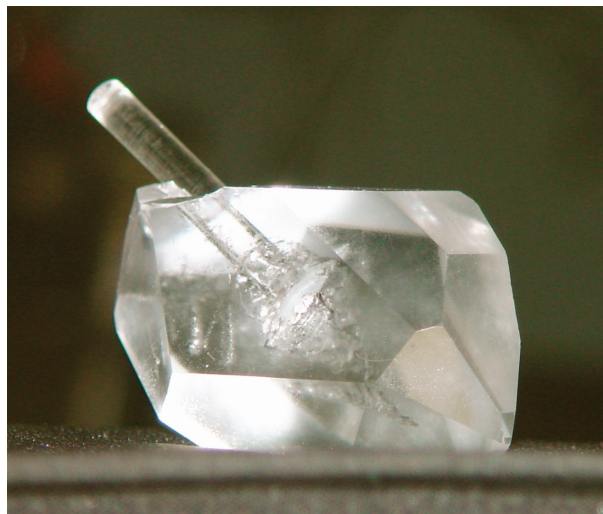

Figure 12. Photograph of a TGS crystal grown at AAMU.

The TGS family-based IR detectors provide the highest R_V, but handling difficulties associated with their water solubility, hygroscopic nature, and fragility have confined their use to these single-element detectors and vidicons, where sensitivity is of prime importance. Furthermore, these crystals depole and the temperature range of their operation is limited.

To improve upon the drawbacks cited above while maintaining the same basic structure, many modifications to TGS have been proposed and evaluated for PIR detection applications. These modifications include deuteration of TGS (DTGS); substitution of sulfuric acid with fluroberyllic acid to give triglycine fluroberyllate (TGFB) with and without deuteration to give (DTGFB); substitution of sulfuric acid with selenic acid to give triglycine selenate (TGSe); doping with cations such as Li, manganese (Mn), cadmium (Cd), zinc (Zn), and copper (Cu) to give Li-doped TGS (LiTGS), Mn-doped TGS (MnTGS), Cd-doped TGS (CdTGS), Zn-doped TGS (ZnTGS), and Cu-doped TGS (CuTGS); substitution of glycine by L-alanine (LATGS); and simultaneously doping with cations like nickel (Ni), chromium (Cr), and cesium (Cs) and L-alanine to give Ni L-alanine-doped TGS (NiLATGS), Cr L-alanine-doped TGS (CrLATGS), and Cs L-alanine-doped TGS (CsLATGS), respectively.[51]

L-alanine has the effect of introducing an internal electric field to produce poled TGS crystals and stabilizing the spontaneous polarization. This is because the alanine molecules possess an extra methyl group that prevents them from rotating within the lattice. The dipole it possesses is thus fixed with respect to the crystal structure and does not disappear at the T_c. LATGS crystals can be thermally cycled through the T_c. They will retain their spontaneous polarization, thereby avoiding the poling process. There is an increase in FOM depending upon the L-alanine content in the TGS lattice. However, the growth yield is not 100% and crystals usually crack during polishing. The uniformity of L-alanine doping in the TGS lattice is also difficult to attain.

Table 2 compares the performance FOMs of modified TGS crystals at their optimum/room temperature over pure TGS crystals.[1] It can be inferred that deuteration of TGS provides a marked improvement to the R_V and also increases the T_c to 60 °C, depending on the deuteration level. This is extremely desirable as it increases the temperature range of detector operation. Bye and Keve[59] studied the pyroelectric properties of x-ray irradiated/field-treated TGS detectors and compared these with LATGS detectors. The improvements in FOMs of x-ray/field-treated TGS detectors were comparable with L-alanine-doped TGS detectors. In this case, uniformity in properties and yield for large-area crystals was 100%. Thus, they proposed that a small-area, single-element detector should preferably be manufactured from LATGS; whereas, for thermal imaging applications requiring large areas of uniform properties, an irradiation/field-treated TGS would be required.

A marginal improvement in FOM has also been proposed by doping with cations. Loiacono and Dougherty[60] suggested that higher concentrations of Zn, Cd, and Cu should give promising results. There have been some encouraging results reported from crystals grown from solutions doped with L-alanine and cations such as Cs, Ni, and Cr. It can be seen that there was a marked increase in FOMs. Furthermore, Cs and alanine doping (CsLATGS) produced more uniformly doped crystals, as is evident from the shape of the hysteresis loop compared with LATGS. However, the growth yield was lower than with pure TGS crystals. In the recent past, doped TGS crystals with organic molecules have been reported with encouraging results such as L-lysine, urea, urea + L-alanine, thiourea, guanidine, and others.[61–66] A higher performance and increase in

Table 2. Material characteristics and FOMs of modified TGS crystals.[1]

Crystals	Temperature of Measurement (°C)	$F_i = p$ (nC/cm²K)	ε'	$F_V = p/\varepsilon'$ (nC/cm²K)	$F_D = p/\sqrt{\varepsilon''}$ (nC/cm²K)
TGS	Room temperature	16–45	20–100	0.5–1.14	0.4–121
DTGS	25	25–70	18–22.5	≈ 1.4	–
LATGS	25	22–70	26–35	≈0.88–2	31.8–92.5
Field x-ray-treated TGS	21	38	26	1.4	41.3
DLATGS	25	25	22	1.13	–
LiTGS	Room temperature	40	40	1	–
MnTGS	Room temperature	56	40	1.4	–
CdTGS	40	–	–	1.28	–
CuTGS	40	–	–	1.28	–
ZnTGS	40	–	–	1.41	–
CrLATGS	35	50	40	1.25	179.7
NiLATGS	35	82	51	1.8	213
CaLATGS	35	134	41	3.26	189.5
ATGSP	25	65	30–32	2	155.5
ATGSAs	25	70	32	2.1–2.3	–
ADTGSP	25	27.5	23	1.19	–
TGFB	60	70	50	1.4	–
ATGAs	25	70	32	2.18	–
TGPS	Optimum temperature	21–25	14–15	1.5	–
DTGPS	Optimum temperature	19–25	11–14	2	–
TGSe	21	420	420	1	40
Oblique cut TGS	35	–	–	≈ 1.7	–
Oblique cut ADTGSP	35	–	–	≈ 1.9	–

range of the operational temperature were offered by TGFB and DTGFB. However, the growth and processing of these crystals is dangerous due to the presence of toxic beryllium.

It has been reported[67–69] that large anisotropy is the principal dielectric, and that constant tensor coefficients can be used to obtain an improved material FOM for high R_V (F_V) from the TGS family crystals by taking oblique crystal cuts, in which the normal to the electroded faces of the detector are no longer parallel to the polar axis. This is because the effective p exhibits a cosine dependence on the angle of rotation, while the dielectric constant depends on a cosine-squared relationship. An improvement by a factor of 2 can be obtained in F_V by cutting the crystal at an optimum angle.

The TGS family-based IR detectors provide the highest R_V, but handling difficulties associated with their water solubility, hygroscopic nature, and fragility have confined their use to these single-element detectors and vidicons, where sensitivity is of prime importance. Various techniques have been explored by which thin films can be prepared as an alternative way to lapping and polishing thin slices and long crystal growth processes.

Whipps and Bye[70] have prepared thin polycrystalline films by using the sedimentation from a fluid suspension of freeze-dried crystallites of TGS onto glass slices, followed by compression to remove porosity. However, the pyroelectric performance from the films was lower than from single-crystal devices of similar dimensions.[71] Hadni et al.[72] developed a technique by which oriented thin films of TGS can be grown by nucleation of crystals in an array of submicroscopic holes etched in a substrate.

Recently, Hadni and Thomas[73] and Hadni[74] have shown that it is possible to grow an epitaxial layer of TGS on a gold (Au) electrode with a thickness smaller than 1 μm, and thus make a pyroelectric detector. The pyroelectric $D*$ was found to be better than bulk TGS detectors at 40 °C. They have also shown that the $D*$ of TGSe epitaxial detectors grown on bulk TGS crystals is six times better than the best detector made by Mullard, UK, under similar conditions.

It is evident from table 2 that one can select a particular crystal depending upon the required application. For high-current R applications, TGSe-based devices will be advantageous. For high-voltage and high-$D*$ applications at room temperature, various doped crystals such as LATGS, NiLATGS, CsLATGS, and alanine-doped triglycine sulfer-phosphate/arsenate ((ATGSP)/arsenic (As)) are more useful. For a high-temperature range of operation applications, DTGFB seems more promising. However, actual use of the above crystals in an IR detector or vidicon tube will determine if the predicted improvement in the signal-to-noise ratio is realized.

4.2 Perovskite Ferroelectrics

Perovskite is the name of the mineral called calcium (Ca) titanate (($CaTiO_3$) (CT)). The perovskite forms a very large family of oxygen octahedral ferroelectrics with the general formula of ABO_3, where A represents a cation with a larger ionic radius, B represents a cation with a smaller ionic radius, and O is oxygen. The structure can be described as a three-dimensional network of corner-sharing BO_6 octahedra within which there is a twelvefold coordinated site occupied by A cations. The A and B cations can be occupied with a wide range of ions to give a ferroelectric structure. Most of the ferroelectrics with perovskite-type structure are compounds of either the $A^{2+}B^{4+}O_3^{2-}$ or $A^{1+}B^{5+}O_3^{2-}$ type formulas.

Most of the useful ceramic, such as $BaTiO_3$, PT, $PbZr_{1-x}Ti_xO_3$ (PZT), PLZT, potassium niobate (KN), K Na niobate ($K_xNa_{1-x}NbO_3$, abbreviated as KNN), and K tantalate niobate ($KTa_xNb_{1-x}O_3$, abbreviated as KTN) have perovskite structures.[75] Two groups of perovskites that have been extensively studied for their pyroelectric properties are rhombohedral structures based on modified Pb zirconate (PZ) and tetragonal structures based on modified PT. A small-sized single crystal can be grown from a variety of fluxes in both cases.

Most of the studies have been conducted on ceramics. Ceramics offer a number of advantages over other candidate crystalline materials such as low cost to manufacture in large areas using standard mixed oxide processes (both mechanically and chemically robust), their ability to process into thin wafers, they possess high T_c (can be operated at high temperatures), and can be modified by introduction of selected dopants into a lattice to control important parameters such as p, dielectric constant and loss, T_c, electrical impedance and mechanical properties, etc.[76] A unit cell of a PZT ABO_3 structure is shown in figure 13.
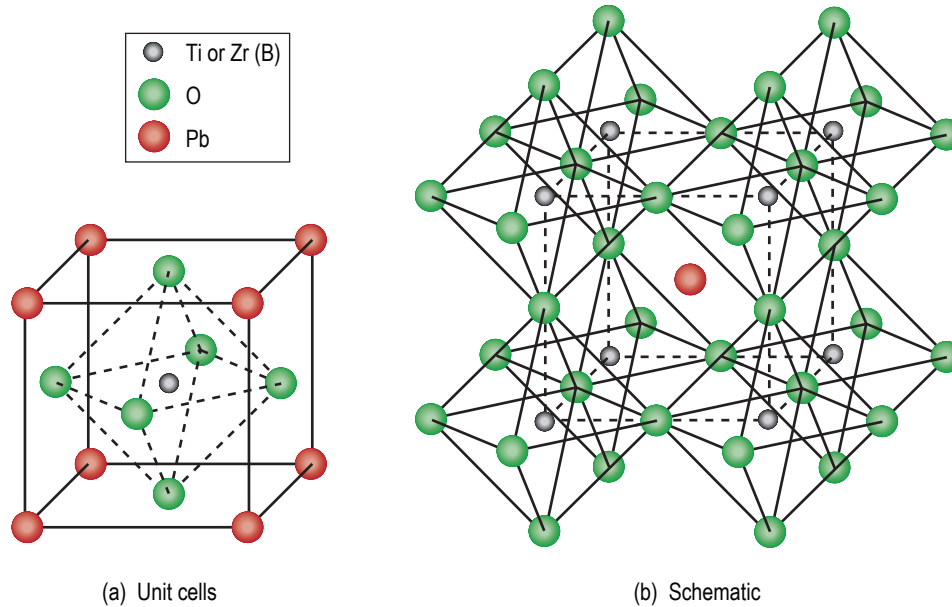
Figure 13. PZT ABO_3 structure: (a) Unit cells and (b) schematic.

4.2.1 Modified Lead Titanate

Lead titanate is a ferroelectric possessing tetragonal structure at room temperature with a high Curie point (490 °C).[77] It also possesses a high spontaneous polarization (up to 75 μC/cm^2). Although the growth of single crystals by flux and top-seeded solution growth is possible, the growth of crystals more than 1 cm in size is very difficult, again restricting the material's practical use to ceramic form. The high spontaneous lattice strain associated with the phase transition makes the fabrication of pure PT ceramics impractical, as they are mechanically unstable at room temperature. Again, a wide range of dopants (which include Mn, rare earths, Ca, and $Pb((Co_{1/2}W_{1/2})O_3)$) has been explored to stabilize the material's properties.

$Pb_{1.05-x}La_xTi_{1-x/4}O_3$ ($x = 0$–0.2) thin films were obtained by the screen printing method on Au bottom electrodes using Si (100) substrates at the annealing temperature of 600 °C. The maximum p of 1.07×10^{-8} C/cm^{2}K was obtained at $x = 0.1$ after poling.[78] The diffusion of (Pb,La) TiO_3 to the Au electrode and then to platinum (Pt) electrodes was on the same level, therefore Au electrodes can be prepared by screen printing for practical use of these films at a low cost.

Lanthanum-modified PT thin films with different La contents were fabricated on Pt/Ti/ SiO_2/Si substrate using the sol-gel method. The p were 1.3–2.5 nC/cm^{2}K and increased as the La content increased.[79]

Pyroelectric PT thin films deposited by sol-gel processing have been characterized for possible use in microsensor applications. Based on a comparison of relevant properties with other integrated circuit (IC)-compatible pyroelectric materials, PT possesses a very high p over a wide operating temperature range. The measured p at 297 K for PT films with thicknesses ranging from

0.2 to 0.6 μm is in the range of 75 to 96 nC/cm^{2}K. This work presents the first use of PT as a pyro-electric material integrated into a micromachined membrane structure.[80] This composite structure offers a key advantage of implementing a low thermal mass for high-sensitivity pyroelectric detection. The measured blackbody R_V for a pyroelectric element with an active area of 4×10^{-5} cm^2 at 297 K and a chopping frequency of 100 Hz is 2.2×10^4 V/W. The normalized D^* at 100 Hz is 1×10^9 cm Hz$^{1/2}$/W. The response time measured by the pulsed laser-beam method for a device area ranging from 2×10^{-6} to 7×10^{-4} cm^2 is in the range of 2 to 20 μs.

The deposition of single-phase perovskite PT thin films by planar multitarget sputtering on Si substrates covered with a thin Pt bottom electrode has been investigated.[81] The films exhibited nearly random crystallographic orientation. The films are self-polarized, which means they exhibited pyroelectric currents without poling treatment. After additional furnace annealing and poling, the p was 1.7×10^{-4} C/m^{2}K. The annealing also reduced the dielectric loss (tan δ) from 0.05 to 0.01.

Thin films in the Pb-CT (PCT) system have been successfully prepared by sol-gel processing on indium (In) tin (Sn) oxide- (ITO-) coated 6059 glass substrates.[82] The perovskite phase of PCT is formed at 650 °C with a polycrystalline tetragonal structure. The electrical properties of these films have been characterized and ferroelectric hysteresis loops have been observed. The pyrocoefficient and FOMs have been calculated and it is observed that PCT films show quite good pyroelectric properties. PCT (76/24) is expected to give high IR detector performance due to its high value of R_V and D^* along with smaller values of dielectric constant and loss tangent.

Chang and Lai used RF sputtering methods to deposit PT thin films with different Ca contents on a Pt/Ti/SiO$_2$/Si substrate.[83] Authors found that, at 50 °C, the p increased from 0.8×10^{-4} to 1.89×10^{-4} C/m^{2}K with Ca content.

For details on pyroelectric thin films for pyroelectric sensors, the reader can refer to an excellent review article by Muralt.[84]

4.2.2 Lead Zirconate Titanate

PZT-based ferroelectric oxide ceramics, for use in PIR detection, offer a number of advantages over single crystalline materials such as TGS, LT, PVDF, etc. PZT is a solid solution phase of the xPbZrO$_3$(1–x)PT ($0 < x < 100$) binary system.

Ferroelectric oxide ceramics for use in PIR detectors are relatively low cost to manufacture by using standard mixed-ceramic oxide processing steps and they are both mechanically and chemically robust. Their good mechanical strength allows large area wafers to be made, which can be easily machined into thin sections. They are not hygroscopic as are high pyroelectric performance TGS single crystals. Furthermore, TGS single crystals are fragile in nature, which causes technical difficulties in the processing. The environmental temperature is also a problem for using and storing these devices. Ferroelectric materials used in PIR detectors operate only below the T_c because they get depoled above T_c. Ferroelectric oxide ceramics also have a high T_c so that there is no danger of depoling during normal usage over a wide range of ambient temperatures (e.g., –50 to

100 ºC). The pyroelectric performance of PZT-type ceramics can be readily modified by inclusion of selected dopants (elements) into the lattice, thereby controlling important desired parameters.

The pyroelectric properties of a hot-pressed PLZT (8/40/60) were investigated in some detail to evaluate its potential as a prospective PIR detector material.[85] The results of measurements show that (8/40/60) has a relatively high dielectric constant, a high p, and favorable thermal and mechanical characteristics comparable with (8/65/35). The calculated FOMs based on the measured properties were compared with other PLZTs of (8/65/35), (12/40/60), and (14/40/60) compositions and the LT single crystal. The results indicate that PLZT (8/40/60) is a promising material for small-area, voltage-mode IR detectors. This material has permanent bias to its polarization, so that repoling is not necessary following a temperature excursion above the T_c.

Suaste-Gomez et al.[86] reported the pyroelectric properties of the $Pb_{0.88}Ln_{0.08}Ti_{0.98}Mn_{0.02}O_3$ (Ln=La, samarium (Sm), and europium (Eu)) ferroelectric system represented as Pb-La titanate manganate (PLTM), Pb-Sm titanate manganate (PSTM), and Pb-Eu titanate manganate (PETM), respectively, in table 3. The values obtained for p, even at T_c, are lower than values obtained in the author's samples.[88] Pyroelectric properties of the multicomponent ferroelectric ceramic materials, on the basis of solid solutions of $PT-PbZrO_3-PbNb_{2/3}Zn_{1/3}O_3-PbSb_{2/3}Mn_{1/3}O_3-PbW_{1/2}Mg_{1/2}O_3$ (system I) and $PT-PbZrO_3-PbNb_{2/3}Zn_{1/3}O_3-PbSb_{2/3}Mn_{1/3}O_3-PbNb_{2/3}Mn_{1/3}O_3$ (system II), prepared using the hot pressing technique, have been investigated at room temperature by Czekaj et al.[87] for both tetragonal and rhombohedral phase areas and morphotropic (M) phase boundary. The average value of the p obtained in the M region was 400 $\mu C/m^2K$ for system I and 500 $\mu C/m^2K$ for system II. The maximum value of dielectric ε obtained in the M region was 1,440 and 1,380, respectively. The value obtained for p of systems I and II makes them prospective candidates for practical applications as materials for pyroelectric detectors for high current R.

Table 3. Physical properties and FOMs of various pyroelectric PZT-type bulk materials.

Ceramic	$F_i=p$ ($\mu C/cm^2K$)	ε'	$F_V=p/\varepsilon'$ ($\mu C/cm^2K$)	$F_D = p/\sqrt{\varepsilon''}$ ($\mu C/cm^2K$)
Modified PZT	380	290	1.3	408.6
PLZT	450	700	0.64	170.4
PLZT	350	1,129	0.31	62.2
PLTM	13.2@T_c	13,236@T_c	0.0001@T_c	–
PSTM	6.14@T_c	6,141@T_c	0.0001@T_c	–
PETM	5.51@T_c	5,510@T_c	0.001@T_c	–
STPZT1	379.5	1,156.6	0.33	79.6
STPZT2	408.5	768.6	0.53	287.6
BM740	300	631.3	0.47	98

Guggilla et al.[88] extensively studied pyroelectric and dielectric properties of various ceramics such as STPZT-1 (PLZT), STPZT-2 (PLZT + MnO_2), and BM740 (modified PZT, obtained

from Sensor Technology Ltd., Canada) for their applications in IR sensors and compared them with other candidate materials including PZT-type ceramics studied by other researchers. The material FOMs at 50 ºC were calculated from measured parameters (dielectric constants and p) for their use in PIR detectors. From the viewpoint of pyrosensor applications, ceramics (namely STPZT-2 and BM740) are remarkably attractive due to their large p and low dielectric loss. It is worthy to mention that the materials investigated are also capable of high operating temperature (up to 100 °C) applications. The results are described in table 3.

Perovskite ceramics of modified PZT type have been extensively studied because of their excellent dielectric, electrooptical, piezoelectric, and pyroelectric properties. Oxygen ions with 200 keV energy and doses of 1×10^{16} ions/cm^2 were irradiated onto a commercially available modified PZT sample having good pyroelectric properties for use in IR detectors. The sample's response was studied in terms of dielectric and pyroelectric properties before and after irradiation. A decrease in dielectric constants (ε', ε'') and the p is observed.[89]

Very thin films of PZT (40/60) (0.26 μm or less) have been prepared on Pt-coated oxidized Si substrates (Pt/Ti/SiO$_2$/Si) by a sol-gel process.[90] These films were of high density with fine grains of about 0.2 μm and annealed in the range of 600 to 700 °C in an oxygen atmosphere. X-ray diffraction patterns taken on this film showed a single-phase, perovskite-type structure. Authors investigated the influence of poling treatment on the dielectric and pyroelectric properties, dielectric constants, and pyroelectric properties. Dielectric constants and p at room temperature were determined as 1,300 and 840 nC/cm^{2}K and 68 for the poled and 10.3 nC/cm^{2}K for the unpoled PZT films. The remanent polarization was 37.8 μC/cm^2 and a coercive field was 146 kV/cm at a switching voltage of 16 V peak to peak and a frequency of 200 kHz. The remanent polarization and coercive field were found to vary slowly with temperature. The material was also difficult to depole. Authors have suggested that these films will be suitable for IR detector applications.

PLZT films around 3 μm thick with compositions of ((Pb$_{0.925}$La$_{0.075}$)(Zr$_y$/Ti$_{1-y}$)$_{0.981}$ + 0.5 mass % MnO$_2$), where $y = 0$–0.1, that have an appropriately small relative dielectric constant (≈ 200) were deposited on Pt(l00)/MgO(l00) by RF magnetron sputtering.[91] The pyroelectric properties of PLZT films as element materials for PIR sensors were investigated in detail.[91] Assuming that the C_V of the present films is 3.2 J/cm^{3}K, the PLZT films exhibited the highest FOM of 1.4×10^{-10} Ccm/J and FOM of D^* (F_{D*}) of 1.6×10^{-8} Ccm/J, which were around 1.8 and 1.5 times larger than those of Pb-La titanate (PLT) films, respectively. Consequently, the FOMs for the PIR sensors could be improved by adding a small amount of Zr to PLT.

PLZT 12/40/60 thick films prepared by screen printing techniques have been characterized electrically.[92] It was found that the sintering time and the poling manner influenced the dielectric and pyroelectric properties. The best results were obtained at sintering parameters of 1,100 °C for 5 hr. Room-temperature poling results in slightly reduced values of the p but allows higher poling fields, up to 5×10^6 V/m. The room-temperature relative ε is about 200 and the dielectric loss is less than 0.014. The room-temperature p is about 1.5×10^{-4} C/m^{2}K. These properties (except the p) are better then those measured on bulk ceramics and are comparable with commonly used single-crystal pyroelectrics. The thick-film technology introduced and discussed by authors can offer significant advantages in pyroelectric sensor production. The possibility of varying the process

parameters allows some flexibility in choosing the characteristics of the resulting pyroelectric layers.

The pyroelectric and dielectric properties of $Pb(Zr_{0.3},Ti_{0.7})O_3$ (PZT) thin films are systematically investigated as functions of film thickness ranging from 0.3 to 1 μm.[93] For better D^* of the film, high p, low-dielectric coefficient, and loss tangent are needed. It can be achieved by highly textured (111) preferred orientation and dense microstructure. To minimize the unwanted preferred orientation with increasing film thickness, a step-by-step annealing process and highly textured (111) Pt bottom electrodes are applied. With increasing film thickness, the squareness of polarization hysteresis loops and remanent polarization values are maximized. Although there is a slight variation of preferred orientation with film thickness, dielectric properties are markedly changed due to microstructural variation. Because of the large improvement of loss tangent, the FOM is improved with minithickness. It is maximized at a thickness of 1 μm. The maximum p measured by the Byer-Roundy method is 38 nC/cm^{2}K.

Epitaxially grown and polycrystalline PT, PLT, and PZT thin films with thicknesses from 1 to 2 μm have been prepared on $Pt/Ti/SiO_2/Si$ substrates by means of a sol-gel spin-coating technique.[94,95] The ferroelectric thin films have good crystallization behavior and excellent dielectric and pyroelectric properties. The p of PT, PLT, and PZT thin films are 2.9×10^{-8} C/cm^{2}K, $(3.37–5.25) \times 10^{-8}$ C/cm^{2}K, and 6.1×10^{-8} C/cm^{2}K, respectively. The FOMs for R_V of PT, PLT, and PZT thin films are 0.6×10^{-10} Ccm/J, $(0.59–0.78) \times 10^{-10}$ Ccm/J, and 0.63×10^{-10} Ccm/J, respectively. The current responsivities of these films are 9×10^{-9} Ccm/J, $(10.5–16) \times 10^{-9}$ Ccm/J, and 19.1×10^{-9} Ccm/J. The D^*s are 0.74×10^{-8} Ccm/J, $(0.79–1.13) \times 10^{-8}$ Ccm/J, and 0.83×10^{-8} Ccm/J, respectively.

The effects of Mn doping on the ferroelectric and pyroelectric properties of $Pb(Zr_{0.3},Ti_{0.7})O_3$ (PZT) thin films on $Pt/Ti/SiO_2/Si$ substrates have been investigated.[96] The Mn-doped (1 mol. %) PZT (PMZT) showed almost no hysteretic fatigue up to 10^{10} switching bipolar pulse cycles, coupled with excellent retention properties. A low-ε interfacial layer that generally formed between the Pt electrode and PZT films does not occur in PMZT. It was proposed that Mn dopants are able to reduce oxygen vacancy mobility in PZT films and Mn^{2+} ions consume the oxygen vacancies generated during repeated switching, forming Mn^{4+} ions. These mechanisms are probably responsible for their low-observed fatigue characteristics. manganese doping brings additional benefits to the electrical properties of PZT films. The relevant p of a 700-μm-thick film are 3.52×10^{-4} C/m^{2}K and FOMs for D^* (F_D) = 3.85×10^{-5} Pa$^{-0.5}$ at 33 Hz for Mn-doped PZT, compared with $p = 2.11 \times 10^{-4}$ C/m^{2}K and $F_D = 1.07 \times 10^{-5}$ Pa$^{-0.5}$ for the undoped PZT films. This means that the Mn-doped PZT thin films are excellent candidates as device materials for both memory and pyroelectric applications.

Highly c-axis oriented PLZT films with compositions of $(Pb_{0.925}La_{0.075})(Zr_yTi_{1-y})_{0.981}O_3$, where $y = 0.2$–0.4, were deposited on Pt(100)/MgO(100) by RF magnetron sputtering, applying an intermittent deposition comprised of the repetition of deposition and nondeposition.[97] It was confirmed that the highest FOMs for the PIR sensors were obtained by using powders with excess PbO of 20 mol. % added to PLZT as sputtering targets in the preliminary experiment. The PLZT film where $y = 0.2$ exhibited the highest FOM for R_V of approximately 5.3×10^{-13} Cm/J among the three samples studied, which was around 1.8 times larger than that of PLZT ceramic where $y = 0.2$.

Thin films of $PbZr_{0.525}Ti_{0.475}O_3$ (PZT) and 1% Ta-oxide-doped PZT titanate $(Pb_{0.9950}(Zr_{0.525}Ti_{0.465}Ta_{0.010})O_3$ (PTZT)) deposited on Pt(200)/SiO$_2$/Si(100) using the dc unbalanced magnetron sputtering (dc-UBMS) method have been investigated.[98] The films were grown at deposition temperatures in the range of 300 to 750 °C for 3 hr, followed by annealing at 700 °C for 1 hr for each deposited film. The films show tetragonal structure with preferred orientation to the (100) and (200) crystal planes. The calculated lattice constants are $a=b=4.056$ Å and $c=4.105$ Å for PZT thin film, and $a=b=4.056$ Å and $c=4.068$ Å for PTZT thin film. The conductivity of PZT films is between 2.24×10^{-13} $(\Omega m)^{-1}$ and 5×10^{-12} $(\Omega m)^{-1}$, whereas the conductivity of PTZT films is between 1.02×10^{-9} $(\Omega m)^{-1}$ and 1.9×10^{-8} $(\Omega m)^{-1}$ for films deposited at the temperature ranges mentioned above. The R_V measured at a chopper frequency of 2,000 Hz and at a wavelength of 947 nm is 62.1–80 µV/W and 61–76.4 µV/W for PZT and PTZT thin films, respectively. Meanwhile, the p is in the range of 9.54 to 12.3×10^{-4} C/m^{2}K for PZT thin films and 9.35 to 11.7×10^{-4} C/m^{2}K for PTZT thin films. These results showed that PZT and PTZT thin films are suitable for use as a PIR sensor.

Epitaxially grown and polycrystalline PT, PLT, and PZT thin films with thickness from 1 to 2 µm have been prepared on Pt/Ti/SiO$_2$/Si substrates by means of the modified sol-gel spin-coating technique.[99] The ferroelectric thin films have good crystallization behavior and excellent dielectric and pyroelectric properties. The p of PT and PLT thin films are 2.9×10^{-8} C/cm^{2}K and $(3.37–5.25)\times10^{-8}$ C/cm^{2}K, respectively. The FOMs for R_V of PT and PLT thin films (F_D) are 0.6×10^{-10} Ccm/J and $(0.79–1.13)\times10^{-8}$ Ccm/J, respectively. The FOMs for current R of these films are 9×10^{-9} Ccm/J and $(10.5–16)\times10^{-9}$ Ccm/J, and the FOMs for D^* of these films are 0.74×10^{-8} Ccm/J and $(0.79–1.13)\times10^{-8}$ Ccm/J, respectively.

Various PLZT films have been prepared on platinized Si wafers. The dielectric constant and dissipation factors decreased and increased respectively with a higher firing temperature due to PbO loss. The pyroelectric activity in the PLZT films was compositional dependent. PZT 53/47 exhibited the highest p at 7.7×10^{-8} C/cm^{2}K (at a heating rate of 1 K/min). The PT film exhibited a low p ($<2\times10^{-9}$ C/cm^{2}K) due to its (100) preferred orientation. It was observed that the p decreased as the rate increased. At high heating rates, the films are unable to conduct heat uniformly, causing a decrease in the calculated p.[100]

PZT films with various Nb doping levels were deposited on Pt(111)/TiO$_2$/SiO$_2$/Si(100) substrate via the CVD technique followed by rapid thermal annealing (RTA).[101] The introduction of the first seeding layer significantly improved the crystallization quality after RTA. The dielectric constant of PMZT films increased with the increase of Nb doping concentration. PZT films with 1% Nb doping exhibit higher remnant polarization (49.33 µC/cm^2), p (4.6×10^{-4} C/m^{2}K), and FOM (1.89×10^{-5} Jm^3/K), which indicates that $Pb(Zr_{0.2}Ti_{0.8})_{0.99}Nb_{0.01}O_3$ would be a good candidate for PIR sensor applications.

$Pb(Zr_{0.52}Ti_{0.48})O_3$, (PZT) thin films fabricated by the magnetron sputtering technique on Pt/Ti/SiO$_2$/Si substrate at room temperature were annealed by means of a carbon dioxide (CO$_2$) laser with resulting temperatures below 500 °C.[102] It was found that the annealed film with laser energy density of 490 W/cm^2 for 25 s has a typical perovskite phase, uniform crystalline particles with size of about 90 nm, and a high p with 1.15×10^{-8} C/cm^{2}K. Thus, laser-annealed PZT thin films are very promising for uncooled detectors and other pyroelectric applications.

36

Dorey and Whatmore investigated uranium- (U-) doped Pb magnesium (Mg) niobate-Pb zirconate titanate (PMN-PZT) (PMNZTU) composite thick film fabricated on Si substrate using a new composite sol-gel technique processed at 700 °C.[103] The maximum FOMs ($F_V = 3.45 \times 10^{-2}$ C/m^{2}K and $F_D = 1.01 \times 10^{-5}$ Pa$^{-1/2}$) calculated were comparable with screen-printed thick films. Authors concluded that the ability of this technique to directly integrate thick film onto Si substrate at temperatures as low as 710 °C, while maintaining competitive FOMs, is of considerable interest for future device applications. Table 4 illustrates the properties of various PZT films grown by different methods.

Table 4. Material characteristics and FOMs of perovskite films.[90–95]

Material	Substrate	$F_i = p$ (nC/cm^{2}K)	ε'	$F_V = p/\varepsilon'$ (nC/cm^{2}K)	$F_D = p/\sqrt{\varepsilon''}$ (nC/cm^{2}K)
PbTiO$_3$ (screen printing)	–	60	200	0.3	–
PbTiO$_3$ (sol-gel)	–	25	190	0.13	23.4
La-modified PbTiO$_3$ (screen printing)	Au-coated SiO$_2$//Si(100)	10.7	–	–	–
La-modified PbTiO$_3$ (sol-gel)	Pt/Ti/SiO$_2$/Si	1.3–2.5	–	–	–
PbTiO$_3$ film (sol-gel)	Polycrystalline Si	85–115	150–400	0.56–0.28	56.6
PbTiO$_3$ film (multitarget sputtering)	Pt-coated Si	17	180	0.09	12.6
Ca-modified PbTiO$_3$ (sol-gel)	ITO-coated glass	46	99	0.46	12.8
PbTiO$_3$ film (sputter)	(001)Pt/MgO	25	97	0.25	32.8
PLZT (ceramic) (8/40/60)	–	120	4,285	0.02	10
PLZT (ceramic)	–	45	700	0.06	17
PZT (40/60) (sol-gel)	Pt-coated oxidized Si	85	1,004	0.08	10.1
Mn-PZT (sol-gel)	Pt/Ti/SiO$_2$/Si	35.3	255	0.13	28.6
PLZT (12/40/60) (screen print)	Pt/alumina	15	190	0.07	9.2
PLZT (12/40/60) (ceramic)	–	35	1,129	0.03	6.2
PLZT (RF-magnetron sputter)	Pt/MgO(110)	81	205	0.39	51.9
PZT (30/70) (spin coat)	Pt/Ti/SiO$_2$/Si	24	600	0.04	10.9
PZT (sol-gel)	(111) Pt/Ti/SiO$_2$/Si	61	300	0.2	28.7

4.2.3 Lithium Tantalate and Lithium Niobate

Lithium tantalate and LN have similar structures. They are one of a large number of ABO$_3$. The neighboring oxygen octahedrals are connected to each other through an oxygen ion that serves a common "tie-end." The symmetry of both crystals belongs to the point group 3m in the trigonal ferroelectric phase at room temperature. The symmetry to the point group 3m changes in the paraelectric phase above T_c. At room temperature, the lattice parameters of the trigonal unit cell are $a = 5.4944$ Å, $\alpha = 55° 52'$ in LN, and $a = 5.4740$ Å, $\alpha = 56° 10'$ in LT. Sometimes, it is more convenient to choose a hexagonal cell for description, with Li and Ta ions occupying two-thirds of the octahedral interstices between the layers. Lithium tantalate also possesses a high melting point (1,650 °C) and is insoluble in water.[104] These factors make the material one of the most stable pyroelectrics with a very wide temperature range of operation.

This material is generally used in single-crystal form, crystals being grown by the CZ method and wafers of more than 50-mm diameter are commercially available. It possesses a moderate pyroelectric effect and dielectric constant that combine to give a response figure about one quarter of TGS. However, very low values of dielectric loss (about 10^{-4}) have been reported for this material, which give it a potential F_D that is about four times greater than that of DTGS, although the loss of commercially available material is rather higher. However, with the lowest loss materials, high $D*$ figures can be achieved with low-noise amplifiers. By using ion beam milling to fabricate very thin (about 2–5 μm) elements in structures and packages in which thermal conductance had been minimized, Stokowski et al. demonstrated $D*$ figures as high as 2×10^9 cm Hz$^{1/2}$/W at 10 Hz.[105]

Roundy[106] has also used LT for one-dimensional detector arrays interfaced to a charge-coupled device (CCD) multiplexing chip. A disadvantage that LT possesses for this application is the high thermal diffusivity, which reduces the array's minimum resolvable temperature difference at high spatial frequencies. The robustness, good performance, and wide availability of this material, including its ability to withstand high-energy IR radiation with a fast response time of 0.5 ns make it a popular choice for commercial detectors. Norkus gives a short review on PIR detectors based on LT.[107] Lithium tantalate thin films ($\approx$0.5 μm) have been successfully deposited on Pt(111)/ SiO$_2$/Si(100) substrates by means of the sol-gel spin-coating technology. FOMs for IR detectors were studied for the LT thin films. High F_V of 2.1×10^{-10} Ccm/J and F_D of 2.4×10^{-8} Ccm/J exist because of the relative low ε' of 35 and high p of 4×10^{-8} C/cm^{2}K of the films. The PIR detector fabricated by the LT thin-film exhibits an R_V of 4,584 V/W at 20 Hz and a high specific $D*$ of 4.23×10^7 cm Hz$^{1/2}$/W at 100 Hz.[108]

Lithium tantalate in single-crystal form is widely applied in pyroelectric point detectors due to its high p of about 230 μC/m^{2}K and a low relative ε of 47. This results in an excellent F_V of 4.9, combined with low dielectric losses of 0.1%. Deposition as thin films from solution precursors would be desirable for integration with readout electronics and simplified processing. In order to optimally use the spontaneous polarization of LT along the c-axis of its hexagonal unit cell, the thin films need to be grown with a (001) orientation of platinized Si. Investigation of different parameters like pyrolysis temperature, heating rate, final heat-treatment temperature, and cooling rate revealed that the heating rate determines the development of the desired (001) orientation. Slow heating with 1 °C/s results in (001)-oriented LT thin films, while faster ramps lead to random or (110) textured films. After precursor deposition by spin coating and pyrolysis at 350 °C of all layers, a gel-like solid amorphous film remains. This layer crystallizes during RTA. Preferred heterogeneous nucleation at the LT/Pt interface can be expected for slow heating, resulting in a (001)-oriented layer due to local epitaxy with the (111) textured Pt. For fast heating rates of 63 °C/s, bulk or surface nucleation may dominate, leading to random or (110) textured films. Electrical measurements after poling the films in an external electric field of 50 kV/cm at 200 °C showed a p of 171 μC/m^{2}K and a dielectric constant of 40, resulting in an FOM of 4.2, comparable to the single-crystal values of 4.9.[109]

An LT thin film has been deposited by RF magnetron sputtering with an Li-enriched target composed of Li$_2$O$_2$/Ta$_2$O$_5$ (55:45 wt. %) on membranes of SiN$_x$ with the aim of improving the performance of thermal microsensors. The best p of LT films (400 nm) obtained was equal to 40 μC/m^{2}K for a growth temperature of 620 °C and a pressure of 0.67 Pa.[110]

Radio frequency sputtering has been used to deposit thin films of LT on ruthenium (Ru) oxide (RuO_2)- or SiO_2-coated Si substrates. Two electrical contact configurations have been used. The first configuration is a thin capacitor with an RuO_2 buried electrode and an Au, Ni, or RuO_2 upper electrode. The second configuration has recourse to RuO_2 interdigitated electrodes fabricated by a photolithographic process. Ferroelectric hysteresis measured with a Sawyer-Tower circuit shows a spontaneous polarization in the range of 20 $\mu C/cm^2$ and an electric coercive field of 3 kV/cm. The dynamic pyroelectric response has been measured as a function of frequency at various temperatures. The pyroelectric current and voltage responses, from 100 Hz to 1 kHz at room temperature, are 12 $\mu A/W$ and 18 V/W, respectively. The authors have investigated the effects of the poling process and significant improvements of the pyroelectric response have been obtained.[111]

Lithium niobate crystals display larger "secondary pyroelectricity," which is caused by a change in the polarization owing to thermal expansion. The p_s of 2.3×10^{-9} C/cm^2K, which is found to be 25% of the first p (8.3×10^{-9} C/cm^2K), has been found.[112] Due to this property, it has found limited commercial application. Recently, Gebre et al. have extensively investigated the general p of pure and doped LN crystals as shown in table 5 and found that iron- (Fe-) doped LN crystals are attractive for use in detectors.[113] A photograph of pure and doped LN crystals grown at AAMU is shown in figure 14.

Table 5. Material characteristics and FOMs of modified LN crystals.[113]

Crystals	$F_i = p$ (nC/cm^{2}K)	ε'	$F_V = p/\varepsilon'$ (nC/cm^{2}K)	$F_D = p/\sqrt{\varepsilon''}$ (nC/cm^{2}K)
LN single crystal (at T=500 °C)	7.2	31.4	0.23	21.1
LN:Fe single crystal (at T=500 °C)	33.8	50.1	0.68	65
LN:Fe/Mn single crystal (at T=500 °C)	9	47.3	0.16	20.9
LN:Eu single crystal (at T=500 °C)	15.3	39.3	0.39	39.2
LN single crystal (at T=250 °C)	4	30	0.13	–

Notes:
• LN—Lithium niobate.
• LN:Fe— LN doped with Fe.
• LN:Fe/Mn—LN doubly-doped with Fe and Mn.
• LN:Eu—LN doped with Eu.

4.2.4 Barium Strontium Titanate Material System

Barium Sr titanate (BST), a perovskite ferroelectric material, has applications in electronic, microwave, and pyroelectric devices. When the Ba:Sr ratio equals 0.7:0.3, the tetragonal to cubic phase is near room temperature. BST ceramic and single crystals have the highest p ever obtained from pyroelectric materials (23 $\mu C/cm^2K$). However, BST ceramic- and single-crystal forms are difficult, expensive, and time consuming to fabricate.[114]

Figure 14. Pure and doped LN crystals grown at AAMU.

Many efforts have been made to integrate thin films of BST Si processing and to grow them thin with higher p. Some of them are described with their important findings in the following paragraphs.

The BST ($Ba_{0.64}Sr_{0.36}TiO_3$) thin films have been prepared by the sol-gel method on a Pt-coated Si substrate. The resulting thin films show very good dielectric and pyroelectric properties. The dielectric constant and dissipation factor for the $Ba_{0.64}Sr_{0.36}TiO_3$ thin film at a frequency of 200 Hz are 592 and 0.028, respectively. The peak p at 30 °C is 1,080 $\mu C/m^2K$. The p at room temperature (25 °C) is 1,860 $\mu C/m^2K$, and the FOM ($p/t\varepsilon''$: t-thickness in μm) of this film is 37.4 $\mu C/m^3K$. The high p and the greater FOMs of $Ba_{0.64}Sr_{0.36}TiO_3$ thin films make them possible to be used for thermal IR detection and imaging.[115] Lee et al. obtained BST films with a considerably high p of 240 nC/cm^2K.[116]

BST ($Ba_{1-x}Sr_xTiO_3$) ferroelectric thin films have been prepared by MOD on $Pt/Ti/SiO_2/Si$ substrates and on a micromachined wafer with an aim to fabricate a dielectric bolometer-type IR sensor.[117] The x-ray diffraction (XRD) pattern and $D–V$ hysteresis curve of the film have been measured in order to investigate the effects of the final annealing temperature and annealing time on the property of the film. The results show that the films annealed at 700 or 800 °C all have good perovskite structure, while the film annealed at 800 °C has better ferroelectric loops. Films annealed at 800 °C with different annealing times from 5 to 60 min show a similar perovskite structure, among which films annealed at 30- and 60-min conditions have the better ferroelectric loops. The temperature coefficient of dielectric constant (TCD) of the MOD made BST thin film on

micromachined substrate is about 1%/K. The uniformity of the BST film on a micromachined Si wafer has also been confirmed to be good enough for operation of a sensor array. Chopperless operation has been attained and IR response evaluation of the fabricated sensor has also been carried out with an R_V of 0.4 kV/W and D^* of 1×10^8 cm Hz$^{1/2}$/W.

Sengupta et al. investigated the films of $Ba_{0.64}Sr_{0.36}TiO_3$, $Ba_{0.94}Sr_{0.36}Ti_{0.06}Zr_{0.18}O_3$, and $Ba_{0.64}Sr_{0.36}TiO_3$/0.50 wt. % MgO compositions by ceramic tape casting and pulsed laser deposition methods, and these compositions were selected as reference materials as they are well represented in the literature.[118] The data obtained from their patented $Ba_{0.64}Sr_{0.36}TiO_3$/0.50 wt. % MgO composition shows a reduction in the dielectric constant and lower dielectric loss, thus contributing to a higher pyroelectric FOM. Their results are presented in detail in tables 6 and 7.

Table 6. Physical properties and FOMs of BST samples.[118]

Tape-Cast Material	$F_i = p$ (μC/cm^{2}K)	ε'	$F_V = p/\varepsilon'$ (μC/cm^{2}K)	$F_D = p/\sqrt{\varepsilon''}$ (μC/cm^{2}K)
$Ba_{0.64}Sr_{0.36}TiO_3$	759	4,478	0.09	103.5
$Ba_{0.94}Sr_{0.06}Zr_{0.18}Ti_{0.82}O_3$	96.5	1,818	0.05	25.39
$Ba_{0.94}Sr_{0.06}TiO_3$/0.25 wt. % MgO	593	2,370	0.25	197.6
$Ba_{0.94}Sr_{0.06}TiO_3$/0.25 wt. % MgO	550	1,370	0.4	183.3

Table 7. Physical properties and FOMs of BST thin-film samples.[118]

Thin Film	$F_i = p$ (μC/cm^{2}K)	ε'	$F_V = p/\varepsilon'$ (μC/cm^{2}K)	$F_D = p/\sqrt{\varepsilon''}$ (μC/cm^{2}K)
$Ba_{0.64}Sr_{0.36}TiO_3$	1,940	594	3.2	520.1
$Ba_{0.94}Sr_{0.06}Zr_{0.18}Ti_{0.82}O_3$	1,260	1,119	1.2	100.8
$Ba_{0.94}Sr_{0.06}TiO_3$/0.25 wt. % MgO	187	505	0.37	93.5
$Ba_{0.94}Sr_{0.06}TiO_3$/0.25 wt. % MgO	129	297	0.43	62.3

Tetragonal $Ba_{0.8}Sr_{0.2}TiO_3$ thin films with large columnar grains 100–200 nm in diameter have been prepared on Pt/Ti/SiO$_2$/Si substrates using a 0.05 M solution precursor by sol-gel processing. The ferroelectric phase transition in the prepared $Ba_{0.8}Sr_{0.2}TiO_3$ thin films is broadened and suppressed to 40 °C with a maximum dielectric constant of ε_r (100 kHz) = 680. The observed low dissipation factor (tan δ = 2.6%) and high $p = 4.586 \times 10^{-4}$ C/m^{2}K at 33 °C render the prepared $Ba_{0.8}Sr_{0.2}TiO_3$ thin films promising for uncooled IR detector and thermal imaging applications.[119]

$(Ba_{0.6}Sr_{0.3}Ca_{0.1})TiO_3$ powders were prepared by the sol-gel method using a solution of Ba, Sr, and Ca acetate and Ti isopropoxide, and the specimens doped with MnCO$_3$ (0.1 mol. %) and Y_2O_3 (0.5 mol. %) were fabricated by the cold isostatic press method. The urethane pot and

zirconia ball were used in the mixing and grinding process, and the green pellets were sintered at 1,450 °C for 2 hr in the alumina crucible. The specimen exhibited a dense and void-free grain structure with a grain size of about 3 μm. The dielectric constant and the dielectric loss at T_c were 16,600 and 1.2%, respectively. The specimen under a 4-kV/cm dc bias field showed the maximum p of 550×10^{-9} C/cm^{2}K at T_c. The F_{D*} of the specimen, applied with a dc 8-kV/cm bias field, was the highest value of 17.6×10^{-9} Ccm/J at T_c.[120]

Silicon dioxide-doped Ba Sr titanate (SiO$_2$-doped Ba$_{0.85}$Sr$_{0.15}$TiO$_3$) (SBST) g-c films with perovskite structure have been prepared on Pt/Ti/SiO$_2$/Si substrates by the sol-gel technique. Differential thermal analysis (DTA), XRD, and atomic force microscopy (AFM) are employed to analyze the synthesizing process and microstructure of SBST g-c films. The ferroelectricity and crystallization behavior of SBST films are discussed. It is found that the staring synthesize temperature of SBST15 film is larger than that of a pure BST film for about 60 °C. The grain sizes decrease and the ferroelectricity of SBST g-c films is degenerated, but their loss tangent and leakage current density decrease with increasing SiO$_2$ content. The TCD and the p of the films are measured. The results show that the TCD and the p of SBST5 film at 20–25 °C are 4.6%/°C and 8.1×10^{-8} C/cm^{2}K, respectively, which is about two-thirds of the value of the pure BST films. BST g-c film with 5 mol. % SiO$_2$ dopant is hopeful to be the advanced candidate material for uncooled IR focal plane arrays (UFPAs) applied at near room temperature.[121]

Liu et al. prepared the BST (Ba$_{1-x}$Sr$_x$)TiO$_3$ thin films with $x = 0$, 0.05, 0.1, and 0.15 (BST, BST5, BST10, and BST15, respectively) on Pt/Ti/SiO$_2$/Si substrate by the improved sol-gel method. The resulting thin films show very good dielectric and pyroelectric properties. At 25 °C and 10 kHz, the dielectric constants of BST, BST5, BST10, and BST15 thin films were 320, 375, 400, and 425, respectively. Their loss tangents were found to be 0.035, 0.041, 0.024, and 0.01, respectively. The maximum p for BST10 film was found to be 12×10^{-8} C/cm^{2}K at 35 °C.[122]

4.2.5 Strontium Barium Niobate

SrBa niobate (SBN) solid-solution series (Sr$_{1-x}$Ba$_x$Nb$_2$O$_6$, where $0.2 < x < 0.8$) has the tetragonal tungsten-bronze-type structure and belongs to the point group 4-mm symmetry. It possesses excellent pyroelectric and electrooptic properties. Due to good mechanical and undeliquescent properties, SBN is an ideal pyroelectric material. By changing the ratio Sr:Ba, the T_c of SBN can be changed in the range of 60 to 250 °C. The tetragonal-type ferroelectric SBN possesses a spontaneous polarization of 32 μC/cm^3 (Sr:Ba = 75:25) and a polar axis along the c-axis of the tetragonal lattice. The p of crystals of different composition of Sr:Ba are listed in table 8.[123] Detectors that were fabricated have high stability in air without a protective window, as in the case of TGS. Furthermore, a thin plate of SBN has a high absorption capacity in the IR region above 10 μm without blackening. The advantage is that it has no apparent piezoelectric response below a frequency of 50 MHz. It is widely used for fast detectors. The main shortcoming of SBN is that its dielectric constant is not low enough for application at high frequencies. Its high-frequency F_V is an order of magnitude less than TGS. So, SBN thin-film detectors are mainly used for small-area, low-frequency applications. Amorin et al. investigated the effect of the La cation as a dopant in the polarization of the La-doped SBN (LSBN) (Sr$_{0.3-3y/2}$La$_y$Ba$_{0.7}$Nb$_2$O$_6$) system where $y = 0.01$, 0.03, and 0.05.[124] It was found that the p and the spontaneous polarization of these materials

Table 8. Physical properties and FOMs of SBN crystals.[123]

Crystal $Sr_{1-x}Ba_xNb_2O_6$	$F_i = p$ ($\mu C/cm^2K$)	ε'
$x = 0.27$	0.28	8,200
$x = 0.33$	0.11	1,800
$x = 0.4$	0.085	610
$x = 0.52$	0.065	380
$x = 0.75$	0.03	180

increase with the La cation doping up to a maximum value of the 3% concentration. For the 5% doping of La, the pyroelectric properties diminish. The results are illustrated in table 9.

Table 9. FOMs of SBN samples at 40 °C.[124]

Sample	$F_i = p$ ($\mu C/cm^2K$)	ε'	$F_V = p/\varepsilon'$ ($\mu C/cm^2K$)	$F_D = p/\sqrt{\varepsilon''}$ ($\mu C/cm^2K$)
LSBN-1% La	1×10^{-4}	850	11.8	–
LSBN-3% La	1.5×10^{-4}	1,100	13.6	–
LSBN-5% La	6×10^{-5}	530	11.3	–

Chen et al. investigated the $Sr_{0.6}Ba_{0.4}Nb_2O_6$ films fabricated on Si and fused silica substrates prepared by the sol-gel method. The p at room temperature was found to be 2×10^{-8} C/cm^{2}K at 27 °C, which is in the same order of magnitude as that of the SBN single crystals.[125]

Venet et al. fabricated textured SBN ($Sr_xBa_{1-x}Nb_2O_6$) ferroelectric ceramics with $x = 0.53$ and 0.63 by the hot forging method.[126] Table 10 summarizes the F_i, F_V, and F_D values for SBN textured ceramics. It can been seen that SBN53/47 ceramic, in the perpendicular direction with respect to the forging axis, has the third highest F_i value, indicating its potential in the fabrication of fast-pulse pyroelectric devices

Table 10. Physical properties and FOMs of textured SBN ferroelectric ceramics.[126]

Ceramic	$F_i = p$ (10^{-4} C/m^{2}K)	ε'	$F_V = p/\varepsilon'$ (10^{-4} C/m^{2}K)	$F_D = p/\sqrt{\varepsilon''}$ (10^{-4} C/m^{2}K)
SBN53/47 HF (⊥)	5.1	980	0.0052	1.2
SBN53/47 HF (∥)	4.0	468	0.0085	2.63
SBN63/37 HF (⊥)	2.3	4,579	0.0005	0.18
SBN63/37 HF (∥)	0.67	1,412	0.00047	0.12

SBN53/47 HF (⊥): Parallel to pressing axis.
SBN53/47 HF (∥): Perpendicular to pressing axis.

4.2.6 Lead Magnesium Niobate-Lead Titanate

Lead Mg niobate-PT (PMN-PT) $((1-x)Pb(Mg_{1/3}Nb_{2/3})O_3\text{-}xPbTiO_3)$ relaxor-based single crystals have rhombohedral symmetry at $x \leq 0.3$, tetragonal symmetry at $x \geq 0.35$, and the morphotropic symmetry at $0.3 < x < 0.35$. PMN-PT, a new generation of single crystals, has been widely investigated due to excellent dielectric, piezoelectric, and optical properties of the crystals; however, few investigations have reported on their pyroelectric performance.[127–136] Table 11 demonstrates some of the noteworthy pyroelectric properties and calculated FOMs of these materials.

Table 11. Physical properties and FOMs of PMN-PT samples.[127–136]

Crystals	$F_i = p$ $(10^{-4}\,C/m^2K)$	ε'	$F_V = p/\varepsilon'$ $(10^{-4}\,C/m^2K)$	$F_D = p/\sqrt{\varepsilon''}$ $(10^{-4}\,C/m^2K)$
PMN-0.13PT <111> direction poled	32.6	3,107	0.01	10.18
PMN-0.21PT <111> direction poled	17.9	961	0.018	10.59
Fe-doped PMN-0.38PT	584×10^{-6}	310	–	–
PMN.29PT	12.8	515	0.024	7.1
Mn-PMN-0.29PT	16.2	688	0.023	27.9

4.2.7 Organic Pyroelectrics

In this section, the properties of polymers used in PIR detectors are discussed briefly.

4.2.7.1 Polyvinylidene Fluoride. With the discovery of pyroelectric responses in PVDF and polyvinyl fluoride (PVF), a new area of organic materials research for their use in PIR detecting devices has come to light. PVDF is inherently polar. The hydrogen atoms are positively charged and the fluorine atoms are negatively charged with respect to the carbon atom in the unit, such as the repeat unit of $(-CH_2\text{-}CF_2\text{-})$ or $(CH_2CF_2)n$, in which the carbon-hydrogen and the electrically polar carbon-fluorine bonds can take up a number of stable configurations determined by the polymer's treatment. PVDF can be crystallized into at least four different polymorphous phases, depending upon film preparation conditions.

Two important forms I or β and II or α are of importance. In the α form, PVDF is non-piezoelectric (which is formed from slow-cooled melts or acetone solution), the bonds are in a trans-gauche-trans-gauche configuration, and molecules stack to give a nonpolar unit cell. The α form can be converted into the β form by stretching and electrically poling with a suitable field. In the β form, the molecular groups are in an all-trans configuration and the molecules are assembled to give a polar unit cell. Form β is orthorhombic, point group Amm2, and $z = 2$ Å, $a = 8.47$ Å, $b = 4.9$ Å, and $c = 2.56$ Å. The density is 1.76 M/gm³.[137] This form of PVDF is pyroelectric and its basic physical properties are presented in table 12.

Table 12. Material characteristics and FOMs of P(VDF-TrFE).

Material	$F_i = p$ (nC/cm^{2}K)	ε'	$F_V = p/\varepsilon'$ (nC/cm^{2}K)	$F_D = p/\sqrt{\varepsilon''}$ (nC/cm^{2}K)
P(VDF-TrFE) 50/50	4	18	0.2	5.06
P(VDF-TrFE) 56/44	3.8	12	0.3	7
P(VDF-TrFE) 70/30	5.5	8	0.68	20
P(VDF-TrFE) 75/25	3.3	7.4	0.4	9.4
P(VDF-TrFE) 80/20	3.1	7	0.44	9.1
PVF$_2$	3	10	0.3	6.8

Recently, in parallel with the findings of PVDF, the polymers of VDF-TrFE have been found to be ferroelectric. Like PVDF, the VDF-TrFE copolymer consists of crystalline and an amorphous fraction. Unlike PVDF, the introduction of a small amount of TrFE causes the copolymer to crystallize directly into the β phase from melt. The VDF-TrFE copolymer is therefore made to be pyroelectric without stretching, as with PVDF. The electrical and physical properties of PVDF and the 65/35 VDF-TrFE copolymer are similar, as shown in table 12.[138]

A comparison of often-used thin-film ferroelectrics shows that the application of P(VDF-TrFE) in low-cost sensors can be advantageous although the FOMs are lower. For instance, a copolymer film can be easily deposited onto a Si wafer in postprocessing after readout circuit fabrication by spin coating of a copolymer solution. Furthermore, the very low thermal conductivity provides good thermal insulation between the pyroelectric film and readout circuitry. The chosen P(VDF-TrFE) with a molar content of 70% VDF shows a spontaneous polarization of 8 µC/cm^2 and a p of 3.5 nC/cm^{2}K, a dielectric constant of 8, and a dielectric loss of about 0.018 at 25 °C. The investigation proved the suitability of the copolymer for use in pyroelectric sensors and arrays.[139] Production of thin-poled films is inexpensive and simple. The properties are comparable to often-used LT sensors. The authors' results will enable relatively simple integration of sensor chip and readout circuits. On the basis of the film technology developed, the realization of two-dimensional arrays is also possible. In the recent past, several other polymers have been using molecular engineering that exhibit a pyroelectric response.[140,141]

4.2.8 Pyroelectric-Polymer Composites

Pyroelectric-polymer composites can be considered an established substitute to conventional electroceramics and to ferroelectric polymers. The composites have a unique blend of polymeric properties such as mechanical flexibility, high strength, formability, and low cost with high electro-active properties of ceramic materials.

The composites contain two or more chemically different materials or phases. In these materials, it is possible to tailor electrical and mechanical properties catering to a variety of applications. Recent studies on ceramic-polymer-based pyroelectric composites show potential usefulness via large-area, lightweight, enhanced-strength, and flexible IR sensing elements. Thus, composites based on pyroelectric ceramic particles embedded in polymer possess hybrid properties

derived from individual components. These hybrid properties include large p of ceramic material and excellent mechanical strength, formability, and robustness of the polymer, eventually useful for IR detectors without the use of a substrate. An overview of the theory, models to predict dielectric behavior and p and fabrication techniques of biphasic composites, and a review of the latest work can be found in reference 142.

The dielectric and p on TGS-PVDF composites with different proportions of TGS have been investigated.[143] It was found that the variation of dielectric coefficients and p with temperature for composites were as reported for TGS single crystals. Furthermore, it was reported that with 50 wt. % of TGS particles in the composite, the FOM is the largest. It was also shown that the $D*$ value of detectors made out of a TGS composite reaches up to $(5–7)\times10^7$ cm Hz$^{1/2}$/W. Wang et al.[144] investigated the 45- to 75-µm TGS particles of different volume fractions (up to 80% volume fraction) dispersed in organic solvent for the preparation of films using the solution casting technique. It was observed that the p increased to 90 µC/m^{2}K and F_V to 3.3 with 80% volume of TGS particles.

A novel technique has been used in the fabrication of LATGS-PVDF-oriented film.[145] A high electric field was applied during preparation of the film. It was also reported that LATGS-PVDF with the highest field grains get oriented to the b-axis when the field is increased perpendicular to the b-axis. With a field of 10 kV/cm, better results for dielectric constant ≈10 and $p \approx$30 µC/m^{2}K at about 30 ºC have been reported. Recently, Yang et al. performed an extensive and noteworthy study on TGS:P(VDF-TrFE) composites with various volume fractions (0.05–0.43) of TGS embedded in P(VDF-TrFE).[146] The p varied from 32 to 102 µC/m^{2}K. The dielectric constant increased from 9.66 to 12.27 while the dielectric loss decreased from 0.021 to 0.008. The two phases of samples were poled in the same direction, in which the p is reinforced while the piezoelectric contribution partially cancels out. The low piezoelectric activity in the pyroelectric composite is an asset, as it reduces the vibration-induced noise. TGS:P(VDF-TrFE) is a good candidate for a sensing element in PIR detecting devices.

The detailed study on the pyroelectric and piezoelectric properties of PT-P(VDF-TrFE) composites gave the maximum value of p, with 54% volume fraction of the particles.[147] The p and dielectric constant were 40.7 µC/m^{2}K and 57.3, respectively, which gives a value of 0.71 for the FOM. However, the maximum value of FOM (0.92) for a composite having 49% volume fractions was obtained when only the ceramic phase was poled. When both phases were poled, the p and dielectric constant were 69.2 µC/m^{2}K and 55, respectively, which gives the FOM value of 1.24.

The pyroelectric properties of PT-P(VDF-TrFE) 0-3 nanocomposite films fabricated using various volume fractions of ceramic particles about 70 nm in size have been investigated by Chen et al.[148] They could only fabricate films with up to a volume fraction of 12% due to the problem of agglomeration. The films were prepared by the spin-coating method on aluminum-coated glass. All the FOMs (F_I, F_V, and F_D) reported by them showed an increase with an increase of volume fraction of PT ceramic particles. The results obtained for pyroelectric properties are shown in figure 15. It was concluded that p of the composite with 12% volume fraction of PT was 40% higher than that of the polymer.
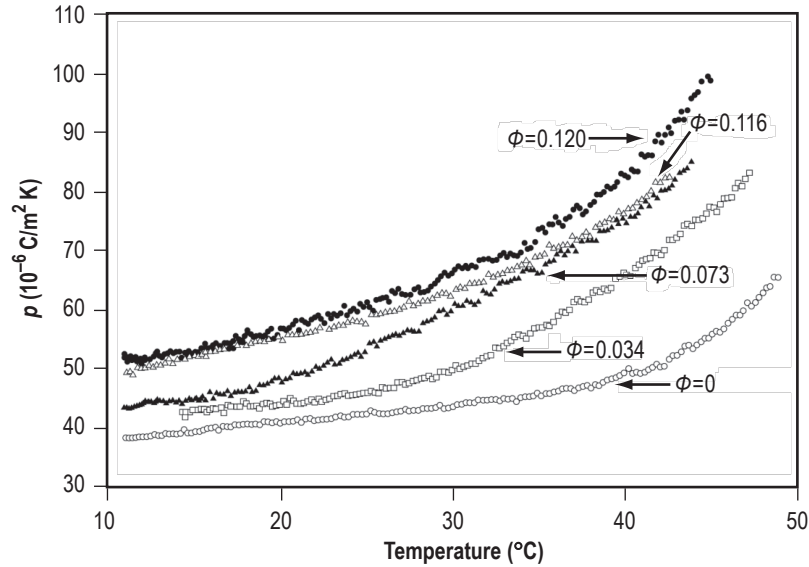
46

Figure 15. Pyroelectric coefficients of the composite films with various volume fractions of ceramic (ϕ) PT as a function of temperature.[148]

A D^* of 1.2×10^7 cm $Hz^{1/2}$/W has been achieved in composite films of (($Pb_{0.8}Ca_{0.2}$)TiO_3:P(VDF-TrFE)) prepared using the appropriate amount of ceramic particles having sizes <100 nm.[149] The values obtained for dielectric coefficients and p by Zhang et al.[150] for nanocrystalline Ca (0.11%)-modified PT (PCLT) are presented in table 1. The F_V and F_D exhibit maxima around 0.11% volume fraction of PCLT nanoparticles. The FOMs were 35% higher than the poled copolymer. A noteworthy study was performed on thin film deposited on Si substrate consisting of 12% volume of nanosized La and Ca modified PT embedded in a P(VDF-TrFE) 70/30 matrix to form pyroelectric sensors with three different configurations. The maximum specific D^* (1.3×10^7 cm $Hz^{1/2}$/W (at 1 kHz), 2.11×10^7 cm $Hz^{1/2}$/W (at about 300 Hz), and 2.8×10^7 cm $Hz^{1/2}$/W (between 5 and 100 Hz), respectively) were reported. Authors suggested that sensors fabricated with PCLT/P(VDF-TrFE) nanocomposites have the potential to be used in Si-based pyroelectric sensors.[151]

Specific D^* of 4.2×10^6 and 3.4×10^7 cm $Hz^{1/2}$/W of film of PCLT/P(VDF-TrFE) have been obtained on a porous Si and plastic (PET) substrate, respectively.[152] This specific D^* was found to be one to two orders of magnitude higher than that of the sensor on bulk Si substrate fabricated under similar conditions. The values for F_V, p, and dielectric constant obtained were 3.74 $\mu C/m^2 K$, 56.5 $\mu C/m^2 K$, and 11, respectively. Lam et al. used thermoplastic elastomer, polyurethane (PU) in fabricating a 0-3 composite with PZT.[153] It was found that, with a 30% volume fraction of PZT, the value of p at room temperature, was found to be 90 $\mu C/m^2 K$. It was more than tenfold higher than the PZT:PVDF composite with the same volume fraction of ceramic. It was concluded that a large electrical conductivity may enhance the pyroelectricity in composites.

Recently, thick films of 0-3 composites of PZT ceramic and P(VDF-TrFE) copolymers have been produced by spin coating on an Au-coated Si wafer.[154] A p of 92 μC/m^{2}K has been measured for composites with 20% volume ceramic. For the composites with 10% and 20% volume ceramic, voltage and current FOMs are higher than PZT thick films.

Lithium tantalate ceramic particles have been incorporated into a P(VDF-TrFE) 70/30 mol. % copolymer matrix to form composite films. The films were prepared using a solvent casting method with the LT powder homogeneously dispersed in the P(VDF-TrFE) copolymer matrix with various volume fractions. Electrical properties such as the dielectric constant, dielectric loss, and p have been measured as a function of temperature and frequency. In addition, materials' FOMs have also been calculated to assess their use in IR detectors. The results show that the fabricated LT:P(VDF-TrFE) composite films have a good potential for uncooled IR sensor applications operating at moderate temperatures.[155]

4.2.9 Other Pyroelectric Materials

4.2.9.1 Aluminum Nitride. Fuflyigin et al. studied pyroelectric properties of high-quality (001) aluminum nitride (AlN) films grown on (111) Si substrates.[156] In these films, the polar axis, <0001>, is oriented perpendicular to the film's plane. The value of p was in the range of 6 to 8 μC/ m^{2}K, yielding an F_V of 0.8–0.95. The p was independent of temperature and applied bias. Leakage current as low as $(1–2)\times10^{-9}$ A/cm^2 was measured at 5 V on large-area devices. These results indicate that AlN films can be good candidates for pyroelectric thin-film devices.

4.2.9.2 Gallium Nitride. The wurtzite gallium (Ga) nitride (GaN) is a natural pyroelectric with pyroelectric polarization in the direction of the c-axis. Bykhovski et al. reported the pyroelectric properties of an n-type GaN film deposited over a basal plane sapphire substrate.[157] The pyroelectric voltage reported by them was of the order of 10^4 V/mK, which is comparable to that of the pyroelectric ceramics such as PZT or BT.

4.2.9.3 Zinc Oxide. Zinc oxide (ZnO) is a unique material that exhibits semiconducting, piezoelectric, and pyroelectric multiple properties.[158] The p are as follows:

• Primary p: –6.8 μC/m^{2}K.
• Secondary p: –2.5 μC/m^{2}K.
• Total p: –9.4 μC/m^{2}K.

5. UNIQUE AND INNOVATIVE TECHNIQUES DEMONSTRATED FOR IMPROVING PERFORMANCE OF PYROELECTRIC INFRARED SENSORS

Enhancing the D^* and thermal resolution of a pyroelectric-type detector is still a main challenge besides developing new ferroelectric thin films and designing advanced architecture. The following unique techniques for enhancing the performance of PIR detectors are being explored. It has been demonstrated that R can be increased many fold by incorporating these techniques.

5.1 Multilayer Structures

The Alexe and Pintile thermal analysis of a pyroelectric bimorph structure, performed for a sinusoidally modulated heat flow, reveals the possibility of obtaining a larger signal than in the case of a homogeneous pyroelectric structure.[159] The ratio between the signal generated from a bimorph structure and the signal generated from a homogeneous structure, in the same conditions, depends on the material properties and on the modulation frequency. This ratio, computed for a particular bimorph, is up to 4:1 at 1,000 Hz. The main conclusion of the above discussion is that, in certain conditions, the signal generated by a pyroelectric bimorph structure could be greater than the signal generated by a homogeneous pyroelectric detector made from only one of the two materials of the bimorph. The thermal analysis of the ratio between the signal generated by the bimorph structure and the signal generated by the homogenous structure (made for the extreme cases on the heat sink and suspended) of a given pair of materials and for a given range of frequencies suggests that it is possible to design a pyroelectric bimorph structure that generates a signal higher than a homogeneous pyroelectric structure made from only one of the two component materials.

Lang and Alexe made theoretical and experimental studies of pyroelectric bimorph radiation detectors.[160] The bimorphs consisted of two thin layers on a substrate, the upper one having a large p and a large ε and the lower one having a smaller p and a smaller ε. The incident radiation is absorbed in the electrode on the upper layer. If the radiation is modulated at a sufficiently high frequency, the thermal waves that are produced will partially penetrate the lower layer so that the effective p will be dominated by that of the upper layer of the bimorph. However, the capacitance of the bimorph will be the series combination of the two layers and will be lower than that of either of them. This gives an R_V that is larger than that of either of the two layers used alone. The analysis was verified experimentally using a PLZT (12/30/70)/PZT (30/70) bimorph. The design of a PLZT (8/35/65)/LT bimorph was simulated. The calculated R_V was more than 100 times that of a PLZT (8/35/65) monomorph having the same thickness. A pyroelectric bimorph IR detector with R_V much higher than that of a monomorph can be constructed. The theory was experimentally verified by tests of a PLZT (12/30/70)/PZT (30/70) bimorph. A much improved design of PLZT (8/35/65)/LT was studied in simulation calculations. The calculations showed that a bimorph could be made that would have an R_V that is more than one hundredfold greater than that of a monomorph of the same thickness.

High-quality multilayer (ML) ferroelectric thin films based on erbium (Er)-doped PT $Pb_{(1-x)1.1}Er_xTi_{1-x/4}O_3$ (PErT) where $x = 0.05$ and $Pb_{1.1}(Zr_{0.58}Fe_{0.2}Nb_{0.2}Ti_{0.02})O_3$ (PZFNT) have been processed via chemical solution deposition on textured (111) $Pt/Ti/SiO_2/Si$ substrates.[161] The dielectric, ferroelectric, and pyroelectric properties have been characterized. It is shown that the ML film exhibits the relaxor-type behavior found for pure PZFNT, and that its transition temperature of 310 °C at 1 kHz lies between those of PErT and PZFNT. The dielectric constant of 520 also lies between those of PErT and PZFNT. The ferroelectric properties are considerably improved over those of the monomorph films. An unusually high p of about 620 $\mu C/m^2K$ was obtained from measurements of the temperature dependence of the remnant polarization between 30 and 80 °C. The voltage and current responses, measured using a modulated near-IR laser, could be improved by two to three orders of magnitude over those of PZFNT. The thermal time constant (τ_T) obtained is found to be three orders of magnitude lower than the electrical time constant (τ_E) and indicates that the high thermal conduction rate in the substrate determines the detector R.

In conclusion, the present work shows that it is possible to tune the dielectric properties of ferroelectric thin films through a proper choice of heterostructures. The FOM for pyroelectric applications can be considerably improved via the use of ML thin films. A poling of the film is not necessary due to self-polarization. High output voltages and currents can be achieved despite the transparency of the films and the use of thick platinized Si substrates. In this respect, the response of the film is expected to improve via the use of micromachined detector elements.

Ferroelectric $Pb(Zr_{0.3}Ti_{0.7})O_3/PT$ ML thin films are fabricated by the sol-gel method.[162] The properties of PZT/PT ML thin films with different PZT and PT layer stacking structures have been systematically studied. All the films are dense and smooth with a single perovskite phase. "Pinched" ferroelectric hysteresis loops are found for ML thin films. The dielectric constant of an ML thin film decreases when the PT volume fraction increases. The dielectric loss of 5PZT/4PT ML thin film is comparable to that of pure PZT; however, all the other ML thin films show much higher dielectric loss. When compared to the pure PZT thin film, the 5PZT/4PT ML film has a comparable p, reduced dielectric constant, and comparable dielectric loss. Therefore, the 5PZT/4PT thin film shows higher pyroelectric F_{D*} (2.1×10^{-5} $Pa^{-1/2}$), which is found to be better than pure PZT thin film and is a promising material structure for pyroelectric application.

Sun et al. did a comparison study on sol-gel prepared $Pb(Zr_{0.3}Ti_{0.7})O_3$ and $Pb(Zr_{0.3}Ti_{0.7})O_3/PT$ ML thin films for PIR detectors and found PZT/PT to be a promising candidate for IR detectors due to the reduced dielectric constant of an ML structure.[163]

5.2 Compositionally Graded Structures

Compositionally graded ferroelectric devices (GFDs) such as those formed from KTN[164] and BST[165] have recently been shown to demonstrate a whole new pyroelectric phenomenon. Effective p as large as 5 $\mu C/cm^2K$ with peak R at approximately 50 °C have also been reported for compositionally graded BaSr ferroelectric thin-film devices formed on Si using unbalanced magnetron sputter deposition.[166] These effective p are nearly two orders of magnitude larger than those observed from conventional pyroelectric thin-film ferroelectric detectors.[167,168]

Tang et al. prepared a compositionally graded structure of $Pb(Zr_xTi_{1-x})O_3$ (PZT) thin films with Zr:Ti ratios from 10:90 to 40:60 grown on $PbZrO_3$-buffered Pt/Ti/SiO$_2$/Si substrates by a simple sol-gel process.[169] The structure, surface morphology, and dielectric properties of the graded PZT films were measured by XRD, field-emission scanning electron microscopy, Auger electron spectroscopy, and by using an impedance analyzer. The results showed that the graded PZT films on $PbZrO_3$-buffered Pt/Ti/SiO$_2$/Si substrates have a preferred (111) orientation. At 100 Hz, the dielectric constant and dissipation factor of the graded PZT film are 255 and 0.032, respectively. The p of compositionally graded PZT film was measured by a dynamic technique. At 25 °C, the p value of the graded PZT film is 349 $\mu C/m^2K$ and the F_{D*} is 16.4×10^{-6} Pa$^{-0.5}$ at 100 Hz.

The typical small-signal dielectric constant and dissipation factor of the graded film at a frequency of 100 Hz were 255 and 0.032, respectively. At room temperature, the p and F_{D*} of the graded PZT film were 349 $\mu C/m^2K$ and 16.4×10^{-6} Pa$^{-0.5}$, respectively. These results make these materials useful for pyroelectric sensors.

Tang et al. also reported the compositionally graded $(Pb_{1-x}Ca_x)TiO_3$ (PCT) thin films of $x = 0$ and 24 mol. % were fabricated on Pt/Ti/SiO$_2$/Si substrates by using a modified sol-gel process.[170] The final structure consists of two-layer, upgraded films starting from PT on the Pt electrode to the top PCT(24) layer; whereas, films with the opposite gradient are called downgraded films. Highly (100)-oriented, graded PCT thin films have been obtained when the graded PCT thin films were annealed at 600 °C. At 100 kHz, the dielectric constants were 79 and 128, respectively, for the upgraded and downgraded PCT films. The p of the graded films was measured by a dynamic technique. At room temperature, the values of p and F_{D*} of the upgraded and downgraded PCT films are 95 $\mu C/m^2K$ and 9.1×10^{-6} Pa$^{-0.5}$ and 112 $\mu C/m^2K$ and 8.6×10^{-6} Pa$^{-0.5}$, respectively.

In conclusion, compositionally graded PCT thin films were grown on Pt/Ti/SiO$_2$/Si substrates by using a modified sol-gel technique with a high degree of preferred orientation (100) in the a-axis direction. At 100 kHz, the relative ε and dissipation factors for the upgraded and downgraded PCT films were 79 and 0.025 and 129 and 0.024, respectively. At room temperature, the p of the upgraded and downgraded PCT films were 95 and 112 $\mu C/m^2K$, respectively. The F_{D*} of the upgraded and downgraded PCT films were 9.1×10^{-6} and 8.6×10^{-6} Pa$^{-0.5}$, respectively. The results make these materials useful for pyroelectric sensors.

5.3 Pyroelectric Heterostructures

Tipton et al. have observed enhanced pyroelectric response in sub-100-nm, epitaxial-heterostructure films of Pb-Zr-Ti-O contacted with conducting perovskite oxide top and bottom electrodes.[171] The enhancements are obtained in capacitors where the bottom electrode is processed under reducing conditions. This leads to an asymmetric, temperature-dependant internal field that is produced within the ferroelectric capacitance and manifests itself as a strongly shifted ferroelectric hysteresis loop. Because the shifted coercive voltage lies near the unbiased operating point, the pyroelectric film has a large value of dP/dE. The product $(dP/dE)(dE/dT)$ gives rise to an enhanced pyroelectric response. This effect is due to introducing oxygen vacancies into the bottom electrode. Their data show that an increase in the pyroelectric response of 10 to 30 times can be obtained from symmetric devices, with a concomitant improvement of sensing F_{D*} by three times.

Infrared detectors consisting of thin-film PZT/YBa$_2$Cu$_3$O$_{7-x}$ oxide-heterostructures have been fabricated.[172] The yttrium (Y) BaCu oxide (YBCO) thin film used as the bottom conductive electrode significantly increases the performance of a PIR detector. A D^* of $\approx10^8$ cm Hz$^{1/2}$/W at room temperature has been obtained for simple heterostructure device configurations in the IR wavelength range of 1 to 20 μm. Reactive ion etching (RIE) has been used to etch the YBCO and the other oxide layers for the development of an air-bridge structure that further reduces thermal mass and increases the operation frequency of the IR detector. Mn- and Sb-doped PZT (MSPZT)/ YBCO heterostructures were epitaxially grown on Y-stabilized Zr (YSZ)/Si and Li aluminum oxide (LAO) Pb(Zr,Ti)O$_3$/YBCO substrates for IR pyroelectric detectors. The p of MSPZT thin films in the heterostructures was ≈80 nC/cm^{2}K, and a D^* of $\approx10^8$ cm Hz$^{1/2}$/W was achieved for the simple MSPZT/YBCO flat detectors. The heterostructure detector with an air bridge showed a three times higher IR photoresponse at a chopper frequency of 30 Hz.

Xu et al.[173] explored new MSPZT/YBa$_2$Cu$_3$O$_{7-y}$ (MSPZT/YBCO) heterostructure fabricated on Si substrate with a YSZ buffer layer by pulsed laser deposition for high-performance, uncooled IR red detectors. This structure resulted in high FOMs.

5.4 Introduction of Nanoporosity

Suyal and Setter successfully deposited PZT thin, porous film by the sol-gel process with the addition of a polymer as a volatile phase.[174] Choosing a polymer of different molecular weight and concentration of polymer can control the pore size. They found the dielectric constant to be strongly dependant on porosity, while p changed moderately. In a PZT film, the relative ε can be decreased from 150 to 95 with a Zr:Ti ratio of 45:55 and 15:85, respectively. For PZT (Zr:Ti = 45:55), the F_V and F_D values increased from 0.28 to 1 μC/m^{2}K and 38 to 80 μC/m^{2}K, respectively; whereas, for PZT (Zr:Ti = 15:85), these values increased from 0.88 to 1.95 μC/m^{2}K and 79 to 139 μC/m^{2}K, respectively, by porous microstructure. This enhancement in values is due to the reduction of relative ε by forming matrix-void composites. Similarly, in PbCa$_{1-x}$TiO$_3$ (PCT), F_V and F_D were shown to be 4.8 and 250 μC/m^{2}K, respectively.[175]

5.5 Other Techniques

Shaulov proposed a broadband thermal detector based on pyroelectric materials with temperature-dependent electrical conductivity.[176] This detector combines the properties (notably the frequency response) of a thermistor bolometer and a pyroelectric detector. He demonstrated that a suitable choice of the detector parameters provides a uniform frequency response above and below the thermal relaxation frequency. Acting simultaneously as a thermistor and as a pyroelectric detector, the pyroelectric thermister bolometer (PTB) combines the advantages of both detectors. Specifically, in the PTB, the thermistor component provides the low-frequency response while the pyroelectric component provides the high-frequency response. As a result, a flat-frequency response can be obtained over a broad band. The characteristic cited above was demonstrated with a PTB made of a Cu$_3$B$_7$O$_{13}$Cl crystal.

Lehman et al. proposed a large-area, domain-engineered pyroelectric radiometer with high spatial and high spectral response uniformity that is an excellent primary transfer standard for measurements in the near- and mid-IR wavelength regions.[177] The domain engineering consisted of inverting the spontaneous polarization over a 10-mm-diameter area in the center of a uniformly poled, 15.5×15.5-mm-square, 0.25-mm-thick LN plate. Gold-black was used as the optical absorber on the detector surface, and an aperture was added to define the optically sensitive detector area. The results indicate significantly reduced acoustic sensitivity without the loss of optical sensitivity. The detector noise equivalent power was not exceptionally low but was nearly constant for different acoustic backgrounds.

In addition, the detector's spatial response uniformity variation was less than 0.1% across the 7.5-mm-diameter aperture, and reflectance measurements indicated that the Au-black coating was spectrally uniform within 2%, from 800 to 1,800 nm. The domain-engineered pyroelectric radiometer is the only alternative compared with mercury (Hg) Cd tellurium (Te) (HgCdTe), indium antimony (InSb) photoconductors, or commercially available pyroelectric detectors capable of measurement uncertainty of the order of 0.1%. The primary role of the radiometer was to extend and improve the National Institute of Standards and Technology spectral R scale from the visible to the near-IR wavelength range.

Nakamura and Itagaki proposed a new structure that consists of interdigital electrodes deposited on periodic inverted domains of a ferroelectric crystal.[178] Since only a shallow region close to the crystal surface is pyroelectrically active in this structure, the surface charges are quickly induced in response to IR irradiation and this structure therefore provides a high R. A pyroelectric detector fabricated using periodic antipolar domains formed by selective proton exchange and subsequent heat treatment of an LT crystal is experimentally demonstrated to exhibit a high current R in the high-frequency range of IR power modulation. It was also recommended that, since only a shallow region just below the irradiated surface serves actively as a pyroelectric material in this detector, it is expected that a higher R would be obtained by decreasing the periods of the domains and interdigital electrodes.

Recently, enhanced ferroelectric and pyroelectric properties have been demonstrated in trilayered bismuth (Bi) La titanate/sodium (Na) Bi titanate/Bi La titanate (BLT/NBT/BLT) and PZT/NBT/PZT thin films fabricated on Pt/Ti/SiO$_2$/Si substrates by chemical solution deposition.[179]

6. APPLICATIONS OF PYROELECTRIC DETECTORS

The applications of uncooled PIR detectors are described in references 180 and 181. These applications consist of air quality monitor, atmospheric temperature measurement, Earth position sensor, Earth resources, engine analysis, fire alarm, gas analyzer, glass processing, horizon sensor, IR detection, IR spectrometer, interferometer, interplanetary probe, intrusion detector, laser detection, laser-power control, liquid-fuel analysis, meteorology, plasma analysis, plastic processing, pollution detection, position sensor, radiometer, reflectance measurements, remote sensing, sky radiance, solar cell studies, human sensors, forest fire detection, pyroelectric vidicons, ear thermometer, terahertz detection, biomedical imaging, satellite-based IR detection at 90 K, optical wave guide studies, x-ray detector, microwave detector, facial recognition, traffic control, vision testing, law enforcement, and border patrol.

7. PYROELECTRIC DETECTORS FOR NASA APPLICATIONS

Uncooled pyroelectric detectors are used for astrophysical, astronomical, and cosmological applications. Pyroelectric detectors are one of many different types of IR radiation detectors. The pyroelectric detectors are of interest for long-term space use because they do not require cooling during operation. They can also detect at very long wavelengths and they have a relatively flat spectral response.

These PIR detectors are very beneficial to space astrophysics, Earth observations from space, and deep space exploration. NASA's commitment to air pollution monitoring and thermal mapping of the Earth, which includes the remote sensing of aerosols and limb scanning IR radiometer projects, requires photodetection in the 6- to 20-μm region of the spectrum. The HgCdTe detectors that are presently used in these wavelengths must be cooled to 50–80 K. The cryogenic systems required to achieve these temperatures are large, complex, and expensive. Pyroelectric detectors can detect radiation in the 1- to 100-μm region while operating at room temperature. This makes the pyroelectric detector a prime candidate to fill NASA's thermal IR detector requirements.

The photopolarimeter-radiometer (PPR) experiment can be designed to measure the linear polarization and intensity of reflected sunlight and the intensity of thermally emitted IR radiation from satellites using a pyroelectric detector.

For Earth horizon sensing applications, PIR detectors can also be used for the following:

• Land-use monitoring.
• Detection of hot events: Volcanic eruptions, fires, hot springs, etc.
• Pollution monitoring.
• Investigation of atmospheric phenomena and processes.
• Thermal imaging.
• Spectrometry.
• Detection and tracking of aircraft and missiles in flight.
• Meteorology.
• Mineral exploration.

7.1 Pyroelectric Materials for Low-Temperature Infrared Detection Space Applications

Only a few pyroelectrics qualify for use as the active layer of a passively cooled, satellite-based pyroelectric detector and other space applications.[181] For example, the temperature on an Earth-orbiting satellite, and thus the passively cooled detector's operating temperature, is around 90 K. Therefore, the pyroelectric material must display a T_c near 90 K to work in the bolometer mode. To allow optimization, ferroelectric solid-solution alloys with composition-dependent T_c have been explored. An alloy-based pyroelectric detector has the added advantage that one should

be able to easily optimize such a detector for use across a wide temperature range simply by changing the alloy composition. Such materials include the following:

- Potassium tantalate niobate (KTN).
- Barium strontium tantalate (BST).
- Lead scandium titanate (PST).
- Sodium tantalate niobate (STN).
- Calcium strontium titanate (CST).

Based on the materials cited above, the compositions having a 77 K T_c are as follows:

- $K(Ta_{0.9}Nb_{0.1})O_3$.
- $(Ba_{0.1}Sr_{0.9})TiO_3$.
- $Na(Ta_{0.8}Nb_{0.2})O_3$.
- $(Ca_{0.1}Sr_{0.9})TiO_3$.

8. CONCLUSIONS

An effort has been made to introduce the basic principles governing pyroelectricity and ferroelectricity and list important materials that exhibit these properties. The processing and characteristics of important pyroelectric materials (from the viewpoint of their applications) in single-crystal, ceramic, and thin- and thick-film forms have been described. Enhancing $D*$ and thermal resolution of a pyroelectric-type detector is still a main challenge. Besides developing new ferroelectric thin films and designing advanced architecture, unique techniques being explored have also been described in this TM.

It is worth mentioning that the thermal flux data collected by the Galileo net-flux radiometer released toward Jupiter's surface helped researchers analyze the chemical composition and structure of the planet's atmosphere. The Mars Exploration Rover mission launched in 2003 carried a miniature thermal emission spectrometer to identify minerals by their IR spectrum and to collect temperature data. The detector materials used in the space missions have usually been DTGS or LT.[182]

According to Lang, "Pyroelectricity has been known for 24 centuries. There is no reason to think the effect will outlive its usefulness anytime soon."[182] Physicists and engineers are likely to develop increasingly sensitive pyroelectric devices including using novel techniques.

REFERENCES

1. Gupta, C.: *Handbook of Photonics*, CRC Press, New York, NY, 1997.

2. Lang, S.B.; and Das-Gupta, D.K.: "Pyroelectricity: Fundamentals and Applications," *Ferroelectrics*, Vol. 2, No. 4, pp. 217–354, 2000.

3. Rogalski, A.: *Infrared Detectors*, Gordon and Breach Science Publishers, The Netherlands, 2000.

4. Whatmore, R.W.; and Watton, R.: *Pyroelectric Materials and Devices Infrared Detectors and Emitters: Materials and Devices*, P. Capper and C.T. Elliott (eds.), Kluwer Academic Publishers, London, England, 2001.

5. *Ferroelectrics*: *Special Issue on Pyroelectricity*, S.B. Lang and A.S. Bhalla (eds.), Gordon and Breach Science Publishers, Berkshire, UK, Vol. 118, No. 104, 1991.

6. Curie, J.R.: "Studies on the Functional Ferroelectric Materials for Infrared Sensors," M.S. Thesis, Alabama A&M University, Normal, AL, 2004.

7. Gautschi, G.: *Piezoelectric Sensorics*, Springer-Verlag Berlin, Heidelberg, Germany, 2002.

8. Nye, J.: *Physical Properties of Crystals*, Oxford University Press, London, UK, 1957.

9. Bauer, S.; and Ploss, B.: "Interference Effects of Thermal Waves and Their Applications to Bolometers and Pyroelectric Detectors," *Sensors and Actuators A*, Vols. 25–27, pp. 417–421, 1991.

10. Aggarwal, M.D.; Currie, J.R.; Penn, B.G.; et al.: "Solution Growth and Characterization of Single Crystals on Earth and in Microgravity," *NASA/TM—2007–215187*, Goddard Space Flight Center, 2007.

11. Brezina, B.; Havrankova, M.; and Vasa, M.: "Enhanced Growth of Non-Polar{001} Growth Sectors of Deuterated Triglycine Sulfate Doped With L-alanine (LADTGS)," *Cryst. Res. Tech.*, Vol. 27, No. 1, pp. 13–20, 1992.

12. Satapathy, S.; Sharma, S.K.; Karnal, A.K.; and Wadhawan, V.K.: "Effects of Seed Orientation on the Growth of TGS Crystals With Large (010) Facets Needed for Detector Applications," *J. Cryst. Growth*, Vol. 240, pp. 196–202, 2002.

13. Banan, M.: "Growth of Pure and Doped Triglycine Sulfate Crystals for Pyroelectric Infrared Detector Applications," M.S. Thesis, Alabama A&M University, Normal, AL, 1986.

14. Zhao-De, D.: "A New Method of Growth of Ferroelectric Crystal," *Ferroelectrics*, Vol. 39, pp. 1237–1379, 1981.

15. Diéguez, E.; Plaza, J.L.; Aggarwal, M.D.; and Batra, A.K.: "Czochralski Growth of Oxide Photorefractive Crystals," in *Springer Handbook of Crystal Growth*, New York, NY, in press, available April 3, 2010.

16. Xu, Y.: *Ferroelectric Materials and Their Applications*, North-Holland, London, England, 1991.

17. Moulson, A.J.; and Herbert, J.M.: *Electroceramics*, John Wiley & Sons, West Sussex, England, 2003.

18. Feldman, Y.: "PT Films by Thermal Evaporation," *The Rev. Sci. Inst.*, Vol. 26, No. 5, pp. 463–465, 1995.

19. Auciello, O.; Kingon, A.I.; and Krupanidhi, S.B.: "Sputtering Synthesis of Ferroelectric Films and Hetro-Structures," *MRS Bull.*, Vol. 21, No. 6, pp. 25–30, 1996.

20. Auciello, O.; and Ramesh, R.: "Laser-Ablation Deposition and Characterization of Ferro-electric Capacitors for Nonvolatile Memories," *MRS Bull.*, Vol. 21, No. 6, pp. 31–36, 1996.

21. de Keijser, M.: "Chemical Vapor Deposition of Electroceramic Thin Films," *MRS Bull.*, Vol. 21, No. 6, pp. 37–43, 1996.

22. Shimizu, M.; and Shiosaki, T.: "MOCVD of Ferroelectric PZT and PLZT Thin Films for Memory Device Applications in Ferroelectric Thin Films," *MRS Bull.*, Boston, MA, Vol. 355, p. 295, 1994.

23. de Keijser, M.; van Veldhoven, P.J.; and Dormans, G.J.M.: "Organometallic Chemical Vapor Deposition of Lead Zirconate Titanate," L.O. Auciello and R. Waser (eds.), *Science and Technology of Electroceramic Thin Films*, Kluwer Academic Publishers, London, England, Vol. 284, p. 75, 1995.

24. Gao, Y.; Cho, D.W.; and Tuttle, B.A.: "Growth and Characterization of $PbTiO_3$ and PZT Thin Films by MOCVD in Ferroelectric Thin Films," *MRS Bull.*, Vol. 355, p. 337, 1994.

25. Budd, K.D.; Dey, S.K.; and Payne, D.A.: "Sol-Gel Processing of PT, PZ, PZT, and PLZT Thin Films," *Proc. Br. Ceram. Soc.*, Vol. 36, pp. 107–121, 1985.

26. Vest, R.W.; and Zhu, Z.: "Films of 64/40 PZT by the MOD Process for Memory Applications," *Ferroelectrics*, Vol. 119, pp. 61–75, 1991.

27. Yi, G.; Wu, Z.; and Sayer, M.: "Preparation of $Pb(Zr,Ti)O_3$ Thin Films by Sol-Gel Processing: Electrical, Optical, and Electrooptic Properties," *J. Appl. Phys.*, Vol. 64, No. 5, pp. 271–274, 1988.

28. Fukushima, J.; Kodaira, K.; and Matsushita, T.: "PZT Films by Sol-Gel," *J. Mater. Sci.*, Vol. 19, pp. 596–601, 1984.

29. Tu, Y.L.; and Milne, S.J.: "Characterization of Single Layer PTT (53/47) Films Prepared From an Air-Stable Sol-Gel Route," *J. Mater. Res.*, Vol. 10, No. 12, pp. 3222–3231, 1995.

30. Tu, Y.L.; and Milne, S.T.: "A Study of the Effect of Process Variables on the Properties of PZT Films Produced by a Single Layer Sol-Gel Technique Route," *J. Mater. Sci.*, Vol. 30, pp. 2507–2516, 1995.

31. Huang, J.: "Microstructure and Properties of Zr-Rich $Pb(ZxTi_{1-x})O_3$ Thin Films Prepared by Metallo-Organic Deposition Technique," Ph.D. Thesis, University of Cincinnati, Cincinnati, OH, 1997.

32. Pilpel, N.: "Properties of Organic Solution Heavy Metal Soaps," *Chem. Rev.*, Vol. 63, pp. 221–225, 1963.

33. Klee, M.; Eusemann, R.; Wiser, W.; and Brand, W.: "Processing and Dielectric Properties of PZT ($x = 0.2$–0.75) Films: Comparison of Metallo-Organic Decomposition and Sol-Gel Process," *J. Appl. Phys.*, Vol. 72, No. 4, pp. 1566–1576, 1992.

34. Haertling, G.H.: "PLZT Thin Films Prepared From Acetate Precursors," *Ferroelectrics,* Vol. 119, pp. 51–56, 1991.

35. Tuttle, B.A.; Headley, T.J.; Bunker, R.W.; et al.: "Microstructure Evolution of PZT Thin Films Prepared by Hybrid Metallo-Organic Deposition," *J. Mater. Res.*, Vol. 7, No. 7, pp. 5007–5013, 1992.

36. Carim, A.H.; Tuttle, B.A.; Doughty, D.H.; and Martinez, S.L.: "Microstructure of Solution-Process PZT Thin Film," *J. Am. Ceram. Soc.*, Vol. 74, No. 6, pp. 1455–1458, 1991.

37. Kwok, C.K.; and Desu, S.B.: "Seeding Layer for PZT Films," *J. Mater. Res.*, Vol. 8, pp. 339–344, 1993.

38. Kwok, C.K.; and Desu, S.: "Transmission Electron Microscopy Study of PZT Thin Films, in Ceramic Transactions: Ferroelectric Films," A. Bhalla and K.M. Nair (eds.), *Am. Ceram. Soc.*, Westerville, OH, Vol. 25, p. 73, 1992.

39. Voigt, J.A.; Tuttle, B.A.; Headley, T.J.; and Lamppa, D.L.: "The Pyrochlore-to-Perovskite Transformation in Solution-Derived Lead Zirconate Titanate Thin Films in Ferroelectric Thin Films IV," *Mater. Res. Soc.*, Boston, MA, Vol. 355, p. 395, 1994.

40. Batra, A.K.; Alim, M.A.; Currie, J.R.; and Aggarwal, M.D.: "The Electrical Response of the Modified Lead Titanate Based Thick-Films," *Physica B*, Vol. 404, pp. 1905–1911, 2009.

41. Ichiki, M.; Zhang, L.; Yang, Z.; et al.: "Lead Zirconate Titanate Film Formation With Spray Coating Method," *Jpn. J. Appl. Phys.*, Vol. 42, pp. 5927–5930, 2003.

42. Kang, S.; Kim, H.; Takahashi, K.; et al.: "Preparation of Modified Lead Zinc Niobate Compound Thick Films by Rapid Quenching," *Jpn. J. Appl. Phys.*, Vol. 32, pp. 4254–4257, 1993.

43. Adachi, H.; Kuroda, Y.; Imahashi, T.; and Yanagisawa, K.: "Preparation of Piezoelectric Thick Films Using a Jet Printing System," *Jpn. J. Appl. Phys.*, Vol. 36, pp. 1159–1163, 1997.

44. Akedo, J.; and Lebedev, M.: "Effect of Annealing Poling Conditions on Piezoelectric Properties of PZT Thick Films by Aerosol Deposition Method," *J. Cryst. Growth*, Vol. 235, pp. 415–420, 2002.

45. Ichiki, M.; Akedo, J.; Schroth, A.; et al.: "X-Ray Diffraction and Scanning Electron Microscopy Observation of PZT Thick Film Formed Gas Deposition Method," *Jpn. J. Appl. Phys.*, Vol. 36, pp. 5815–5819, 1997.

46. Dias, C.J.; and Das-Gupta, D.K.: "Inorganic Ceramic/Polymer Ferroelectric Composite Electrets," *IEEE Trans. Diel. Elect. Ins.*, Vol. 3, No. 5, pp. 706–734, 1996.

47. *Polymer Sensors and Actuators*, Y. Osada and D.E. DeRossi (eds.), Springer Verlag, New York, NY, 2000.

48. Guggilla, P.: "Studies on Pyroelectric Materials for Infrared Sensor Application," Ph.D. Thesis, Alabama A&M University, Normal, AL, 2007.

49. Guggilla, P.; Batra, A.K.; Aggarwal, M.D.; and Lal, R.B.: "Investigation on Nanocomposites for Pyroelectric Infrared Sensors," *Proc. SPIE*, Vol. 5725, pp. 295–297, 2005.

50. Guggilla, P.; and Batra, A.K.: "0-3 Composite Film Preparation," unpublished.

51. Lal, R.B.; and Batra, A.K.: "Growth and Properties of Triglycine (TGS) Sulfate Crystals," *Ferroelectrics*, Vol. 142, pp. 51–82, 1993.

52. Alexandru, H.V.; Berbecaru, C.; Stanculescu, F.; et al.: "Doped TGS Crystals for IR Detectors and Sensors," *Sensors and Actuators A*, Vol. 113, pp. 387–392, 2004.

53. Banan, M.; Batra, A.K.; and Lal, R.B.: "Growth and Morphology of TGS Crystals," *J. Mat. Sci. Lett.*, Vol. 8, pp. 1348–1349, 1989.

54. Banan, M.; Lal, R.B.; Batra, A.K.; and Aggarwal, M.D.: "Effect of Poling on the Morphology and Growth Rate of TGS Crystals," *Cryst. Res. Tech.*, Vol. 24, No. 3, p. K53, 1989.

55. Nakatani, N.: "Ferroelectric Domain Structure and Internal Bias Field in TGS Crystals," *Jpn. J. Appl. Phys.*, Vol. 30, No. 12A, pp. 3445–3449, 1991.

56. Yang, L.; Batra, A.K.; and Lal, R.B.: "Growth and Characterization of Triglycine Sulfate (TGS) Crystals Grown by Cooled Sting Technique," *Ferroelectrics*, Vol. 118, Nos. 1–4, pp. 85–91, 1991.

57. Banan, M.; Lal, R.B.; and Batra, A.: "Modified Triglycine Sulfate (TGS) Single Crystals for Pyroelectric Infrared Detector Applications," *J. Mater. Sci.*, Vol. 27, pp. 2291–2297, 1992.

58. Zhao-De, D.: "A New Method of Growth Ferroelectrics Crystal," *Ferroelectrics*, Vol. 39, pp. 1237–1239, 1981.

59. Bye, K.L.; and Keve, E.T.: "Structural Inhibition of Ferroelectric Switching in Triglycine Sulfate X-Ray Treatment," *Ferroelectrics*, Vol. 4, pp. 87–95, 1972.

60. Loiacono, G.M.; and Dougherty, J.P.: Final Technical Report (contract no DAAK70–77–C–0098) Submitted to Night Vision and Electrooptics Laboratories, Fort Belvoir, VA, 1978.

61. Lee, M.H.; Guo, R.; and Bhalla, A.S.: "Pyroelectric Sensors," *J. Electroceramics*, Vol. 2, pp. 229–242, 1998.

62. Chang, J.; Batra, A.K.; and Lal, R.B.: "Growth and Properties of Urea-Doped Triglycine Sulfate (UrTGS) Crystals," *J. Cryst. Growth*, Vol. 158, pp. 284–288, 1996.

63. Novotny, J.; Zelinka, L.; and Moracev, F.: "Broadband Infrared Detectors on the Basis of PATGS/Pt(IV) Single Crystals," *Sensors and Actuators A*, Vol. 119, pp. 300–304, 2005.

64. Batra, A.K.; Aggarwal, M.D.; and Lal, R.B.: "Growth and Characterization of Doped DTGS Crystals for Infrared Sensing Devices," *Mat. Lett.*, Vol. 57, pp. 3943–3948, 2003.

65. Su, G.; He, Y.; Yao, H.; et al.: "A New Pyroelectric Crystal L-Lycine-Doped TGS (LLTGS)," *J. Cryst. Growth*, Vol. 209, pp. 220–222, 2000.

66. Meera, K.; Muralidharan, R.; Tripathi, A.K.; et al.: "Growth of Thiourea-Doped TGS Crystals and Their Characterization," *J. Cryst. Growth*, Vol. 260, pp. 414–421, 2004.

67. Shaulov, A.; Smith, W.A.; and Rao, N.Y.: "Advantages of Obliquely Cut TGS Crystals in Pyroelectric Applications," *Ferroelectrics*, Vol. 38, pp. 967–970, 1981.

68. Shaulov, A.; and Smith, W.A.: "Optimum Cuts of Monoclinic m Crystals for Pyroelectric Detectors," *Ferroelectrics*, Vol. 49, pp. 223–228, 1984.

69. Shaulov, A.: "Improved Figure of Merit in Obliquely Cut Pyroelectric Crystals," *Appl. Phys. Lett.*, Vol. 39, No. 2, pp. 180–183, 1981.

70. Whipps, P.W.; and Bye, K.L.: "Polycrystalline Triglycine Sulphate-Selenate Materials for Pyroelectric Applications," *Ferroelectrics*, Vol. 7, pp. 183–185, 1974.

71. Bye, K.L.; Whipps, P.W.; and Keve, E.T.: "High Internal Bias Fields in TGS (L-alanine)," *Ferroelectrics*, Vol. 4, pp. 253–256, 1972.

72. Hadni, A.; Thomas, R.; and Erhard, C.: "An Unusual Type of Epitaxial Growth," *Phys. Status Solidi* (*a*), Vol. 39, pp. 419–424, 2006.

73. Hadni, A.; and Thomas, R.: "The Use of a Regular Distribution of Minute Pinholes for the Epitaxial Growth of an Oriented Thin Film," *Thin Solid Films*, Vol. 81, pp. 247–256, 1981.

74. Hadni, A.: *Infrared and Millimeter Waves*, Academic Press, New York, NY, 1986.

75. Xu, Y.: *Ferroelectric Materials and Their Applications*, North-Holland, London, England, 1991.

76. Curie, J.R.: "Studies on the Functional Ferroelectric Materials for Infrared Sensors," M.S. Thesis, Alabama A&M University, Normal, AL, 2004.

77. Yamaka, E.; Hayashi, T.; and Matsumoto, M.: "$PbTiO_3$ Pyroelectric Infrared Detector," *Infrared Phys.*, Vol. 11, pp. 247–248, 1971.

78. Futakuchi, T.; and Tanino, K.: "Pyroelectric Properties of La-Modified $PbTiO_3$ Thin Films Prepared by Screen Printing," *Jpn. J. Appl. Phys.*, Vol. 33, pp. 5294–5296, 1994.

79. No, K.; Choi, C.G.; Yoon, D.S.; et al.: "Pyroelectric Properties of Sol-Gel Derived Lanthanum Modified Lead Titanate Thin Films," *Jpn. J. Appl. Phys.*, Vol. 35, pp. 2731–2733, 1996.

80. Ye, C.; Tamagawa, T.; Schiller, P.; and Polla, D.L.: "Pyroelectric $PbTiO_3$ Thin Film for Microsensor Applications," *Sensors and Actuators A*, Vol. 35, pp. 77–83, 1992.

81. Pachaly, B.; Bruchhuas, R.; Pitzer, D.; et al.: "Pyroelectric Properties of Lead Titanate Thin Films Deposited on Pt-Coated Si Wafers by Multitarget Sputtering," *Integrated Ferroelectrics*, Vol. 5, pp. 333–338, 1994.

82. Chopra, S.; Sharma, S.; Goel, T.C.; and Mendiratta, R.G.: "Structural, Dielectric, and Pyroelectric Studies of $Pb_{1-x}Ca_xTiO_3$ Thin Films," *Solid State Communications*, Vol. 127, pp. 299–304, 2003.

83. Chang, C.C.; and Lai, Y.C.: "The Fabrication and Characterization of $(Pb,Ca)TiO_3$ Pyroelectric Thin Films With Different Ca Contents," *J. Appl. Phys.*, Vol. 101, pp. 104,106-1– 104,106-6, 2001.

84. Muart, P.: "Micromachined Infrared Detectors Based on Pyroelectric Thin Films," *Rep. Prog. Phys.*, Vol. 64, pp. 1339–1388, 2001.

85. Deb, K.K.: "Pyroelectric Characteristics of a Hot-Pressed Lanthanum-Doped PZT (PLZT (8/40/60))," *Mat. Lett.*, Vol. 5, pp. 222–226, 1987.

86. Suaste-Gómez, E.; González-Ballesteros, R.; and Castillo-Rivas, V.: "Pyroelectric Properties of $Pb_{0.88}Ln_{0.08}Ti_{0.98}Mn0_{.02}O_3$ (Ln=La, Sm, Eu) Ferroelectric Ceramic System," *Mat. Character.*, Vol. 50, pp. 349–352, 2003.

87. Czekaj, D.; Lisinska-Czekaj, A.; Kuprianov, M.F.; and Zakharov, Y.N.: "Pyroelectric Properties of the Multi-component Ferroelectric Ceramic Materials," *J. Euro. Ceram. Soc.*, Vol. 19, pp. 1149–1152, 1999.

88. Guggilla, P.; Batra, A.K.; Currie, J.R.; et al.: "Pyroelectric Ceramics for Infrared Detection Applications," *Mat. Lett.*, Vol. 60, pp. 1937–1942, 2006.

89. Batra, A.K.; Guggilla, P.; Aggarwal, M.: and Lal, R.B.: "Effects of O^+ Irradiation on Infrared Sensing Characteristics of Modified PZT Ceramic," *Nucl. Instrum. Methods Phys. Res. B*, Vol. 246, pp. 369–373, 2006.

90. Deb, K.K.; Bennett, K.W.; Brody, P.S.; and Melnick, B.M.: "Pyroelectric Characteristics of Thin PZT (40/60) Film on Platinum Film for Infrared Sensors," *Integrated Ferroelectrics*, Vol. 6, pp. 253–264, 1996.

91. Kobune, M.; Fujii, S.; Takayama, R.; and Tomozawa, A.: "Preparation and Pyroelectric Properties of PLZT Thin Films," *Jpn. J. Appl. Phys.*, Vol. 35, pp. 4980–4983, 1996.

92. Loziński, A.; Wang, F.; Uusimäki, A.; and Leppävuori, S.: "PLZT Thick Film for Pyroelectric Sensors," *Meas. Sci. Tech.*, Vol. 8, pp. 33–37, 1997.

93. Yang, J-S.; Kim, S-H.; Park, D-Y.; et al.: "Thickness Effects on the Pyroelectric Properties of Chemical-Solution–Derived $Pb(Zr_{0.3}Ti_{0.7})O_3$ Thin Films for Infrared Devices," *Jpn. J. Appl. Phys.*, Vol. 42, pp. 5956–5959, 2003.

94. Yang, J-S.; Kim, S-H.; Yeom, J-H.; et al.: "Piezoelectric and Pyroelectric Properties of $Pb(Zr,Ti)O_3$ Films for Microsensors and Actuators," *Integrated Ferroelectrics*, Vol. 54, pp. 515–525, 2003.

95. Shi, C.; Meidong, L.; Churong, L.; et al.: "Investigation of Crystallographic and Pyroelectric Properties of Lead-Based Perovskite-Type Structure Ferroelectric Thin Films," *Thin Solid Films*, Vol. 375, pp. 288–291, 2000.

96. Zhang, Q.; and Whatmore, R.W.: "Improved Ferroelectric and Pyroelectric Properties in Mn-Doped Lead Zirconate Titanate Thin Films," *J. Appl. Phys.*, Vol. 94, pp. 5228–5233, 2003.

97. Kobune, M.; Ishito, H.; Mineshige, A.; et al.: "Relationship Between Pyroelectric Properties and Electrode Sizes in (Pb, La)(Zr, Ti)O_3 (PLZT) Thin Films," *Jpn. J. Appl. Phys.*, Vol. 37, pp. 5154–5157, 1998.

98. Irzaman, Y.; Darvina, A.; Faud, P.; et al.: "Physical and Pyroelectric Properties of Tantalum-Oxide-Doped Lead Zirconium Titanate ($Pb_{0.995}(Zr_{0.525}Ti_{0.465}Ta_{0.010})O_3$) Thin Films and Their Application for IR Sensors," *Phys. Status Solidi* (*a*), Vol. 199, Iss. 3, pp. 416–424, 2003.

99. Shaobo, L.; and Yanqiu, L.: "The Crystallization and Electrical Properties of Lead-Based Ferroelectric Thin Films for Uncooled Pyroelectric Infrared Detector," *J. Mater. Sci.: Materials in Electronics*, Vol. 15, pp. 545–548, 2004.

100. McCarthy, K.C.; McCarthy, F.S.; Teowee, G.; et al.: "Pyroelectric Properties of Various Sol-Gel Derived Thin Films," *Integrated Ferroelectrics*, Vol. 17, pp. 377–385, 1997.

101. Han, H.; Kotru, S.; Zhong, J.; and Pandey, R.K.: "Effect of Nb Doping on Pyroelectric Property of Lead Zirconate Titanate Films Prepared by Chemical Solution Deposition," *Infrared Phys. Tech.*, Vol. 51, pp. 216–220, 2008.

102. Tian, X.; Li, Y.; and Xu, Z.: "Laser Annealing of $Pb(Zr_{0.52}Ti_{0.48})O_3$ Thin Films for Pyro-electric Detectors," *Thin Solid Films*, Vol. 517, Issue 20, pp. 5855–5857, 2009.

103. Dorey, R.A.; and Whatmore, R.W.: "Pyroelectric PZT/PMNZTU Composite Thick Films," *J. Eur. Ceram. Soc.*, Vol. 25, pp. 2379–2382, 2005.

104. Xu, Y.: *Ferroelectric Materials and Their Applications*, North-Holland, London, England, 1991.

105. Stokowski, S.E.; Venables, J.D.; Byer, N.E.; and Ensign, T.C.: "Ion-Beam Milled, High-Detectivity Pyroelectric Detectors," *Infrared Phys.*, Vol. 16, pp. 331–334, 1976.

106. Roundy, C.B.: "Pyroelectric Self-Scanning Infrared Detector Arrays," *Appl. Opt.*, Vol. 18, pp. 943–945, 1979.

107. Norkus, V.: "Pyroelectric Infrared Detectors Based on Lithium Tantalate: State-of-the-Art and Properties," *Proc. SPIE 5251*, pp.121–128, 2003.

108. Kao, M.C.; Chen, H.Z.; Wang, C.N.; and Chen, Y.C.: "Pyroelectric Properties of Sol-Gel Derived Lithium Tantalite Thin Films," *Physica B*, Vol. 329–333, pp. 1527–1528, 2003.

109. Seifert, A.; and Muralt, P.: "$LiTaO_3$ Thin Films for Pyroelectric Devices," unpublished.

110. Nougaret, L.; Combette, P.; and Pascal-Dalannoy, F.: "Growth of Lithium Tantalate Thin Films by Radio Frequency Magnetron Sputtering With Lithium Enriched Target," *Thin Solid Films*, Vol. 517, pp. 1784–1789, 2009.

111. Schmid, P.F.; and Levy, F.: "Ferro- and Pyro-Electric Properties of Lithium Tantalate (LiTaO$_3$) Thin Films," *J. Korean Phys. Soc.*, Vol. 32, pp. S1454–S1456, 1998.

112. *Properties of Lithium Niobate*, K. Wong (ed.), IET, Michael Faraday House, Hartfordshire, UK, 2002.

113. Gebre, T.; Batra, A.K.; Guggilla, P.; et al.: "Properties of Pure and Doped Lithium Niobate Crystals for Infrared Sensors," *Ferroelectric Lett.*, Vol. 31, pp. 131–139, 2004.

114. Lines, M.E.; and Glass, A.M.*: Principles and Applications of Ferroelectrics and Related Materials*, Clarendon Press, Oxford, UK, 1979.

115. Zhang, T.; and Ni, H.: "Pyroelectric and Dielectric Properties of Sol-Gel Derived Barium-Strontium-Titanate (Ba$_{0.64}$Sr$_{0.36}$TiO$_3$) Thin Films," *Sensors and Actuators A*, Vol. 100, pp. 252–256, 2002.

116. Lee, J-S.; Park, J-S.; Kim, J-S.; et al.: "Preparation of (Ba,Sr)TiO$_3$ Thin Films With High-Pyroelectric Coefficients," *Jpn. J. Appl. Phys.*, Vol. 38, pp. L574–L576, 1999.

117. Zhu, H.; Miao, J.; Noda, M.; and Okuyama, M.: "Preparation of BST Ferroelectric Thin Films by Metal Organic Decomposition for Infrared Sensors," *Sensors and Actuators A*, Vol. 110, pp. 371–377, 2004.

118. Sengupta, S.; Sengupta, L.C.; Synowczynski, J.; and Rees, D.A.: "Novel Pyroelectric Sensor Materials," *IEEE Trans. Ultra., Ferro., and Freq. Cont.*, Vol. 45, No. 6, pp. 1444–1452, 1998.

119. Cheng, J.; Meng, X.; Tang, J.; et al.: "Pyroelectric Ba$_{0.8}$Sr$_{0.2}$TiO$_3$ Thin Films Derived From 0.5M Solution Precursor by Sol-Gel Processing," *Appl. Phys. Lett.*, Vol. 75, pp. 3402–3404, 1999.

120. Kang, D.; Han, M.; Lee, S.; and Song, S.: Dielectric and Pyroelectric Properties of Barium Strontium Calcium Titanate Ceramics," *J. Eur. Ceram. Soc.*, Vol. 23, pp. 515–518, 2003.

121. Liu, S.; Liu, M.; Jiang, S.; et al.: "Fabrication of SiO$_2$-Doped Ba$_{0.85}$Sr$_{0.15}$TiO$_3$ Glass-Ceramic Films and the Measurement of Their Pyroelectric Coefficient," *Mater. Sci. Eng.*, Vol. B99, pp. 511–515, 2003.

122. Liu, S.; Liu, M.; Jiang, S.; et al.: "Preparation and Characterization of Ba$_{1-x}$Sr$_x$TiO$_3$ Thin Films for Uncooled Infrared Focal Plane Arrays," *Mater. Sci. Eng. C*, Vol. 22, pp. 73–77, 2002.

123. Glass, A.M.: "Investigation of the Electrical Properties of Sr$_{1-x}$Ba$_x$Nb$_2$O$_6$ With Special Reference to Pyroelectric Detection," *J. Appl. Phys.*, Vol. 40, pp. 4699–4313, 1969.

124. Amorin, H.; Guerreo, F.; Portelles, J.; et al.: "Effect of La^{3+} Doping on the Polarization of the LSBN Ceramic System," *Solid State Comm.*, Vol. 106, pp. 555–558, 1998.

125. Chen, C.J.; Xu, Y.; Xu, R.; and Mackenzie, J.D.: "Ferroelectric and Pyroelectric Properties of Strontium Barium Niobate Films Prepared by the Sol-Gel Method," *J. Appl. Phys.*, Vol. 69, pp. 1763–1765, 1991.

126. Venet, M.; Santos, I.A.; Eiras, J.A.; and Garcia, D.: "Potentiality of SBN Textured Ceramics for Pyroelectric Applications," *Solid State Ionics*, Vol. 177, pp. 589–593, 2006.

127. Wan, X.; Tang, X.; Wang, J.; et al.: "Growth and Pyroelectric Properties of 0.2 mol. % Fe-Doped $Pb(Mg_{1/3}Nb_{2/3})O_3$-0.38PbTiO$_3$ Single Crystals by a Dynamic Technique," *App. Phys. Lett.*, Vol. 84, pp. 4711–4713, 2004.

128. Tang, Y.; Zhao, X.; Wan, X.; et al.: "Comparison, DC Bias and Temperature Dependence of Pyroelectric Properties of <111> - Oriented $(1–x) Pb(Mg_{1/3}Nb_{2/3})O_{3–x}PbTiO_3$ Crystals," *Mater. Sci. Eng. B*, Vol. 119, pp. 71–74, 2005.

129. Tang, Y.; Wan, X.; Zhao, X.; et al.: "Large Pyroelectric Response in Relaxor-Based Ferroelectric $(1–x)Pb(Mg_{1/3}Nb_{2/3})O_{3–x}PbTiO_3$ Single Crystals," *J. Appl. Phys.*, Vol. 98, pp. 084,104-1–084,104-4, 2005.

130. Wang, J.T.; and Zhang, C.: "Pyroelectric Properties of $0.7Pb(Mg_{1/3}Nb_{2/3})O_3$-0.3PbTiO$_3$ Ceramics," *J. Appl. Phys.*, Vol. 98, pp. 054,103-1–054,103-4, 2005.

131. Sebald, G.; Seveyrat, L.; Guyomar, D.; et al.: "Electrocaloric and Pyroelectric Properties of $0.75Pb(Mg_{1/3}Nb_{2/3})O_3$-0.25PbTiO$_3$," *J. Appl. Phys.*, Vol. 100, pp. 124,112-1–124,112-6, 2006.

132. Aleksandrov, S.E.; Gavrilov, G.A.; Kapralov, A.A.; et al.: "Relaxer Ferroelectrics as Promising Materials for IR Detectors," *Solid-State Electronics*, Vol. 74, pp. 72–76, 2004.

133. Kumar, P.; Sharma, S.; Thakur, O.P.; et al.: "Dielectric, Piezoelectric, and Pyroelectric Properties of PMN-PT (68:32) System," *Ceram. Internat.*, Vol. 30, pp. 585–589, 2004.

134. Tang, Y.; Luo, L.; Jia, Y.; et al.: "Mn-Doped $0.71Pb(Mg_{1/3}Nb_{2/3})O_3$-0.29PbTiO$_3$ Pyroelectric Crystals for Uncooled Infrared Focal Plane Arrays Applications," *Appl. Phys. Lett.*, Vol. 89, pp. 162,906-1–162,906-3, 2006.

135. Kochary, F.; Aggarwal, M.D.; Batra, A.K.; et al.: "Growth and Electrical Characterization of the Lead Magnesium Niobate-Lead Titanate (PMN-PT) Single Crystals for Piezoelectric Devices," *J. Mater. Sci.: Mat. Electron.*, Vol. 19, pp. 1058–1063, 2008.

136. Davis, M.; Damjanovic, D.; and Setter, N.: "Pyroelectric Properties of $(1–x Pb(Mn_{1/3}Nb_{2/3}O_{3–x}PbTiO_3$ and $(1–x)Pb(Zn_{1/3}Nb_{2/3}O_{3–x}PbTiO_3$ Single Crystals Using a Dynamic Method," *J. Appl. Phys.*, Vol. 96, pp. 2811–2815, 2004.

137. *Ferroelectric Polymers*, H.S. Nalwa (ed.), Marcel Dekker, Inc., New York, NY, 1995.

138. Ploss, B.; and Bauer, S.: "Characterization of Materials for Integrated Pyroelectric Sensors," *Sensors and Actuators A*, Vols. 25–27, pp. 407–411, 1991.

139. Neumann, N.; Kohler, R.; and Hofmann, G.: "Pyroelectric Thin Film Sensors and Arrays Based on P(VDF-TrEF)," *Integrated Ferroelectrics*, Vol. 6, pp. 213–230, 1995.

140. Capan, R.; Alp, I.; Richardson, T.H.; and Davis, F.: "Pyroelectric Figure of Merit for an Acid/Amine Alternate Layer Langmuir-Blodgett Film," *Mat. Lett.*, Vol. 59, pp. 1945–1948, 2005.

141. Tesnel, B.; Topacli, A.; Topacli, C.; et al.: "Characterization of Langmuir-Blodgett Films of Arachidic Acid and 1,2-bis(dodecyloxy)04,5-Diaminobenzene in Pyroelectric Devices," *Colloids and Surfaces A: Eng. Aspects*, Vol. 299, pp. 274–251, 2007.

142. Aggarwal, M.D.; Currie, J.R.; Penn, B.G.; et al.: "Polymer-Ceramic Composite Materials for Pyroelectric Infrared Detectors: An Overview," *NASA/TM—2007–215190*, Goddard Space Flight Center, 2007.

143. Wang, M.; Fang, C.S.; and Zhuo, H.S.: "Study on the Pyroelectric Properties of TGS-PVDF Composites," *Ferroelectrics*, Vol. 118, pp. 191–197, 1991.

144. Wang, Y.; Zhong, W.; and Zang, P.: "Pyroelectric Properties of Ferroelectric-Polymer Composite," *J. Appl. Phys.*, Vol. 74, No. 1, pp. 512–524, 1993.

145. Changshui, F.; Qingwu, W.; and Hongsheng, Z.: "Preparation and Pyroelectric Properties of Oriented Composite ATGS-PVDF Film," *J. Korean Phys. Soc.*, Vol. 32, pp. S1843–S1845, 1998.

146. Yang, Y.; Chan, H.L.W.; and Choy, C.L.: "Properties of Triglycine Sulfate/Poly(Vinylidene Fluoride-Trifluoroethylene) 0-3 Composites," *J. Mater. Sci.*, Vol. 41, pp. 251–258, 2006.

147. Chan, H.L.W.; Chan, W.K.; Zhang, Y.; and Choy, C.L.: "Pyroelectric and Piezoelectric Properties of Lead Titanate/Polyvinylidene Fluoride-Trifluoroethylene 0-3 Composites," *IEEE Trans. Dielec. Elec. Ins.*, Vol. 5, No. 4, pp. 505–512, 1998.

148. Chen, Y.; Chan, H.L.W.; and Choy, C.L.: "Pyroelectric Properties of $PbTiO_3$/P(VDF-TrFE) 0-3 Nanocomposite Films," *Thin Sold. Films*, Vol, 323, pp. 270–274, 1998.

149. Zhang, Q.Q.; Ploss, B.; Chan, H.L.W.; and Choy, C.L.: "Integrated Pyroelectric Arrays Based on PCLT/P(VDF-TrFE) Composite," *Sensors and Actuators A*, Vol. 86, pp. 216–219, 2000.

150. Zhang, Q.Q.; Chan, H.L.W.; Ploss, B.; and Choy, C.L.: "PCLT/P(VDF-TrFE) Nanocomposite Pyroelectric Sensors," *IEEE Trans. Ultra., Ferro., and Freq. Cont.*, Vol. 48, No. 1, pp. 154–160, 2001.

151. Zhang, Q.Q.; Chan, H.L.W.; and Choy, C.L.: "Dielectric and Pyroelectric Properties of P(VDF-TrFE) and PCLT–P(VDF-TrFE) 0-3 Nanocomposite Films," *Composites Part A: Appl. Sci. and Manuf.*, Vol. 30, pp. 163–167, 1999.

152. Jinhua, L.; Ningyi, Y.; and Chan, H.L.W.: "Preparation of PCLT/P(VDF-TrFE) Based on Plastic Film Substrate," *Sensors and Actuators A*, Vol. 100, pp. 231–235, 2002.

153. Lam, K.S.; Wong, Y.W.; Tai, L.S.; et al.: "Dielectric and Pyroelectric Properties of Lead Zirconate Titanate/Polyurethane Composites," *J. Appl. Phys.*, Vol. 96, No. 7, pp. 3896–3899, 2004.

154. Dietze, M.; Krause, J.; Solterbeck, C.H.; and Es-Souni, M.: "Thick Film Polymer-Ceramic Composites for Pyroelectric Applications," *J. Appl. Phys.*, Vol. 101, pp. 054,113-1–054,113-7, 2007.

155. Batra, A.K.; Corda, J.; Guggilla, P.; et al.: "Dielectric and Pyroelectric Properties of $LiTaO_3$:P(VDF-TrFE) Composite Film," *Proc. of SPIE*, Vol. 7213, pp. 721,313-2–721,313-9, 2009.

156. Fuflyigin, V.; Salley, E.; Osinsky, A.; and Norris, P.: "Pyroelectric Properties of AlN," *Appl. Phys. Lett.*, Vol. 77, No. 19, pp. 3075–3077, 2000.

157. Bykhovski, A.D.; Kaminski, V.V.; Sur, M.S.; et al.: "Pyroelectricity in Gallium Nitride Thin Films," *Appl. Phys. Lett.*, Vol. 69, No. 21, pp. 3254–3256, 1996.

158. Wang, Z.L.: "Nanostructures of Zinc Oxide," *Appl. Phys. Lett.*, pp. 26–33, June 2004.

159. Alexe, M.; and Pintilie, L.: "Thermal Analysis of the Pyroelectric Bimorph as Radiation Detector," *Infrared Phys. Tech.*, Vol. 1, pp. 949–654, 1995.

160. Lang, S.B.; and Alexe, M.: "Optimization and Experimental Verification of a Pyroelectric Bimorph Radiation Detector," *Appl. Ferroelectrics*, *07803–4959–8/98 IEEE*, pp. 195–198, 1998.

161. Es-Souni, M.; Iakovlev, S.; and Solterbeck, C-H.: "Multilayer Ferroelectric Thin Film for Pyroelectric Applications," *Sensors and Actuators A*, Vol. 109, pp. 114–119, 2003.

162. Sun, L.; Tang, O.K.; Liu, W.; et al.: "Characterization of Sol-Gel Derived $Pb(Zr_{0.3}Ti_{0.7})O_3$/$PbTiO_3$ Multilayer Thin Films," *Ceram. Internat.*, Vol. 30, pp. 1835–1841, 2004.

163. Sun, L.L.; Tan, O.K.; Liu, W.G.; et al.: "Comparison Study on Sol-Gel $Pb(Zr_{0.3}Ti_{0.7})O_3$ and $Pb(Zr_{0.3}Ti_{0.7})O_3$/$PbTiO_3$ Multilayer Thin Films for Pyroelectric Infrared Detectors," *Microelectronic Eng.*, Vol. 66, pp. 738–744, 2003.

164. Schubring, N.W.; Mantese, J.V.; Micheli, A.L.; et al.: "Dynamic Pyroelectric Enhancement of Homogeneous Ferroelectric Materials," *Phys. Rev. Lett.*, Vol. 68, p. 1778, 1992.

165. Mantese, J.V.; Schubring, N.W.; Micheli, A.L.; and Catalan, A.B.: "Ferroelectric Thin Films With Polarization Gradients Normal to the Growth Surface," *Appl. Phys. Lett.*, Vol. 67, pp. 721–723, 1995.

166. Mantese, J.V.; Schubring, N.W.; Micheli, A.L.; et al.: "Slater Model Applied to Polarization Graded Ferroelectrics," *Appl. Phys. Lett.*, Vol. 71, pp. 2047–2049, 1997.

167. Zhong, S.; Alpay, S.P.; Ban, Z.G.; and Mantese, J.V.: "Effective Pyroelectric Response of Compositionally Graded Ferroelectric Materials," *Appl. Phys. Lett.*, Vol, 86, pp. 092,903-1–092,903-2, 2005.

168. Jin, F.; Auner, G.W.; Naik, R.; et al.: "Giant Effective Pyroelectric Coefficient From Graded Ferroelectric Devices," *Appl. Phys. Lett.*, Vol. 73, No. 19, pp. 2838–2840, 1998.

169. Tang, X.G.; Wang, J.; Chan, H.L.W.; and Ding, A.L.: "Growth and Electrical Properties of Compositionally Graded $Pb(Zr_xTi_{1-x})O_3$ Thin Film on $PbZrO_3$ Buffered $Pt/Ti/SiO_2/Si$ Substrates," *J. Cryst. Growth*, Vol. 267, pp. 117–122, 2004.

170. Tang, X.G.; Chan, H.L.W.; and Ding, A.L.: "Electrical Properties of Compositionally Graded Lead Calcium Titanate Thin Films," *Solid State Comm.*, Vol. 127, pp. 625–628, 2003.

171. Tipton, C.W.; Kirchner, K.; Godfey, R.; et al.: "Enhanced-Response Pyroelectric Hetero-Structures," *Appl. Phys. Lett.*, Vol. 77, No. 15, pp. 2388–2390, 2000.

172. Wu, N.J.; Xu, Y.Q.; Chen, Y.S.; and Ignatiev, A.: "Pyroelectric/Superconducting Oxide Hetero-Structures for Uncooled Wide-Band Infrared Detection," *Physica C*, Vols. 341–348, pp. 2743–2744, 2000.

173. Xu, Y.Q.; Wu, N.J.; and Ignatiev, A.: "(Mn,Sb) Doped-$Pb(Zr,Ti)O_3$ Infrared Detector Arrays," *J. Appl. Phys.*, Vol. 88, No. 2, pp. 1004–1007, 2000.

174. Suyal, G.; Seifert, A.; and Setter, N.: "Pyroelectric Nanoporous Films: Synthesis and Properties," *Appl. Phys. Lett.*, Vol. 81, No. 2, pp. 1059–1061, 2002.

175. Suyal, G.; and Setter, N.: "Enhanced Performance of Pyroelectric Microsensors Through the Introduction of Nanoporosity," *J. Eur. Ceram. Soc.*, Vol. 24, pp. 247–251, 2004.

176. Shaulov, A.: "Broad Band Infrared Thermal Detector," *Sensors and Actuators*, Vol. 5, pp. 207–215, 1984.

177. Lehman, J.; Eppeldauer, G.; Aust, J.A.; and Racz, M.: "Domain-Engineered Pyroelectric Radiometer," *Appl. Optics*, Vol. 38, No. 34, pp. 7074–7055, 1999.

178. Nakamura, K.; and Itagaki, M.: "Pyroelectric IR Detectors Using Periodic Inverted Domains of $LiTiO_3$," *Jpn. J. Appl. Phys.*, Vol. 33, pp. 5404–5406, 1994.

179. Guo, Y.; Li, M.; Zhao, W.; et al.: "Ferroelectric and Pyroelectric Properties of $(Na_{0.5}Bi_{0.5})TiO_3$-$BaTiO_3$ Based Trilayered Thin Films," *Thin Solid Films*, Vol. 517, pp. 2974–2978, 2009.

180. Hossain, A.; and Rashid, M.H.: "Pyroelectric Detectors and Their Applications," *IEEE Trans. on Industry Applications*, Vol. 27, No. 5, pp. 824–829, 1991.

181. Schloss, L.F.: "Development of Novel Thin Film Pyroelectric Infrared Detectors," Ph.D. Thesis, University of California, Berkeley, CA, 2001.

182. Lang, S.B.: "Pyroelectricity: From Ancient Curiosity to Modern Imaging Tool," *Phys. Today*, pp. 31–36, August 2005.

REPORT DOCUMENTATION PAGE

1. REPORT DATE *(DD-MM-YYYY)*	2. REPORT TYPE	3. DATES COVERED *(From - To)*
01–03–2010	Technical Memorandum	

4. TITLE AND SUBTITLE	5a. CONTRACT NUMBER
Pyroelectric Materials for Uncooled Infrared Detectors: Processing, Properties, and Applications	5b. GRANT NUMBER
	5c. PROGRAM ELEMENT NUMBER

6. AUTHOR(S)	5d. PROJECT NUMBER
M.D. Aggarwal,* A.K. Batra,* P. Guggilla,* M.E. Edwards,* B.G. Penn, and J.R. Currie, Jr.	5e. TASK NUMBER
	5f. WORK UNIT NUMBER

7. PERFORMING ORGANIZATION NAME(S) AND ADDRESS(ES)	8. PERFORMING ORGANIZATION REPORT NUMBER
George C. Marshall Space Flight Center Marshall Space Flight Center, AL 35812	M–1273

9. SPONSORING/MONITORING AGENCY NAME(S) AND ADDRESS(ES)	10. SPONSORING/MONITOR'S ACRONYM(S)
National Aeronautics and Space Administration Washington, DC 20546–0001	NASA
	11. SPONSORING/MONITORING REPORT NUMBER
	NASA/TM—2010–216373

12. DISTRIBUTION/AVAILABILITY STATEMENT

Unclassified-Unlimited
Subject Category 25
Availability: NASA CASI (443–757–5802)

13. SUPPLEMENTARY NOTES

*Alabama A&M University, Normal, Alabama
Prepared by Spacecraft and Vehicle Systems Department, Engineering Directorate

14. ABSTRACT

Uncooled pyroelectric detectors find applications in diverse and wide areas such as industrial production; automotive; aerospace applications for satellite-borne ozone sensors assembled with an infrared spectrometer; health care; space exploration; imaging systems for ships, cars, and aircraft; and military and security surveillance systems. These detectors are the prime candidates for NASA's thermal infrared detector requirements. In this Technical Memorandum, the physical phenomena underlying the operation and advantages of pyroelectric infrared detectors is introduced. A list and applications of important ferroelectrics is given, which is a subclass of pyroelectrics. The basic concepts of processing of important pyroelectrics in various forms are described: single crystal growth, ceramic processing, polymer-composites preparation, and thin- and thick-film fabrications. The present status of materials and their characteristics and detectors' figures-of-merit are presented in detail. In the end, the unique techniques demonstrated for improving/enhancing the performance of pyroelectric detectors are illustrated. Emphasis is placed on recent advances and emerging technologies such as thin-film array devices and novel single crystal sensors.

15. SUBJECT TERMS

pyroelectric infrared detector, pyroelectric materials, ferroelectrics, uncooled detectors, ceramic and thick film processing

16. SECURITY CLASSIFICATION OF:			17. LIMITATION OF ABSTRACT	18. NUMBER OF PAGES	19a. NAME OF RESPONSIBLE PERSON
a. REPORT	b. ABSTRACT	c. THIS PAGE			STI Help Desk at email: help@sti.nasa.gov
U	U	U	UU	88	19b. TELEPHONE NUMBER *(Include area code)* STI Help Desk at: 443–757–5802

National Aeronautics and
Space Administration
IS20
George C. Marshall Space Flight Center
Marshall Space Flight Center, Alabama
35812